DISCRIMINATION OF SUSPENDED SEDIMENT CONCENTRATIONS USING MULTISPECTRAL REMOTE SENSING TECHNIQUES

by

Jeffrey Lee Liedtke

B.A., University of California, Santa Barbara, 1982

THESIS SUBMITTED IN PARTIAL FULFILLMENT OF

THE REQUIREMENTS FOR THE DEGREE OF

MASTER OF SCIENCE

in the Department

of

Geography

SIMON FRASER UNIVERSITY

July 27, 1987

APPROVAL

Name: Jeffrey Lee Liedtke

Degree: Master of Science

Title of Thesis: Discrimination of Suspended Sediment Concentrations Using Multispectral Remote Sensing Techniques.

Examining Committee:

Chairman: I. Hutchinson

A.C.B. Roberts
Senior Supervisor

M.C. Roberts

J.L. Luternauer
Research Scientist
Geological Survey of Canada

J.F.R. Gower
External Examiner
Research Scientist
Institute of Ocean Sciences

Date Approved: 19 August 1987

PARTIAL COPYRIGHT LICENSE

I hereby grant to Simon Fraser University the right to lend my thesis, project or extended essay (the title of which is shown below) to users of the Simon Fraser University Library, and to make partial or single copies only for such users or in response to a request from the library of any other university, or other educational institution, on its own behalf or for one of its users. I further agree that permission for multiple copying of this work for scholarly purposes may be granted by me or the Dean of Graduate Studies. It is understood that copying or publication of this work for financial gain shall not be allowed without my written permission.

Title of Thesis/Project/Extended Essay

Discrimination of Suspended Sediment Concentrations Using Multispectral Remote Sensing Techniques

Author: _____
(signature)

Jeffrey Lee Liedtke
(name)

August 21, 1987
(date)

ABSTRACT

The objective of this study was to use the spectral characteristics of inorganic suspended sediment to estimate suspended sediment concentrations using less expensive multispectral remote sensing systems and techniques.

Identification of suspended sediment was achieved by digitally processing multispectral video and photographic imagery utilizing spectral bands which optimized sediment discrimination. After imaging variable suspended sediment concentrations (SSCs) concurrent with surface sampling, the relative behavior of discrete spectral bands were used to develop procedures and techniques for identifying and quantifying SSC.

Spectral characteristics of suspended sediment in varying concentrations were examined in a controlled laboratory study under natural light conditions. These results were then compared with previously collected field data obtained in the Fraser River sediment plume in the Strait of Georgia. Additionally, airborne multispectral video and photographic imagery were taken at varying scales to examine the influence of atmospheric factors on target radiance. Extraneous factors contributing to the suspended sediment signal, such as shallow water bottom reflection and littoral vegetation, were also examined.

It was concluded that both narrow (10-16.8 mg/l) and wide (31-380 mg/l) ranges of SSC could be estimated with multispectral video and small format photographic imagery. Results showed that reflectance increased non-linearly (except for narrow concentration ranges) with SSC. Accompanying this non-linear increase in reflectivity was a spectral shift of peak reflectivity from green to red wavelengths of light.

Results from airborne imagery acquired at two altitudes (2000-4000 feet A.M.S.L.) demonstrated that the affects of extraneous atmospheric and environmental factors (noise) that contributed to the spectral return from sediment-laden water could be reduced. This reduction in noise resulted in an improved classification of SSC.

The red portion of the spectrum provided the most consistent information over the broadest range of sediment and atmospheric conditions. The green spectral region was also useful, especially for broad SSC ranges where its behavior could be compared with that of the red band by ratio techniques. A channel in the reflected infrared portion of the spectrum was necessary to extend the analytical range of the sensor system and insure that image overexposure (i.e., image saturation) did not occur at high SSCs. In addition, the infrared band could be used to help delineate shallow water and/or the land-water interface since these wavelengths are attenuated within the first few centimeters of the water. Thus, the rationale for a multispectral approach to water quality remote sensing was reaffirmed by these findings.

The procedures and techniques used in this study support the findings of other researchers who used orbital, airborne, and ground-based remote sensing systems to estimate SSC. The results also demonstrate that less expensive multispectral video and photographic remote sensing systems could be developed for practical water quality assessment.

THE FUTURE....

"The challenge before the international scientific community is to continue to develop the science and technology of remote sensing, while on the other hand, develop an intregrated understanding of our global life support system, and work toward a quantitative science of the biosphere. For only if we do this will we truly begin to understand the nature of the only known closed life support system capable of sustaining life for more than a few decades."

Estes and Star, (1986)

ACKNOWLEDGEMENTS

I thank my supervisor, Dr. Arthur Roberts, for his help during the course of the research, and letting me 'run with the ball'. His many ideas and perceptions will continue to be food for thought for many years to come.

The strength of these findings are a direct result of the considerable efforts of the surface sampling crews; the importance of their role cannot be overemphasized. Their triumphs over all adversities (in the name of 'science') was most humbling and unforgettable, and the following cavalcade of persons does not belie the appreciation of each. Thus, I acknowledge and thank: Jim Bowers, Mike 'Boats' Brown, Valerie Cameron, Susan 'Su-san' Chow, Debbie Duggan, David J. Evans, Lori 'Miz Griz' Griswold, Dennis 'Cowboy' Jelinski, Demetrios 'Clem' Karagatzides, Dr. John Luternauer, Anna 'Slim' Nilsson, Jerry 'Patch' Patchell, Ian Saunders, Anna 'ACE' Schlecht, Susan Smythe, Mirjam 'L. W.' Stadelmann, Jodey Udell, Martine Udell, Robert Wielgus, Haryy Williams, Guy 'Gee' Worthington, and the Canadian Coast Guard Hovercraft Search and Rescue crews. Thanks also go to the imaging system operators: Davey Evans, Edward 'Mr. Ed' Higginbottom, and John MacDonald. The assistance of Brian Radcliffe (Instructional Media Centre, Technical Services) was instrumental in 'trouble-shooting' and modifying the sensor system and digitizing imagery; his assistance is greatly appreciated. And thank you, Dr. Hickin, for donating the outboard motor to 'the cause'.

I thank Trudy Forbes (Pacific Geoscience Centre, Sediment Laboratory) for her assistance in water sample analyses. I must also thank the SFU Department of Biology for lending me (with and without permission) much needed sampling equipment. It was all returned in the same or better condition.

I gratefully acknowledge Dr. Michael Roberts, Dr. John Luternauer, and Dr. James Gower for their well-founded editorial comments. I also thank Jodey and Martine Udell, Mirjam Stadelmann, Clem Karagatzides, and Martin W. W. Feuchtwanger for

their assistance in compiling this manuscript.

I thank my wife, Elizabeth Hubbs, for her unflagging support and patience. I also thank my family for both moral and financial support.

The assistance of Dr. John Luternauer and the Geological Survey of Canada made this research possible, and are gratefully acknowledged for providing equipment, logistical, and financial support.

TABLE OF CONTENTS

LIST OF TABLES

LIST OF FIGURES

CHAPTER 1

INTRODUCTION

The objective of this study was to use less expensive multispectral remote sensing systems and techniques to estimate suspended sediment concentrations.

The suspended material was comprised primarily of silt and fine sand transported by the Fraser River, twenty miles south of Vancouver, British Columbia. The remote sensing system consisted of four ('off-the-shelf') video cameras sensitive in the blue, green, red, and reflected infrared spectral regions respectively, and two photographic cameras using color and false color infrared film.

Spectral characteristics of suspended sediment in varying concentrations were examined in a controlled laboratory study under natural light conditions. These result were then compared with previously collected field data obtained in the Fraser River sediment plume in the Strait of Georgia. Airborne multispectral video and photographic imagery were taken at varying scales to examine the influence of atmospheric factors on target radiance. Extraneous factors contributing to the suspended sediment signal, such as shallow water bottom reflection, submerged vegetation, and physical environmental factors were also examined. Therefore, a secondary objective was to identify and evaluate sources of problems resulting from atmospheric effects, differences in illumination (sun angle), instrument noise and noise introduced as a result of specular reflectance from water surfaces. Identification of suspended sediment was achieved through digital processing of multispectral imagery utilizing spectral bands which optimize sediment discrimination. After imaging variable suspended sediment concentrations (SSC) concurrent with surface sampling, the relative behavior of discrete spectral bands was used to develop procedures and techniques for identifying and quantifying SSC.

1.1 Introduction

Marine studies have often been limited by the inability to collect synoptic data. Extrapolation of surface sample results to unsampled areas have been tenuous and inaccurate. Investigators examining water quality parameters and phenomena have also been hampered by equipment, personnel, and cost contraints. These difficulties are particularly acute in estuarine studies where significant changes in conditions occur over short distances and time periods. Remote sensing data can overcome this difficulty by allowing analysis of complex phenomena such as suspended sediment concentrations and circulation patterns over entire estuaries and sea basins.

Most remote sensing studies of water quality have utilized orbital multispectral scanner imagery and relatively large water bodies. Many studies have been successful in determining various aspects of sediment loads, but were limited by spatial and spectral resolution and atmospheric restrictions (Bowker *et al.*, 1975; Viollier and Baussart, 1978; Aranuvachapun and LeBlond, 1981; Carpenter and Carpenter, 1983).

Landsat Multispectral Scanner (MSS) has been the principal orbital system used to date. Landsat MSS was designed for terrestrial applications, and is not well suited for accurate analysis of water quality. Consequently, data processing and presentation techniques were designed for differentiation of land cover classes, not water quality and related dynamic environments (Carpenter and Carpenter, 1983). Landsat MSS data are subject to analog-to-logarithmic compression, analog-to-digital conversion, and digital calibration and decompression before being distributed to the user. The character of the raw data values, and their proximity to other image data, determine the statistical decision rules for image calibration and rectification. Therefore, the statistical calibration and data transformation processes administered to the digital imagery are difficult to invert, making the retrieval of the original data values extremely difficult to achieve (Viollier and Baussart, 1978; Carpenter, 1981).

A further problem with Landsat MSS is its low spatial resolution (80 meters). The reflectance of any number of discrete sub-pixel objects are represented by a single reflectance value averaged for the 79m x 79m area. This affects studies concerned with small or narrow water bodies, and highly variable environments such as coastal marine environments. These environments are typically made up of nearshore and foreshore features with marsh communities and shore deposits, and shallow and deep water, with and without suspended sediment. Many of these features are 'sub-pixel' in size and would be masked or averaged together in an image pixel.

Spectral resolution limitations of Landsat MSS include the lack of a channel in the blue spectral region (420-500nm) and fixed wide-band channels ($\geq$ 100nm) (see Figure 1). In a study to determine SSC in a macrotidal system using MSS data, Amos and Alföldi (1979) achieved high correlations between SSC and radiance despite the large variety of grain sizes, compositions, and shapes of the suspended particles. Therefore, they concluded that MSS broad-band channels smooth-over or mask these variables, and that they were undetectable.

The signal return from relatively clear water is very low compared to terrestrial features because most light incident on a water surface is absorbed by the water body. For a solar zenith angle of 60°, Davis (1978) determined that the total upwelling irradiance, due to reflected sun and skylight, plus that due to upwelling subsurface light, was approximately 7.4% of the total incident light, integrated over the visible spectrum. The subsurface component (i.e., that portion containing water quality information) was approximately 2.5% of total incident sunlight. This low spectral return translated to a grey intensity range of about 1-9 (with a possible range of 0 - 127) on a Landsat image of moderately turbid waters in the Chesapeake Bay (Kritikos *et al.*, 1974). Included in this small density number (DN)[1] range were atmospheric contributions to the returned signal. Over clear deep water, more than 95% of the signal measured by

---

1 the grey-scale density numbers which make up the digital image representing reflectance from the ground scene. They range between 0 (black) and 64, 127, or 255 (white), depending whether the image data is represented by 6 bit, 7 bit, or 8 bit format (see footnote '2').

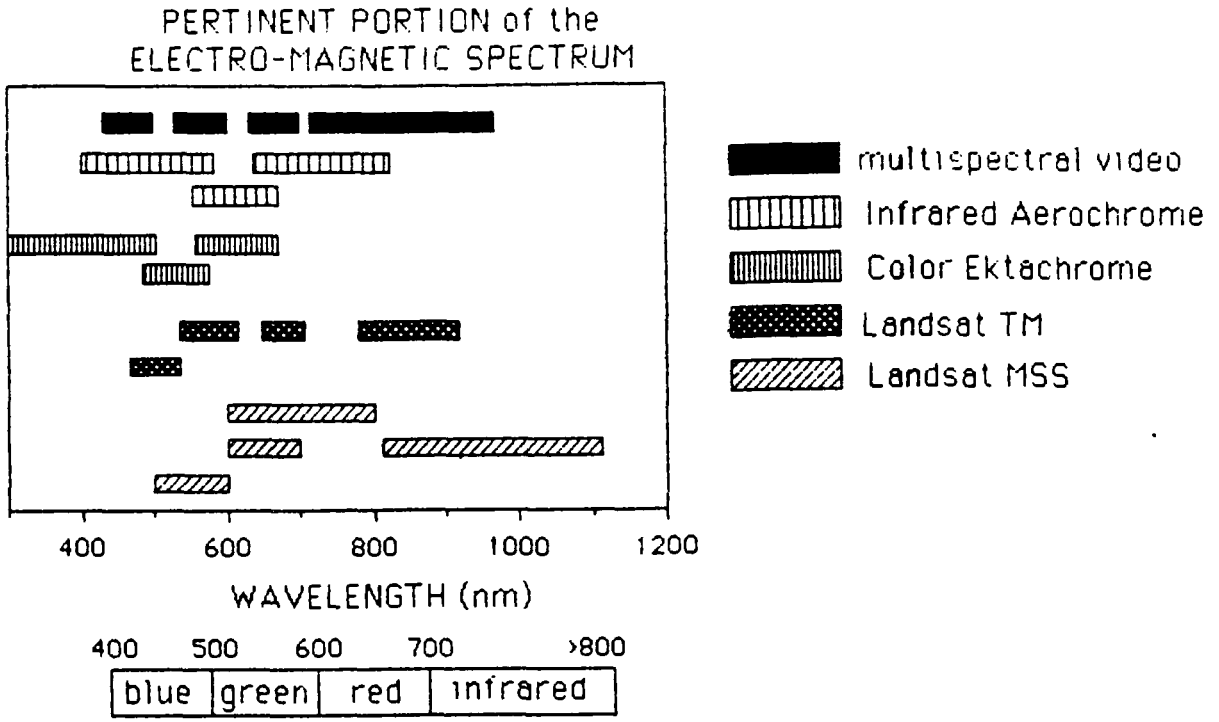

Figure 1: VISIBLE PORTION OF THE ELECTRO-MAGNETIC SPECTRUM, INCLUDING NEAR INFRARED. THE VARIOUS SENSOR BANDS OF LANDSAT* AND THE MSV ARE INDICATED.

*Both Landsat MSS and TM have non-visible (infrared) bands that are not shown in the diagram.

Landsat MSS originates as atmospheric scattering caused by aerosol content alone. In terms of reflectivity, this translates as more than the difference between 10-100 mg/l of suspended silt (Moore, 1978).

Electronic aberrations in the early MSS data resulted in an error of about 7-16% (Williamson *et al.*, 1973) of the signal returned from the water (from 1-3 grey levels; Kritikos, 1974). The six detectors comprising each spectral band [2] had slightly different characteristics which were not completely accounted for in the calibration process. Carpenter (1981) noted that with the small range in DNs over water, classification of water quality tended to respond to differences between detectors within a band as much as to differences between areas. Williamson *et al.*, (1973), and Whitlock (1976) indicated that more recent Landsat data had system noise comprising 5-10% of the return from water. Because of the low spectral return from the water, the signal-to-noise ratio (S:N) was low (i.e., $\simeq$ 4:1; Viollier and Baussart, 1978). MSS noise and atmospheric noise comprise a large portion of the spectral return over water and hinder the quantitative assessment of water quality.

Landsat Thematic Mapper (TM) may present a viable alternative to Landsat MSS for measurement of SSC. TM has improved spatial (30m versus 79m), spectral (7 channels versus 4 channels), and radiometric (8 bit versus 7 bit)[3] resolution. TM channel bandwidths are narrower than those of MSS, and the addition of a blue band has greatly enhanced the utility of the imagery for water quality studies. However, significant atmospheric alteration of the recieved signal and periodicity of coverage (16 days) coupled with infrequent cloud-free days in the Pacific Northwest still pose problems for some studies.

---

2 Scene radiance was measured in four channels which were comprised of six detectors each. The sensitivities of these six detectors were averaged by on-board calibration functions to produce a single output value representing ground radiance.

3 In digital computer terminology, this is a binary digit that is an exponent of the base 2. Therefore, 8 bit is 2^8 or '255'; 6 bit is 2^6 or 64; 7 bit is 127. These numbers indicate the dynamic range of the sensor.

Prior to 1968, when the first airborne multispectral scanner was designed and developed, aerial photography was used to map water turbidity and depth (Moore, 1947; Jones, 1957). Aerial photography can provide satisfactory quantitative results by employing careful calibration techniques (Moore, 1947; Piech and Walker, 1971; Scherz and Van Domelen, 1975; Villemonte *et al.*, 1974; Lillisand *et al.*, 1975). However, the use of color-pack films results in degradation of color separation images used in densitometric analysis. 'Color pack' film refers to multi-emulsion film used to generate color photographs. The emulsion layers are designed to be sensitive to light of certain wavelengths. However, the red and green light-sensitive layers are partially exposed by blue light because they overlay each other. Thus, color pack films have overlapping spectral sensitivity between layers. For studies focusing on the radiometric characterization of features or phenomena, analyses using multi-layered film must cope with reduced spectral resolution.

A number of airborne multispectral scanners have been used for water quality remote sensing (e.g., Coastal Zone Color Scanner (CZCS), NASA's Ocean Color Scanner (OCS), and Bendix Modular Multispectral Scanner (M^2S). Noise in the data ranged from 2-30+% of the water radiance values, depending on the scanner being used, particular band under analysis, and instrument gain (Whitlock, 1976). These airborne scanners were flexible remote sensors because appropriate bandwidths could be selected to optimize feature discrimination, with possible bandwidths usually as narrow as 10 nanometers (nm). Also, the number of possible bands could be more than ten, although the number of bands analyzed was seldom more than four due to computer data handling and cost constraints. Airborne flexibility allowed good spatial resolution for many applications. Thus, these systems provided excellent spatial and/or spectral resolution, but were very expensive and highly technical systems that required expensive aircraft and specialized system operators. These costs could be prohibitive for many site-specific resource oriented water quality applications.

To establish the utility of remote sensing for a certain application, two criteria must be met: 1) the analytical capability of the method, and 2) the economic competitiveness of the approach as compared with alternative methods for obtaining the same information. Optimally, many users could combine budget resources ti obtain useful imagery to suit the requirements of each of the different studies in a cost effective manner; however, this would necessitate a level of cooperation and communication between engineers, users, and agencies which is often unrealistic. Many projects are site or application specific, requiring that the sensor system be flexible enough to adequately meet the various needs of each study. In reality, even similar projects may be spatially or spectrally incompatible, and be approached as separate studies. As the number of potential users decrease, the cost of remote imagery increases. The tradeoff has been to compromise unique site-specific detail for managable costs. The cost of sophisticated airborne MSS imagery could easily exceed the budget for some practical investigations or applications.

One other important consideration in remote sensing of water quality is the fact that different spectral bands respond differently to different suspended sediment concentrations. A particular band may be extremely sensitive to changes in SSC at low concentrations (e.g., green), but be saturated, or insensitive, at high SSCs; whereas another band (e.g., red or near infrared) may not be highly sensitive at low SSCs but is not saturated at higher concentrations, thus extending the useful analytical range. In order to maximize both analytical range and sensitivity, a multispectral approach is superior to single-band methods (Holyer, 1978).

In light of the limitations of orbital multispectral scanners, the lack of spectral fidelity of color-pack films, and the high cost of airborne multispectral scanners, an alternative for aquiring, analyzing, and processing remote sensing data of water quality for practical resource management purposes is evident. A low cost, spectrally suitable and versatile remote sensing system needs to be developed for water quality analysis, along with compatible methodologies for information extraction from such a system.

Both the sensor system and methods need to be developed so that a range of [sediment] conditions can be related on a spatial, spectral, and temporal basis. For example, an ideal system for aquiring and analyzing SSC data would be able to reliably determine variable SSCs in different geographical locations at different times. Important considerations that need to be addressed in formulating this methodology are:

1) knowledge of energy-matter interactions in atmosphere and water,
2) knowledge of the sensor system employed,
3) appropriate control or correction for extraneous influences of image data (e.g., atmosphere and system noise),
4) proper data manipulation conforming to physical and statistical criteria,
5) consistency of results, and,
6) applicability, in terms of analytical ability and cost.

CHAPTER 2

SIGNAL RESPONSES IN WATER BODIES

Absorption of light in clear water increases with increasing wavelength. The maximum transmission and reflection peak for clear water is in the blue region of the spectrum (400-460 nanometers (nm)), and more light is absorbed through the green and red portions of the spectrum (500-600nm; 600-700nm). Water attenuates nearly all incident energy in the reflected infrared (720-1100+ nm; see Figure 2).

The spectral characteristics of a water body change with the introduction of suspended particles. These particles backscatter impinging radiation that would otherwise penetrate deeper into the water body and be absorbed by the water. The stronger reflectance from the turbid water is accompanied by a spectral shift of peak reflectivity towards longer wavelengths. The strength of the backscattered radiation increases with increasing sediment concentrations, and the magnitude of the peak spectral return to the sensor can be correlated with particular sediment types and concentrations. Examination and evaluation of these relative shifts of object reflectivity as conditions change is central to multispectral remote sensing.

Some important variables that can affect remote sensing of physical water-quality characteristics, and that must be accounted for in both empirical and radiative transfer modeling equations (Moore, 1978), are:

a. Time of year – The Earth recieves 7 percent more energy from the sun on January 1 than on July 1 because of its orbit.

b. Sun-elevation angle – More solar energy is specularly reflected from water surfaces at low sun-elevation angles than at high angles. Also, the path length of solar energy through the atmosphere is longer at low sun-elevation angles, and more solar energy is absorbed and scattered.

c. Aerosol and molecular content of the atmosphere – These constituents determine the amount of solar energy absorbed and scattered by the atmosphere.

d. Specular reflection of skylight from the water surface – Specularly reflected skylight

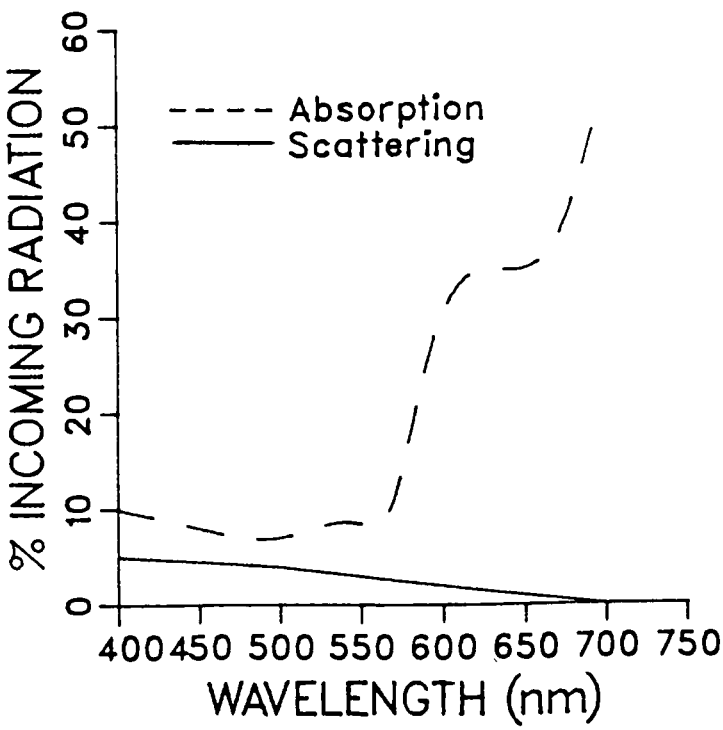

Figure 2: ABSORPTION AND SCATTERING PROPERTIES OF LIGHT IN PURE WATER.

is recieved by a sensor, and hence, influences the spectral return from both sediment-laden and clear water. The intensity and wavelength distribution of this energy depends on atmospheric scattering and absorption.

e. Roughness of the water surface — A rough surface may produce more or less specular reflection than a smooth surface.

f. Water color — Dissolved colored materials increase absorption of solar energy in water.

g. Reflectance and absorption characteristics of suspended sediment — When present in high concentrations, particles affect the spectral distribution of backscattered energy.

h. Depth of water and reflectance of bottom sediment — Water clarity determines the importance of bottom reflectance. Light reflected from the bottom of a water body may be confused with increasing SSC. Solar energy may not reach the sea-bed in turbid water, or water deeper than 100 meters.

2.1 Energy-Matter Interactions

Remote sensing surveys of water quality are based on the assumption that a meaningful relationship exists between reflectance and water quality. However, radiance values derived from remote sensing hardware do not directly relate to ground reflectance values because of differences in physical environments and atmospheric influences. If ground features are to be characterized in terms of their spectral reflectivity, atmospheric noise must be eliminated. Additionally, if multi-date comparisons are to be made, even limited to one location, adjustment of the remote sensing data is required to allow for differences in sun illumination, atmospheric backscattering and attenuation of energy, and the resulting surface reflection effects. These atmospheric effects obscure and reduce the contrast between adjacent surface features on the imagery and make feature identification more difficult.

The phenomena affecting water color can be classified into three categories (Piech and Walker, 1971): 1) atmospheric and source effects; 2) surface reflection; and 3)volume

reflection ('true' water color). Only volume effects provide information about water quality; the other effects obscure and degrade the desired spectral information by changing the apparent water color, and should be corrected

Source and Atmospheric Effects: Source effects refer to the two energy sources available for passive remote sensing, incoming direct sunlight and skylight (diffuse). These sources differ in relative energy content, spectral distribution, and in the degree to which they are reflected from water surfaces (due to their different angular distribution) (Figure 3; Piech and Walker, 1971; Sydor, 1980). Direct sunlight is collimated, and three to six times more intense than diffuse skylight (Whitlock, 1976). The constituents of the atmosphere selectively scatter shorter wavelengths more severely than longer wavelengths. Thus, skylight has a large ultra-violet and blue energy component, with reduced scattering for longer visible wavelengths, and virtually no scattering of near-infrared energy. Atmospheric attenuation is predominant in numerous longwave infrared regions due to absorption by water vapor and carbon dioxide, but is less important at near-infrared wavelengths (Sabins, 1979).

The amount of atmospheric scatter is not only a function of humidity and dust content, but also sun angle. When the solar altitude decreases from 90° (sun directly overhead), the atmospheric luminance increases due to longer effective scattering volume caused by the longer path length of solar radiation through the atmosphere (Figure 4). The atmospheric luminance at a solar altitude angle of 30° is about twice the value for a solar altitude of 90°. Increasing absorption of light in the longer atmospheric path begins to be the dominant factor for smaller angles. Thus, the atmosphere affects energy sensed by remote detectors in three ways (Turner *et al.*, 1971): 1) it modifies the spectral and spatial distribution of the radiation incident on water; 2) the energy returned from the water is decreased by scattering and absorption along the path to the sensor (atmospheric transmittance); 3) the apparent energy returned from the water is increased due to skylight scattered into the field-of-view (FOV) of the detector.

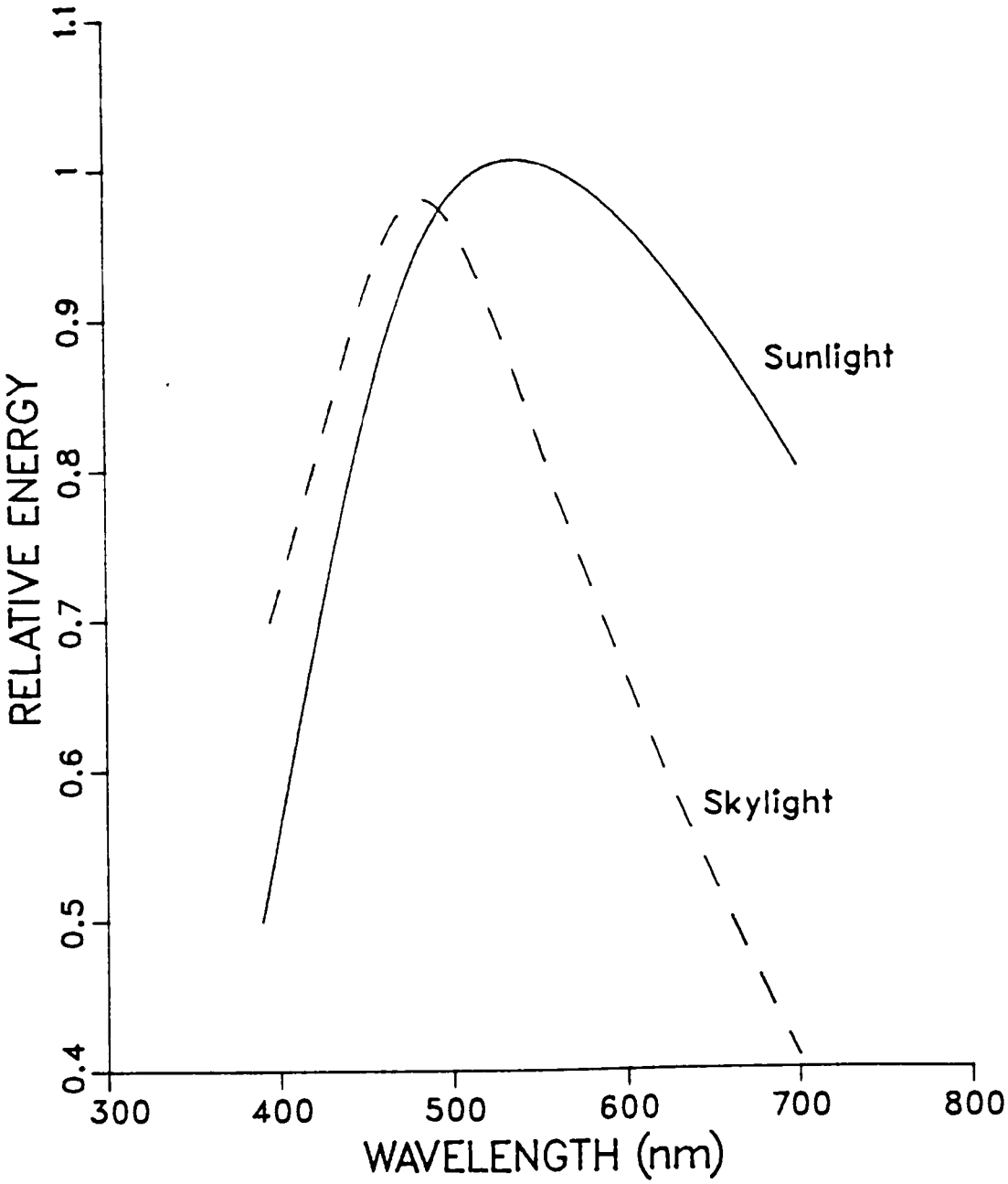

Figure 3: APPROXIMATE SPECTRAL DISTRIBUTIONS OF SUNLIGHT AND SKYLIGHT ON A CLEAR DAY (after Piech and Walker, 1971).

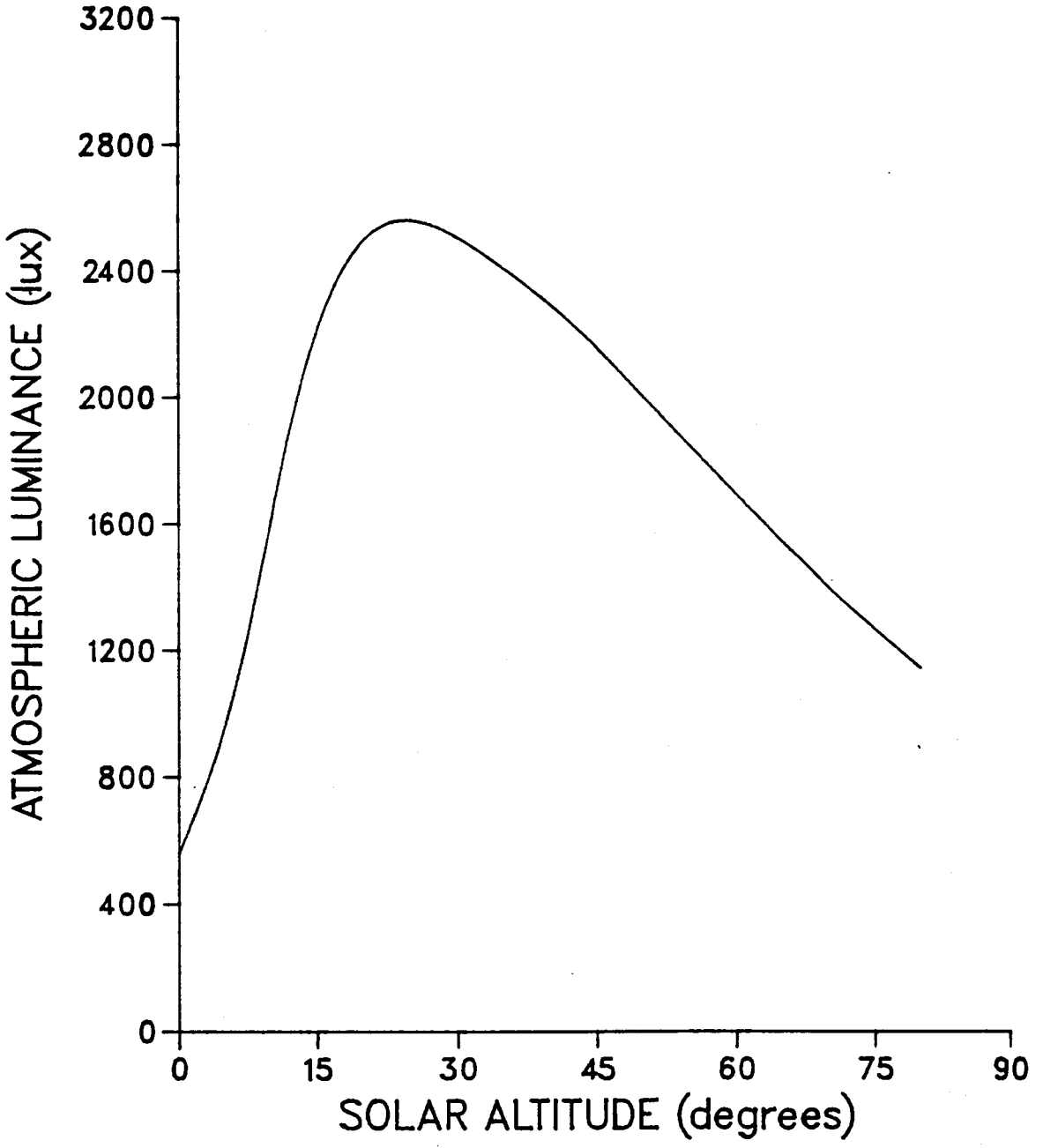

Figure 4: ATMOSPHERIC LUMINANCE AS A FUNCTION OF SOLAR ALTITUDE ANGLE (after Slater, 1975).

A study by Turner *et al.* (1971) illustrated the influence of diffuse radiation on object reflectivity. They attempted to quantify spectral path radiance by measuring the spectral return from grey reflectance panels. The resulting path radiance spectrum looked suspiciously like a reflectance spectrum for green vegetation, and they discovered that radiation from nearby objects outside the sensor's FOV (grass) were being scattered into the FOV of the reciever. Similarly, Griggs (1973) found that Landsat MSS radiance data obtained within 1300 feet of the shoreline was contaminated by the high albedo of land.

Transmittance of the atmosphere and amount of skylight depends on meteorological conditions, quantity and size of water vapor and dust particles within the atmosphere, solar angle, and the altitude of measurement. The atmospheric transmission will decrease with increasing altitude due to the increased influence of the intervening atmosphere. Since radiance from the water is much less than the average radiance of the surroundings (i.e., sun, atmosphere, and clouds), the apparent radiance from the water increases with altitude because the noise from the surroundings is greater than the target radiance (Horvath *et al.*, 1970). The tendency towards increase in apparent radiance is significantly strengthened by hazy atmospheric conditions, and is inversely related to wavelength (Horvath *et al.*, 1970). Measurements by Hovis and Leung (1977) show that the radiance at high altitudes can be several times that at low altitudes. As a result, the apparent differences in reflectivity between targets will decrease with increasing altitude.

Surface Reflection Effects: Water surfaces reflect light due to the discontinuity in refractive index at the air-water interface. Portions of the imagery affected by specular reflection of direct sunlight are useless for water quality analysis since the returned radiation is nearly identical to the incident radiation, and overwhelms the volume reflected energy from the water. Specular reflectance is recorded by the sensor as 'white', resulting in loss of information. Information may be obtained from areas on the imagery affected by skylight reflected energy (diffuse) if the volume reflected energy

from the water is stronger. The percentage of energy reflected from calm water depends on sun-elevation angle (Figure 5; Table 1) (List, 1971).

Only small amounts of information are lost by specular reflection at sun-elevation angles greater than 30°, whereas specular reflection is a serious problem at sun angles less than 30°.

Changes in sea-state induce changes in sea surface reflection coefficients (Cox and Munk, 1956; Wald and Monget, 1983). Rough water increases the area of sunglint on imagery because many waves have slopes that specularly reflect light towards the sensor. This effect is complex because of multiple reflections and differences in wavelength, height, and slope of surface waves. These surface roughness factors affect imagery according to wind/wave direction, direction of flight (look angle), and solar altitude.

Sunglint reflects visible energy at all wavelengths (white light) and changes the absolute level of the remotely measured flux, with little effect on the relative spectral signature (Johnson *et al.*, 1983). While portions of the imagery affected by specular reflection of direct sunlight can be avoided or eliminated from image analysis, surface

Table 1: **Percent Reflection of Solar Energy From Calm Water.**

Solar Elevation Angle	Percent Reflection
Horizon	100
5°	58
10°	35
20°	13
30°	6.0
40°	3.4
50°	2.1
90°	2.0

(after List, 1971)

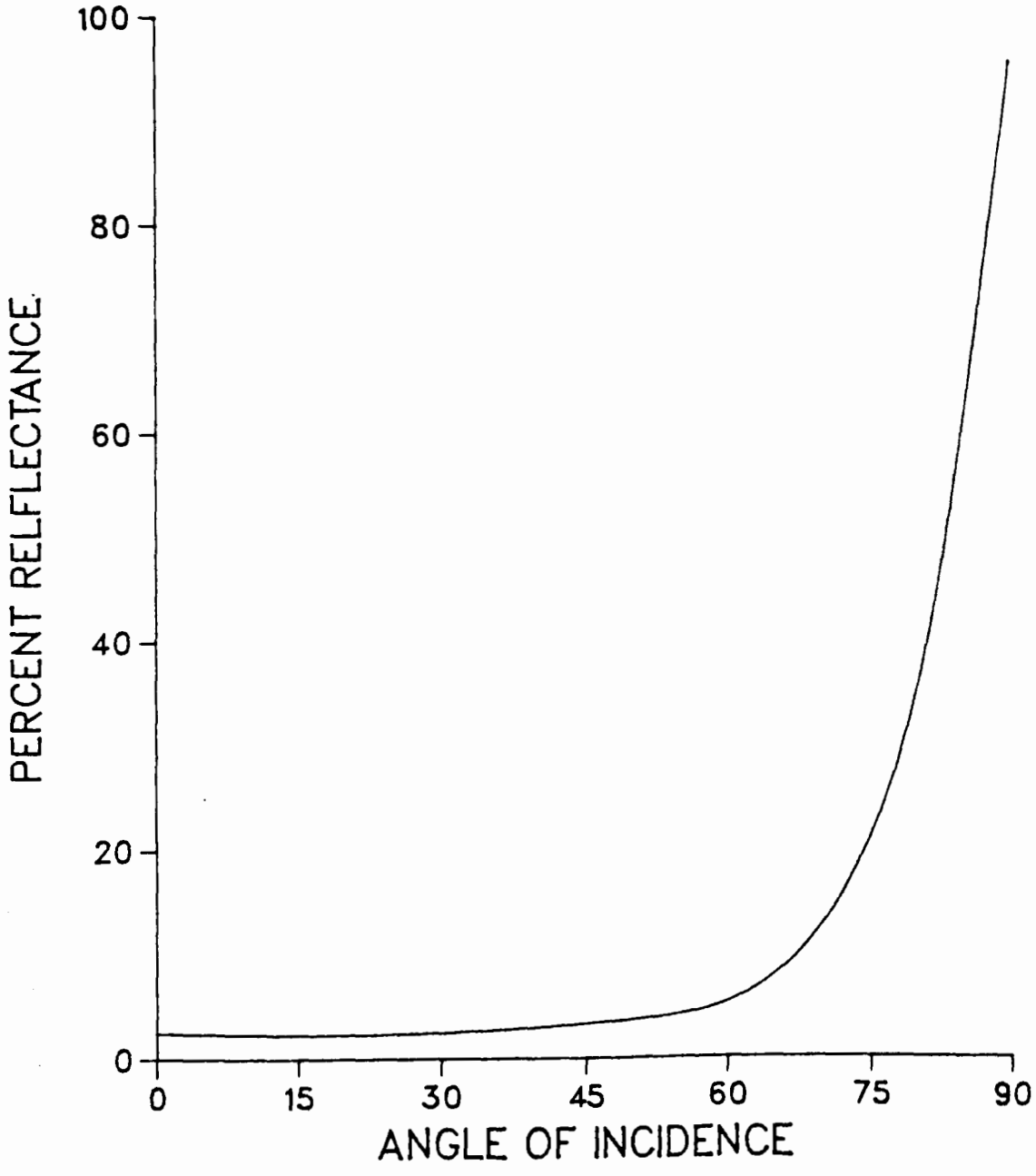

Figure 5: PERCENTAGE REFLECTANCE FROM AIR-WATER INTERFACE AS A FUNCTION OF ANGLE OF INCIDENCE, MEASURED FROM VERTICAL (values are for unpolarized light only)(after Piech and Walker, 1971).

reflected skylight occurs at every point within the scene. The amount of surface reflected skylight is a function of meteorological conditions, but typically constitutes about 10% of the reflected signal for a clear day (Moore, 1978; Piech and Walker, 1971). Since diffuse skylight is not specularly uniform, it not only increases the volume reflectance from the water, but also distorts its spectral shape towards the blue wavelengths. Jerlov (1968) inferred that reflectance under clear sky conditions was only weakly dependent on wind speed and air-mass turbidity, and was primarily a function of solar altitude.

Volume Reflection: The color of water is a function of its own optical properties and the type and concentration of dissolved and suspended particles. Sunlight (direct solar radiation and diffuse sky radiation) that is not specularly reflected is refracted downward at the air-water surface and is depleted due to molecular absorption and scattering by the water, as well as absorption, defraction, and reflection by suspended particles in the water (McCluney, 1976; Gordon, 1974). Molecular scattering by the water is so small that it may be neglected (Moore, 1947). Scattering by suspended particles in coastal waters will generally be in a forward direction; its extent depending on the size and amount of suspended particles and on the wavelength of light being considered (Di Toro, 1978). Forward scattering refers to light scattered deeper into the water body, i.e., in a forward direction. Thus, wavelengths which are susceptible to absorption by water (e.g., red) can actually penetrate deeper into the water body than some of the more deeply penetrating wavelengths, such as the blue-green wavelengths in clear water. Some of the forward-scattered energy is absorbed by both the water and the suspended material in the water. The remaining energy is 'backscattered' by the suspended particles. The fewer suspended particles, the lower the backscattered energy component. The re-emerging light resulting from backscattering was used in this study to predict sediment concentrations. In clear deep water, only about 1-3% of incident energy is backscattered, and about ten times more blue light is scattered than red light (Moore, 1978). After passing through the seawater, light reaching the sea-bed will be partially diffuse from scattering by both atmosphere and water, and partially parallel

(Moore, 1947), the proportions varying over a wide range. The sea-bed will then act as a diffuse reflector, the fraction reflected depending on the color and texture of the bottom and the wavelengths considered.

Backscattered energy reaching the water surface at an angle greater than 48° will be internally reflected back into the water body (Moore, 1947; Di Toro, 1972; Holyer, 1978). The volume reflection of water is the portion of upwelling irradiance which emerges from the water surface after selective scattering, reflection, and absorption by suspended particles. This irradiance is measured by the remote sensors after additional atmospheric absorption and scattering.

2.2 Quantifying Volume Reflection

Penetration of radiation in pure water is described by an extinction coefficient ω, which is the sum of the absorption coefficient α and the scattering coefficient β; both the α and the β coefficients vary with wavelength and SSC (Moore, 1947). Table 2 illustrates the interaction between these coefficients in pure water. Basically, the extinction coefficient increases with increasing wavelength and depth (Tyler *et al.*, 1972). Absorption dominates the extinction coefficient at wavelengths longer than 500 nm, and at 600 nm (red) the absorption and extinction are approximately equal. Absorption is low at visible wavelengths less than 500 nm and the extinction coefficient is influenced by molecular scattering. The scattering coefficient varies inversely with wavelength, and at wavelengths greater than 600 nm, scattering in pure water is negligible (See Table 2).

These values of the extinction coefficient only apply for pure water. Various types of inorganic and organic particles, with different size distributions and shapes, yield different volume scattering functions (Ghovanlou *et al.*, 1977; Gupta and Ghovanlou, 1978). Scattering is almost entirely in the forward direction for turbid waters; Di Toro (1978) found that about 50% of scattered light was scattered within 5% of its incident direction.

Table 2
Spectral Coefficients for Pure Water

λ (nm)	ω (m^{-1})	β (m^{-1})	α (m^{-1})
380	0.030	0.0073	0.023
390	0.027	0.0066	0.020
400	0.024	0.0058	0.018
410	0.022	0.0052	0.017
420	0.021	0.0047	0.016
430	0.019	0.0043	0.015
440	0.019	0.0039	0.015
450	0.018	0.0035	0.015
460	0.019	0.0032	0.016
470	0.019	0.0029	0.016
480	0.021	0.0027	0.018
490	0.022	0.0024	0.020
500	0.028	0.0022	0.026
510	0.038	0.0020	0.036
520	0.050	0.0018	0.048
530	0.053	0.0017	0.051
540	0.058	0.0016	0.056
550	0.066	0.0015	0.064
560	0.072	0.0013	0.071
570	0.081	0.0013	0.080
580	0.109	0.0012	0.108
590	0.158	0.0011	0.157
600	0.245	0.00101	0.245
610	0.290	0.00094	0.290
620	0.310	0.00088	0.310
630	0.320	0.00082	0.320
640	0.330	0.00076	0.330
650	0.350	0.00071	0.350
660	0.410	0.00067	0.410
670	0.430	0.00063	0.430
680	0.450	0.00059	0.450
690	0.500	0.00055	0.500
700	0.650	0.00052	0.650

(after Morel and Prieur, 1977)

λ = wavelength (nm)
ω = extinction coefficient (m^{-1})
β = scattering coefficient (m^{-1})
α = absorption coefficient (m^{-1})

The scattering and absorption coefficients are often expressed as a ratio; β/α. The β/α ratio of the water mixture is much lower than that of sediment alone (Whitlock, 1976). Inorganic sediments have β/α ratios much larger than unity throughout the visible spectrum; hence, the input of sediments into a water body will increase the volume reflectance and turbid water will appear brighter than clear water (Ghovanlou *et al.*, 1977; Gupta and Ghovanlou, 1978). As sediment concentration increases, the scattering coefficient increases at a much faster rate than the absorption coefficient until sediment concentration becomes so high that absorption for the pure water component alone is small in comparison to absorption of the suspended particles (Bowker *et al.*, 1975; Whitlock, 1975). Mueller (1973) showed that an increase in the absorption within the suspended particles produced a reduction in β with ω being decreased only slightly. Many workers have found that particle size rather than texture or color is the predominate factor relating SSC to volume reflectance (Bowker *et al.*, 1975; Whitlock, 1976; Holyer, 1978; Moore, 1978). As the particle size increases, and the number of these larger particles increase, the minimum extinction coefficient shifts from the blue to the red portion of the spectrum (due to increased reflection from the sediment-laden water) (Moore, 1947).

Potentially, many dissolved substances can contribute to the color of a water body and affect its absorption characteristics. One important dissolved substance which affects the absorption properties of marine waters is gelbstoff (or "yellow substance"). Højerslev (1979) has shown that gelbstoff and its fluorescent by-products are dependent on erosion and river runoff and salinity, not organic matter or temperature, as previously thought. Temperature and salinity have been shown to have very little direct influence on water color (Moore, 1947; McCluney, 1976; Moore, 1978; Khorram, 1985).

2.3 Approaches to Suspended Sediment Concentration Prediction

There are two different approaches which can be taken to analyze remote sensing data of water quality, theoretical modeling and an empirical approach. The two are complementary and interrelated, and should be pursued simultaneously. This would require the cooperation of many investigators in a substantial laboratory and field measurement program (McCluney, 1976).

Theoretical modeling approaches have two phases, micro- and macroscopic (McCluney, 1974a). Microscopic models assume knowledge of the particle size distribution and concentration of particulate matter. Classical absorption and scattering theories are then used with mathematical simulations to model the absorption and scattering properties of pure water and any combination of suspended matter. A simpler and less expensive approach (in terms of computer time) is to use known scattering/absorption properties of the suspended material to simulate changes of water color with changing particulate concentrations (McCluney, 1974a).

Macroscopic models use the absorption, scattering, and extinction properties of light in turbid water (determined in the microscopic models), along with atmospheric components, incident sunlight and skylight, water surface roughness, and bottom effects to predict the volume reflectance of a water body (Jerlov, 1968; Gordon and Brown, 1973a; 1973b; 1974; McCluney, 1974a). The macroscopic model is based on radiative transfer theories of both atmosphere and water, and should include the effects of multiple scattering within the water body (Gupta and Ghovanlou, 1978, McCluney, 1976). Gordon and others (Gordon and Brown, 1973; Gordon, 1973; Gordon, *et al.*, 1975; Maul and Gordon, 1977; see also McCluney, 1974a; Gupta and Ghovanlou, 1978) developed a quasi-single scattering model using Monte-Carlo techniques to simulate multiple scattering of diffuse light in turbid water, with and without bottom reflection. These techniques trace movements of photons (i.e., life histories) after entry into the water body. Such models may not be feasible for practical investigations because 100,000 separate computer cases may be required to define the upwelled radiance (Whitlock, 1976).

Another macroscopic model was proposed by Di Toro (1978) utilizing a combination of an exponential and a quasi-single scattering approximation to the radiative transfer equations. Di Toro assumed an exponential decay of both downwelling and upwelling irradiance with depth and a strong scattering component in a forward direction, with scattering in all other directions being isotropic.

In an investigation which compared the Gordon *et al.* (1975) and the Di Toro models, Bukata *et al.* (1979) found that these models may be brought into close agreement with sun angle corrections. When theoretical results of the Monte Carlo method were compared with experimental results of extremely clear ocean water in the Sargasso Sea, it was found that the shape of the two spectra were similar (McCluney, 1974a.). Di Toro's predicted absorption and scattering coefficients also agreed closely with actual values, and when particle concentration and types were measured, an application of the method to the turbid waters in the San Francisco Bay was satisfactory (Di Toro, 1976). Futher testing is needed to evaluate the accuracy of the quasi-single scattering model for more turbid waters. One limitation is that these models apply only to calculations of general irradiance, not specific radiance. Although initial results look promising, furthur work is needed to establish the validity and accuracy of this method. Other analytical solutions of radiative transfer equations have tended to be extremely complex (Morse and Feshbach, 1953) unless the problem is so simplified that the solutions are nearly meaningless (McCluney, 1976).

Once models have been developed and multispectral data collected, these models need to be inverted to predict water quality parameters from the apparent water color spectrum (McCluney, 1976; Di Toro, 1978). The more complex the model, the more difficult it is to correctly perform the mathematical inversion required to determine suspended sediment concentrations. Theoretically, the complete spectral definition of the absorption and scattering properties of all particulates in the sea would permit a solution to the general problem of quantifying ocean color (Jerlov, 1968).

The empirical approach correlates surface sediment values with simultaneously collected imagery of the apparent radiance of the sea. Multispectral algorithms utilize radiance values at separate discreet wavelength intervals, which can be overlapping (e.g., color photography) or non-overlapping, to determine sediment concentrations. The empirical approach is closely tied with the remote sensing concept of 'supervised classification'. Supervised classification is the correlation of remotely measured radiance values of a feature to some property or characteristic about that feature, usually determined by surface survey. This study correlated SSC with optical DNs obtained from photographic and video imagery. Supervised classification techniques are based on surface 'truth' observations, the breadth of which depends on the accuracy required and the cost of misclassification.

Unsupervised classification is the process by which image DNs are statistically assigned to spectrally distinct groups, with the identity of the groups determined independently. The features are classified by the pre-determined spectral signature of a feature, and no surface truth data is collected. Inter-planetary probes employ unsupervised classification techniques, unless they can remotely collect actual ground truth samples as well as imagery. Totally unsupervised classification seldom occurs due to the inquisitive nature of researchers, resource managers, and other users; many potential users and investigators need to be convinced of the accuracy and validity of remote sensing techniques over other accepted methods. Unsupervised classification techniques are generally based on models developed by extensive surface truth studies (i.e., supervised classification techniques.). Usually some sort of validation and/or adjustments are made to the classifier by examining ancillary data sources, e.g., maps or air photos. Lillisand and Kiefer (1978) refer to this process as "hybrid" classification.

If features are to be identified by their spectral signatures, all variables contributing to the feature's reflectance spectra need to be quantified. This would require the standardization and/or control over phenomena affecting image data, namely,

variable atmospheric conditions, since measurements of many meteorological factors is important in developing analytical corrections for orbital and high altitude imagery. These data are often not available for a particular site and are usually summarized as average values over an entire scene or are estimated from tables of prior measurements, given that some important meteorological data was obtained. The accuracy of the classification is dependent on the accuracy of the atmospheric models of overpass conditions. If some meteorological measurements are unavailable (e.g., archival imagery), they must be estimated using ancillary information or physical relationships evident in the remote sensing data (e.g., see Aranuvchapun and LeBlond, 1983; Holyer, 1984).

Many of these sophisticated atmospheric relationships can be summarized by empirically derived relationships between objects' reflectivity. The spectral deviation of a 'standard reflector'[4] in the scene can be estimated by comparison to its 'true' reflectivity. This deviation can be used to radiometrically adjust other image DNs. For example, a black object or shadow can represent the baseline for scene radiance (see Chapter 3.2). Other atmospheric factors can become insignificant with low altitude imagery. Such corrections for atmospheric scatter can be simplified with the use of low altitude multispectral imagery (Bukata, 1981).

Once remote sensing imagery and surface truth measurements have been obtained, relationships can be evaluated with multispectral algorithms in order to predict SSC. Image DNs can be systematically processed and manipulated in a predictable manner with the use of these algorithms. Algorithms are based on the energy-matter interactions, physical environmental dynamics and components, properties of the employed sensor system, and other specific criteria dictated by the study. The object of multispectral algorithms is to determine the linear or non-linear relationship between the radiance values of each channel (independent variables) and suspended sediment concentration (dependent variable). The complexity of these algorithms range from simple linear relationships between one channel and SSC, to linear combinations of the

---

4 An object that is spectrally stable and usually either black or white, such as airport tarmacs or concrete dams; or a target with a known spectral distribution.

channels, to ratio combinations of channels, to third order polynomials (Johnson, 1975; Bartolucci *et al.*, 1977; Holyer, 1978; Bukata and Jain, 1979). Regression with radiance and SSC data statistically determine the fitting coefficients for maximum correlation. The accuracy and prediction capabilities of the developed algorithm can then be evaluated by application to additional data. Literature reviews by Johnson and Harriss, (1980), Cracknell, (1981), Geraci *et al.* (1980), Witzig and Whithurst, (1981), Colwell (1983), and Virdin (1985) showed that suspended sediment can be statistically correlated with radiance using optical techniques.

2.4 Summary

The amount and spectral distribution of energy that an object reflects provides information about that object. Scene reflectivity is influenced by numerous physical and environmental factors which can be measured, controlled, or uncontrolled. Regardless of all the influencing factors, ground radiance is translated into image density numbers (DNs). The value of these DNs provide the basic information for countless remote sensing studies; it is the way these DNs are manipulated that enhances the desired information while de-emphasizing unrelated information (noise).

The spectra of clear water is well known, and provides a reliable 'baseline' with which to make comparisons. Deviations from this baseline (evaluated by multispectral remote sensing techniques) is caused primarily by inorganic sediment (in this study), and secondly, by extraneous factors such as atmospheric contributions, bottom reflection, and submerged vegetation. Because of the low spectral return from water, it is important to control and correct for different light conditions (e.g., sun angle and clouds), variable atmospheric conditions, surface reflection (e.g., sunglint), and sea-state. The accuracy of an empirically derived multispectral algorithm depends on the accurate assessment of atmospheric contributions to target (i.e., SSC) radiance. The spatial and spectral resolution of orbital remote sensors will be continually improved, resulting in improved classification of water quality parameters in small-scale studies. Atmospheric components

will always be important terms in water quality classification algorithms, and periodicity and spectral rigidity may render orbital imagery deficient for some site-specific applications.

Many difficult meteorological measurements, or their estimation, can be avoided by using low altitude aerial survey. Subsequently, the remotely sensed water volume reflectance has minimum atmospheric interference, while other secondary factors influencing the signal response from the water can be estimated from the remote sensing data (e.g., surface reflection and sea-state), or measured directly in a straight-forward manner (e.g., sun angle). Aerial survey missions also allow for:

- co-ordination with complex surface observations,
- variable image scales,
- unique, site-specific target conditions,
- rapidly changing environments (both spatially and temporal),
- flexible scheduling of missions, and
- satisfactory data collection under conditions inappropriate for high altitude sensors (e.g., cloud cover).

The airborne flexibility and excellent spatial and spectral resolution of airborne multispectral scanner imagery makes it an attractive alternative to orbital sensors, especially for site-specific studies. The primary limitation of these sensors systems is cost. Therefore, a need for applications-oriented remote sensing of water quality is evident. Ideally, this system needs to be inexpensive, spectrally flexible, and flown at low altitudes to obtain 'true' feature reflectivity. Multiple overpasses at different altitudes allows atmospheric profiles to be developed if smaller scale imagery is required. Additionally, the methods of image analysis need to be analytically capable of providing the desired information, reliably, over time. The feasiblity of using a particular remote sensing system depends on the analytical ability and cost of the employed methods, compared with other methods for obtaining the same information. This thesis addresses the former criteria; however, the sensors and methods employed in this investigation are

substantially less expensive than multispectral scanner systems and platforms (i.e., aircraft and satellite). Additionally, with the privatization of the Landsat program and initial cost of SPOT[5] imagery, this less-expensive system may compete economically with orbital imagery.

---

5 French earth-imaging satellite.

CHAPTER 3

REMOTE SENSING OF WATER QUALITY

This chapter is divided into two sections. The first section describes energy-matter interactions in water as defined from many studies. This 'background' information forms the physical foundations on which this research was based. The second section traces the evolution of empirical water quality remote sensing pertinent to this study. The body of previous work presented herein forms a basis for comparison and evaluation of the methods employed in this study. Of particular relevence is the work using regression techniques to correlate scene radiance with surface sampling measurements.

3.1 Signal and Water Parameter Relationships

Peak transmission and reflection of energy in pure water occurs at blue wavelengths (Duntley, 1963). Calculations by Williams (1970) show that light at 470nm is transmitted 100 meters in distilled water. In nature, peak transmission for infinately deep clear water bodies occurs at blue-green (490-530nm) wavelengths. Theurer (1959) and Goldman (1974) measured blue-green light at 60 and 40 meters in Puerto Rico and Lake Tahoe, California, respectively. Hulbert (1945), Clark and James (1939), and Specht *et al.* (1973) calculated transmittance values for various water types at 10-meter depths (Figure 6). Tranmittance (and reflection) remains high through the green (500-580 nm) portion of the spectrum, then rapidly declines through the yellow and red (580-700 nm) wavelengths. McCluney (1974a) estimated that wavelengths sensed by Landsat MSS channels 4 and 5 (green, red) penetrated 1.8 and .16 meters, respectively, in turbid water based on a quasi-single scattering model. Pure water attenuates nearly all incident energy in the near-infrared (MSS channels 6 and 7) within the first few centimeters.

The introduction of fine particles shifts the reflectance peak from blue to green wavelengths. Gordon and McCluney (1975) indicated that maximum penetration depths

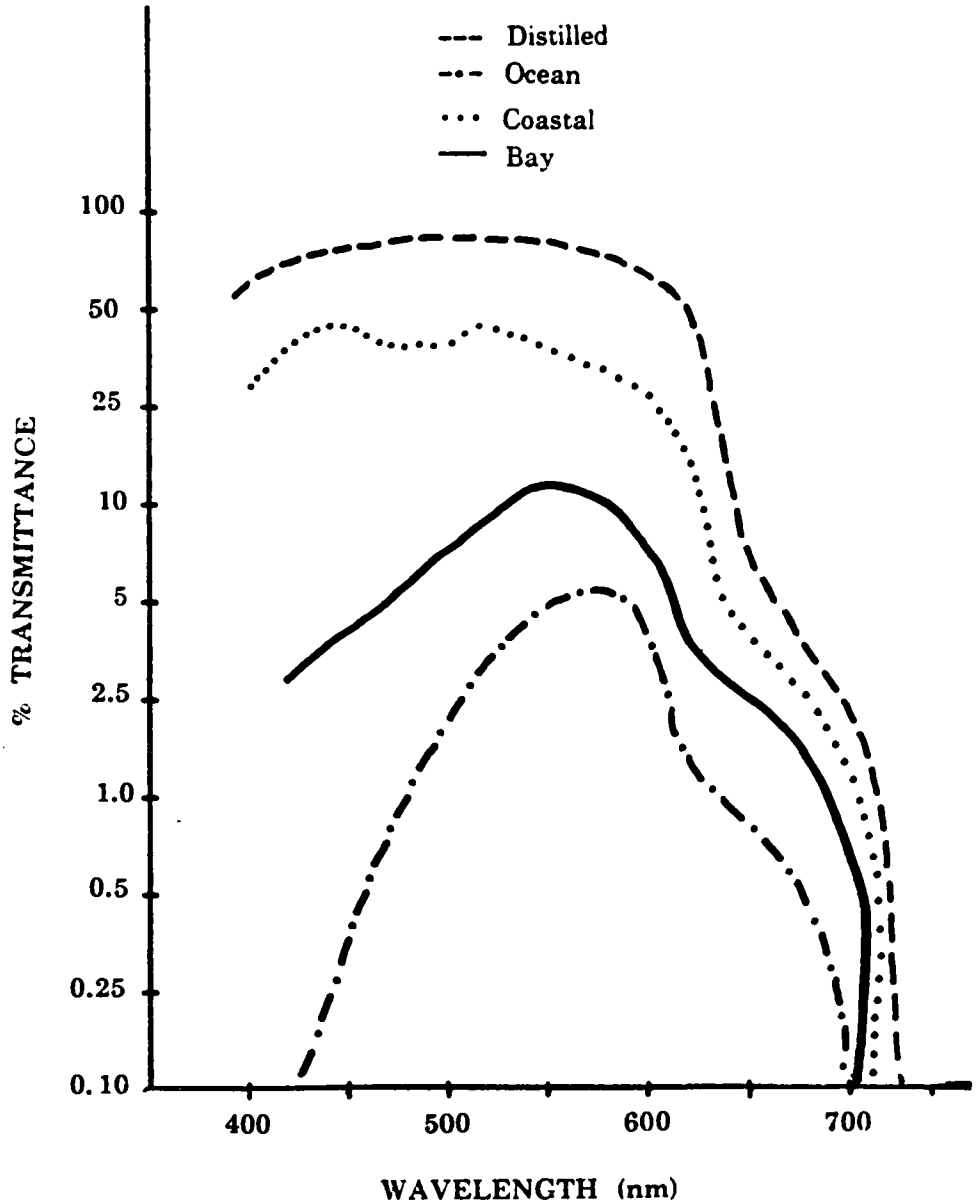

Figure 6: SPECTRAL TRANSMITTANCE FOR 10 METERS OF VARIOUS WATER TYPES (after Specht *et al.*, 1973).

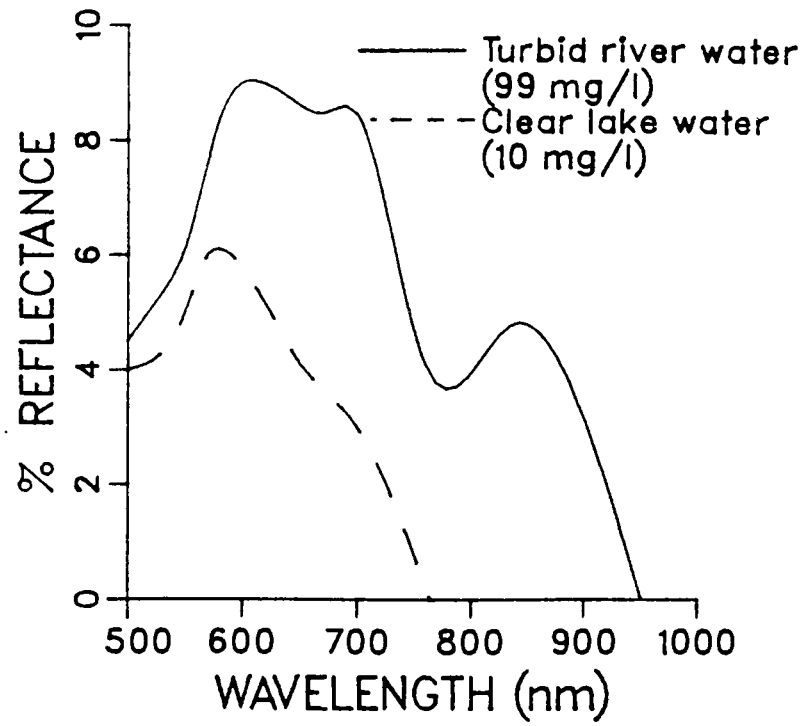

FIGURE 7: SPECTRAL CHARACTERISTICS OF TURBID RIVER WATER AND CLEAR LAKE WATER (after Bartolucci *et al.*, 1977).

for coastal waters occur in the green range, and Whitlock (1976) calculated values for penetration depths based on optical coefficients at 540 nm. Transmittance for natural waters decreases as the level of turbidity increases, and the peak wavelengths for maximum transmittance/reflectance shifts to longer (red) wavelengths (Figure 7) (Pestrong, 1968; Polcyn, 1970). As the size of the particles increase and the relative influence of the water medium is reduced, the color of the signal peak approaches that of the material which forms the particle (Lepley, 1968; Scherz and Van Domelen, 1977). Any near infrared return is due to the spectral reflectance caused by particles on or near the water surface, and near-surface chlorophyll components (e.g., eelgrass, algae). The direction and magnitude of the peak reflectivity in turbid waters depends on the size, quantity, and composition of the suspended material. If the water is sufficiently clear and/or shallow, incident energy will also be reflected from the sea-bed. Thus, the water color spectrum will be influenced by the color and scattering characteristics of the bottom, and be affected by interactions similar to those of turbid water.

3.2 Previous Research

Research on the interpretation of aerial photographs of turbid waters began at the end of World War II (Moore, 1947) as a result of attempted military landings on South Pacific Islands. The objective of these early studies was to determine depths of shallow water; and the turbidity effects on the depth of light penetration in water naturally followed.

Compiling and updating nautical charts was of obvious importance, and the use of aerial photography to this end has been ongoing (Jones, 1957; Theurer, 1959; Harris and Umbach, 1972). In these studies, aerial photography was effective in mapping intertidal reaches and shallow and deeper water, depending on water clarity. Other studies were concerned with qualitative assessment of changing shorelines and coastal, estuary, and turbidity mapping (El-Ashry and Wanless, 1967; Schneider, 1968; Piech and Walker, 1972). At the same time, the first satellite photographs were being studied for

potential applications in water investigations. Color transparencies from orbital GEMINI missions were studied in order to pinpoint coastal areas where aerial photography would enable synoptic depth contouring and shoreline mapping, while also noting atmospheric effects on orbital imagery (Lepley, 1968). Color and color photographic separations from the Apollo orbital missions were used to detect water masses, small scale suspended sediment patterns, and infer coastal and continental shelf processes (Mairs, 1970). Meanwhile, special films were being designed for water penetration and pollution detection (Helgeson, 1970; Specht *et al.*, 1978)

Scherz *et al.* (1969) compared the reflection characteristics of various industrial wastes discharged into different water bodies in Wisconsin. Various film and filter combinations were used to enhance the identification of different pollutants. It was concluded that no one film/filter combination was adequate for general water quality assessment, but that the best combination depended on the pollutant and type of water in which it was dispersed (e.g., acid or tannin lakes). Schmer *et al.* (1972) evaluated lake water quality in South Dakota using airborne color, color infrared, and multispectral photography at 4000 and 10000 feet, coordinated with ground survey. Film densities were measured with a transmission densitometer and correlated with water sample data. The investigators found that the correlation coefficients for the infrared layer of the color infrared film showed the best results over all the aerial missions. The highest correlation between SSC and infrared was 0.59, significant at the 0.05 probabltity level. No information was given about the other layers of the infrared film, the color film, or any of the separate multispectral images. Blanchard and Leamer (1973) also reported that color infrared film was consistently more sensitive to changes in SSC than color film.

Villemonte *et al.* (1973) conducted an ongoing study using aerial photography to quantitatively map mixing zone characteristics in order to provide data for the establishment of water quality guidelines for the State of Wisconsin. Their remote sensing efforts focused on the development of mathematical models identifying and

correlating turbidity and SSC with aerial photographic imagery. Laboratory reflectance analyses performed by Klooster and Scherz (1973) were used to demonstrate that reflectance was a function of turbidity and SSC. A model was developed which permitted the estimation of SSC from measuring image density, and it was concluded that the developed nonlinear model could be used with confidence if each roll of film was calibrated separately using a greyscale stepwedge, and if a standard reflector (white target) was included in the scene.

Modern digital remote sensing techniques have been applied to water quality data concurrent with the launch of the first Landsat (ERTS-1) satellite in June of 1972. Image data format and computer image processing allowed automatic pattern-recognition techniques to be employed for analyzing remotely sensed multispectral data. These techniques facilitated discrimination of several spectrally different classes of water and the subsequent mapping of general turbidity and circulation patterns (Klemas *et al.*, 1973, 1974a; Bukata *et al.*, 1974; Clark *et al.*, 1974; Abiodun, 1976)

Klemas was one of the first workers to use Landsat MSS data to investigate water quality, and mapped circulation patterns in Delaware Bay using suspended sediment as a natural tracer (Klemas *et al.*, 1973a, 1973b; Klemas *et al.*, 1974a, 1974b). These studies correlated MSS band 5 (red) radiance with SSC by using an exponential determined by a least squares fit. The correlation coefficient was questionably high for an initial study (0.99), and no information was given about the standard error of the estimate, significance level, amount of bias, or sources of error.

McCauley *et al.* (1973) analyzed several early Landsat images of reserviors in Kansas to relate water quality parameters to Landsat radiance. Plotting MSS density values against SSC exhibited a uniform nonlinear relationship while radiance was linear for secchi depth (turbidity). The correlation between secchi depth, SSC, and radiance was high for individual days, but comparisons between days were not made because sun angle changed with changing SSC. Thus, lower radiance could not be solely attributed to either the reduced sun angle or lower SSCs.

The SSCs of 14 Oklahoma impoundments were related to airborne MSS data by Pionke and Blanchard (1975). The derived equation related SSC (y) to reflectance (x) as an exponential: $y=x^n$, where x (radiance) was 530-580nm for SSC between 13-75mg/l, and 588-690nm for SSC between 13-232mg/l. Values of n were greater than 1 (also see Blanchard and Leamer, 1973), causing sediment concentrations to be increasingly sensitive to incremental increases in measured reflectance. This limited the range of the relationship because errors in the reflectance measurements had to be small or the stability and accuracy of the relationship would be destroyed.

Johnson (1975) conducted one of the earliest remote sensing water quality studies using statistical analyses, and derived a linear regression equation to determine SSC in the tidal James River, Virginia, using a 10-band airborne MSS (M^2S). A single band (700-740nm) was adequate for determining SSC, with a correlation coefficient of 0.89 and the standard error of the estimate was 4.76mg/l for SSCs up to 50mg/l. Five additional bands, covering a frequency range of 540-860nm, all showed high correlations with SSC. In another study, Johnson and Bahn (1977) used the same data set with a more rigorous criteria for selecting appropriate ground truth values. Only sea-truth measurements treated with consistent sample-handling techniques and collected closest to sensor overpass were used. These 'more refined' data resulted in a regression equation that correlated SSC with band 2 (440-490nm) and band 6 (620-660nm); the resulting correlation coefficient was 0.899 and a standard error of 5.23 mg/l (about 38%). Bowker *et al.* (1975) regressed Landsat MSS band 5 radiance data, corrected for the different sun angles on different days, against SSC obtained in the lower Chesapeake Bay area. The relationship was linear for the low concentration values measured (1-14 mg/l), with a correlation coefficient of 0.92, although some samples were collected up to 6 hours after satellite overpass, and concentration values may have changed. No values were given for the standard error of the estimate or level of significance. The attenuation coefficient of the turbid water was also compared with MSS band 5 radiance, resulting in a $r^2 >$ of 0.95.

Ritchie (1976) measured the reflected solar radiation of 6 Mississippi lakes from a boat using a spectroradiometer. Linear regression analysis showed that the best relationship was between SSC and reflectance (i.e., ratio of reflected solar radiation to incident solar radiation) between 700-800 nm. The correlation coefficient for sun angles between 10°-70° was 0.84. The correlation coefficient was 0.96 for sun angles less than 40°, and SSC ranged between 20-350 mg/l.

In a Geological Survey of Canada report of activities, Amos (1976) presented preliminary results quantifying SSC in the Minas Basin using Landsat MSS data. Initial analyses involved normalizing MSS band 4 chromatic intensities by dividing the DNs of a particular band by the sum of the DNs in all bands and regressing the transformed value against SSC. This resulted in an inverse relationship with a correlation coefficient of -0.87, significant at the 99.9% confidence level.

Bartolucci *et al.* (1977) measured reflectance of turbid river water (99 mg/l) and relatively clear lake water (10 mg/l) with a spectroradiometer mounted on a truck boom. The spectra from the water was normalized by comparison to the spectral reflectance of a known standard (pressed barium sulfate). Their findings showed that the greatest difference between the turbid and clear water occured in the 700-800 nm range, which corresponds to Landsat MSS band 6. Additionally, bottom reflectance did not affect the spectral response of turbid water deeper than 30 centimeters.

Some general models have been developed to estimate sediment loads under a wide range of conditions and phenomena. Holyer (1978) made surface radiance measurements from a boat at Lake Mead, Nevada, along with surface sampling. Field data were only collected at sites where water depth exceeded secchi extinction depth to exclude bottom effects. The recorded surface radiance was corrected for surface reflection of skylight at the air-water interface. The correction for surface reflected skylight assumed a uniform distribution of sky radiance, i.e., clear or overcast conditions, or a partly cloudy sky with a rough water surface. Three 'universal' algorithms were developed for volume reflectance at 652 nm (red), 782 nm (infrared), and a model using both wavelengths.

The error of the estimate was similar (variance = 0.05) for the red-infrared algorithm and the infrared algorithm, with the errors from the red algorithm being much larger. When sediment was expressed in terms of nephelometric turbidity (NTU), the resulting volume reflection signatures were relatively invariant (for NTU less than 15) between sediment types, thus suggesting the turbidity algorithm may have universal applicability. Unfortunately, turbidity cannot be directly converted to SSC (Amos and Alföldi, 1979), thus limiting the usefulness of the algorithm. No direct measurements of algorithm accuracy were given, except that the nephelometric turbidity model met the Environmental Protection Agency's accuracy standard that the variance not exceed 0.05 down to a detectable threshold of 25 mg/l.

Munday and Alföldi (1979) reviewed models from the literature applied to empirical Landsat MSS and suspended sediment data. Three sets of data collected on different days were studied separately and together with and without solar angle correction. Regression with these data showed that solar angle correction generally enhanced the data and that the logarithmic and nonlinear Gordon (1973) models produced much higher correlation coefficients than linear models (except for small ranges of SSC). The correlation coefficients for the simple logarithmic(SSC) model were generally very close to those of the complex quasi-single scattering diffuse reflectance Gordon model (see Chapter 2.3) The correlation coefficients for the linear, logarithmic, and Gordon models were 0.65 verses 0.95 and 0.96, respectively, for all three data sets combined and corrected for sun angle.

Scarpace *et al.* (1979) evaluated Landsat MSS as a way to classify thousands of lakes in Wisconsin. Using band 5 radiance, 34 lakes were classified into tropic categories based on turbidity caused mainly by chlorophyll-*a*, and to a lesser degree on mineral sediment. Regression with tropic class and band 5 provided generally high correlations, but no analytical information was provided about the relationships between turbidity, Landsat data, and tropic class. The 'standard radiance' of clear lakes and an airport runway were used to adequately correct for atmospheric influences.

Aranuvachapun and LeBlond (1981) calculated the portion of reflected energy contributed by the atmosphere and the air-water interface to estimate SSC in the Fraser River sediment plume in the Strait of Georgia. Atmospheric components of the reflected signal were estimated from work done by researchers in the atmospheric sciences and other users of Landsat data. MSS DNs were converted to radiance values; the calculated atmospheric influences were then removed from the total radiance leaving the diffuse reflectance component due to the optical properties of the seawater. Holyer's (1978) nonlinear algorithm for estimating SSC using MSS data was then applied to SSC data published by Munday and Alföldi (1979). Aranuvachapun and LeBlond found that Holyer's algorithm was unsatisfactory, and subsequently considered the nonlinear model of diffuse reflectance by Maul and Gordon (1975), and a logarithmic relationship. While the highest correlation coefficient for the nonlinear model was 0.98, they selected the logarithmic model for simplicity, which gave a correlation coefficient of 0.96. The logarithmic relationship was then applied to estimate SSC in the Fraser River plume. No surface truth samples were collected so that the method was evaluated on 'plausible' SSC values. In a reply to Aranuvachapun and LeBlond, Holyer (1982) subtracted MSS band 6 radiance values for SSC less than 3 ppm from total radiance to estimate atmospheric influences (see APPENDIX A). The results from Holyer's atmospheric correction supported his earlier algorithm, but he concluded that further research was needed.

Carpenter and Carpenter (1983) used multiple regression techniques to develop a model having MSS bands 4, 5, and 6 as predictors of the logarithm of turbidity. When the sine of the sun angle was included as a predictor, as a simple way to compensate for atmospheric effects, the the multiple regression coefficient (r) was 0.96, with no values given for variability. The model was tested with other lakes in the area; the resulting correlation between the observed and predicted data was 0.88 for (log)turbidity. Khorram (1985) also used multiple regression techniques to estimate suspended solids concentration in the Neuse River estuary, North Carolina. The best regression equation was complex, with the independent variables being ratios and

combinations of Landsat MSS bands 4, 5, 6, and 7. The coefficient of determination was 0.64 for the model, and when tested with new data from the same data set, $r^2>$ was 0.47. These results compared with those obtained in the San Francisco Bay (Khorram, 1981, 1982). Multiple regression equations were derived to predict 4 water quality parameters; the $r^2>$ for SSC was 0.609.

The importance of understanding the optical properties of pure and natural waters in order to directly relate suspended sediment concentrations with different radiance measurements was recognized by many researchers (see section 2.2.3). Development of physical models using radiative transfer theories has been an integral part in developing remote sensing techniques for water quality assessment. Theoretical modeling provides insight and understanding of the processes which are summarized in empirical measurements. However, simulation models suffer from a deficiency of *in situ* measurements of optical properties that could contribute to, and benefit from, these theories.

Some studies have focused on measurement of apparent optical characteristics of water bodies in order to predict water quality parameters. The apparent optical properties—reflectance, attenuation, and scattering— were used with models such as those developed by Gordon *et al.* (1973) and Di Toro (1978) to infer the *inherent* optical properties of a water body. Statistical techniques such as multiple regression (Bukata *et al.*, 1979, 1981a, 1981b) and principle components analysis (Mueller, 1976), were applied to determine the absorption, scattering, and backscattering cross sections of specific suspended constituents. Bukata *et al.* (1981a) developed a five-component optical water quality model of Lake Ontario in which the standard deviation for inorganic suspended sediment was greater than 35%. Because Lake Ontario is optically complex, the high uncertainty may be misleading, and futher work is needed in a homogeneous aqueous environment to properly evaluate this model.

Detection and measurement of suspended sediment has been successfully demonstrated for individual studies, utilizing airborne (Johnson, 1975, 1980) and satellite

(Bowker *et al.*,1975; Alföldi and Munday, 1978; Aranuvachapun and LeBlond, 1981) multispectral scanners. Some general models have been developed to estimate sediment loads under a wide range of conditions and phenomena (Holyer, 1979; Munday and Alföldi, 1979). However these models have been developed for high altitude remote sensing platforms where atmospheric alteration (noise) is an important term in the algorithms, and is difficult to quantify. Correction for atmospheric scatter can be simplified, or eliminated, by the use of low altitude multispectral imagery (300+ m) (Miller *et al.*, 1977). Low altitude aerial survey using multispectral photography and video imagery can provide high spatial and spectral resolution, minimum atmospheric alteration of object reflectivity, and intensive area coverage. The use of aircraft also allows the versitility of multi-date data to be collected (for temporal parameters) under a variety of weather conditions that would not permit satellite imaging.

3.2.1 Atmospheric Corrections

Remote sensing surveys of water quality are based on the assumption that a meaningful relationship exists between reflectance and water quality. However, radiance values derived from remote sensor channels do not directly relate to ground reflectance values because of physical environmental and atmospheric influences. If ground features are to be characterized in terms of their spectral reflectivity, atmospheric interference must be eliminated. Additionally, if multidate comparisons are to be made, even limited to one location, some adjustment of the remote sensing data is required to allow for differences in sun illumination, atmospheric backscattering and attenuation of energy, and the resulting surface reflection effects. Atmospheric haze obscures and reduces the contrast between adjacent surface features on the imagery and makes feature identification more difficult.

Turner *et al.* (1971) observed that "in spite of all the research over the past thirty years or so, no detailed comprehensive [atmospheric] radiative transfer model has been developed which can be applied directly to the problems of remote sensing." Additionally, because of the many variables, it may not be practical to directly

determine an atmospheric correction for remotely sensed data (Moore, 1978). So many factors would have to be monitored, measured, and calculated that it would probably be cheaper to collect and analyze water samples.

It is possible to enhance spectral data and define an adequate atmospheric correction factor by using the remote sensing data itself. The observed color spectra of a turbid water body represented on imagery is made up of hue, saturation, and brightness. Brightness information, containing atmospheric noise components, can be removed with chromaticity techniques which use the normalized hue and saturation values to determine water quality parameters (Jerlov, 1968). These techniques remove brightness information by converting image DNs to radiance values and ratioing the radiance measured by each band with the other bands. These techniques essentially remove brightness information and use the color differences to determine SSC.

Munday and Alföldi have applied chromaticity analysis to remote sensing data of southern Ontario lakes with good results, obtaining correlation coefficients as high as 0.97 for three combined dates. Lindell (1981) and Smith and Baker (1978) have also noted satisfactory results, but Bukata *et al.* (1983) reported 'severe' restrictions in the application of chromaticity techniques to water quality prediction of western Lake Ontario.

Other researchers have used objects with constant reflectance (e.g., black objects, clear lakes, airport tarmacks, etc.) to calibrate imagery and remove unwanted atmospheric noise (Klooster and Scherz, 1973; Moore, 1947; Piech and Walker, 1971; Scherz and Van Domelen, 1974; Yarger, 1974; Scarpace *et al.*, 1979).

Spectral band ratio procedures are valuable for isolating spectral differences between targets under varying light conditions. The presence of suspended sediment affects the spectral response of the green and red bands differently; this spectral difference can be enhanced by dividing the DN's of one band by another. Subsequently, inferences can be made about water quality based on the resulting band ratio. Ratios of the spectral DNs from different channels also reduce or negate the effects of

extraneous factors that influence the sensor data. For example, Yarger (1974) used a concrete dam with constant percent reflectance to investigate sun angle and atmospheric variability on remote sensing data. The resulting spectral band ratios appeared to be nearly independent of solar and atmospheric effects, and provided satisfactory enhancement of image data. Additionally, the process of ratioing of radiance data can normalize some temporal differences in imaged spectral values between aerial surveys (Amos and Topliss, 1985). The resulting radiance transformations are therefore considered isoluminous, and spectral differences result from changing SSC, not changing solar brightness or sea state (Amos and Topliss, 1985). Theoretically, ratio techniques compensate only for those factors that act equally on the various channels, such as vignetting and some atmospheric effects (e.g., sun elevation angle; Moore, 1978).

Because some atmospheric effects are additive (Moore, 1978; Scarpace *et al.*, 1979), ratio techniques alone cannot normalize atmospheric influences between scenes. Dark objects with near-zero reflectance (e.g., deep shadows and black rooftops) can be used to determine additive atmospheric influences. These objects should have a DN of '0', and any spectral return from these objects is due to atmospheric backscatter. Since the atmosphere selectively scatters the shorter wavelengths, each channel must be corrected separately. The pixels (picture elements) of each channel can be radiometrically adjusted by subtracting the portion of the signal contributed by scattering from the total scene irradiance, determined by the spectral return from the dark object (Moore, 1978; Sabins, 1978).

3.3 Development and Evaluation of Regression Models

Many researchers have used regression techniques to estimate a variety of water quality parameters with varying degrees of success (Johnson, 1975; 1977; Johnson and Bahn, 1977; Rogers *et al.*,1975; 1976; Whitlock and Kuo, 1979). The theoretical justification for using this particular method can be found in Whitlock (1977), Whitlock and Kuo (1979), and Whitlock *et al.* (1982). Basically, the remote sensing signal

responses to various concentrations of different constituents suspended in water (in terms of optical physics) can be summarized in a straight-forward manner by a multiple regression equation. Regression models for predicting SSC were developed by applying multiple regression techniques between surface truth measurements and radiance values represented either by densitometric optical counts (film), or grey density numbers (electronic sensors). The reflectance data of the different bands, or layers of film, were treated as independent variables, while the measured SSC values were the dependent variables. The resulting models are of the form:

$$SSC = J + K_w(Rad_w) + \ldots + K_z(Rad_z) + e$$

where:

J = the y intercept.

K = the partial regression coefficient.

Rad = the optical count values and grey density numbers from film and video imagery, respectively.

w, ...z = the different sensor bands.

e = error.

The J and K coefficients are a function of surface reflection, atmospheric scattering and absorption, and inherent upwelled radiance components from the background water. These various water and atmospheric factors have a significant influence on volume reflectance, and must be determined empirically. The regression task is to determine the J and K coefficients by least squares fitting techniques. Thus, the J and K coefficients are chosen in such a way that the sum of the squared vertical deviations between the regression line and the scatter of points is minimized.

3.3.1 Measures of Adequacy

It was not known how many channels (or in what combination) would be required to make a reliable prediction of SSC. Several statistical parameters were used as indicators of precision of the regression equation, such as the coefficient of determination (r^2), standard error of the estimate (SE), F-values, and the total squared error (Cp/p)

statistic (Whitlock and Kuo, 1979).

A common measure of prediction accuracy and linear association is the ratio of explained variation in SSC to the total variation in SSC, or $r^2>$. The coefficient of determination ($r^2>$) describes the variation in SSC explained by the combined linear influence of the radiances for the different bands. Conversely, the proportion of variance in radiance *not* explained by the regression equation is $1-r^2>$. Theoretically, $r^2>$ should approach 100%. but values greater than .7 may indicate a reliable regression model for predicting water quality (Mace, 1983). The correlation coefficient, r, is not a good indicator of precision when the number of estimated coefficients (independent variables) approach the number of observations (sample sites) (Draper and Smith, 1966). Therefore, the number of ground truth points should exceed the number of spectral channels by a wide margin, or the number of channels should be limited (Whitlock and Kuo, 1979).

The overall test for goodness of fit of the multiple regression equation tests the null hypothesis that the multiple correlation is zero, and any observed multiple correlation is due to sampling variability and/or measurement error. The statistical parameter used to evaluate the adequacy of the least squares process is the F-test, which can be expressed as (Whitlock and Kuo, 1979):

$F = (r^2>/k) \; / \; [(1-r^2>)/(n-k-1)]$

where:

k = the number of independent variables.

n = the number of field observations.

In order for the regression equation to be deemed a valid predictor (of sediment) the calculated F-value should be at least 4 times the tabular critical F-value (F/F_{cr}) (Daniel and Wood, 1971). The F-ratio is approximately distributed as the F distribution with k and n-k-1 degrees of freedom. A problem with this parameter is that the confidence level must be arbitrarily selected before the F/F_{cr} can be calculated. A confidence level of 0.95 is commomly selected, meaning that the risk of being incorrect was no more

than 5 percent.

Daniel and Wood (1971) recommended the total squared error as a criterion for goodness of fit. This statistic, called Cp, measures the sum of the squared biases plus the sum of the squared random errors for the dependent variables at all n data points. Given a multiple regression equation with p estimated coefficients (Whitlock, 1977):

$$Cp = RSS_p / s^2 - (n - 2p)$$

where:

RSS_p = sum of the squared residuals for the p-term equation,

s^2 = unbiased estimate of the variance.

Given a multiple regression equation with P estimated coefficients, a low value of Cp coupled with a Cp/P ratio of less than 1.0 is considered to indicate a good fit with negligible bias (Whitlock *et al.* ,1982; Huang and Lulla, 1986). The Cp/P ratio is the only one of the discussed statistical parameters which is indicative of bias in the fitted equation.

To summarize the criteria used to select the optimum regression equation to predict SSC:

- The $r^2 > \geq .70$,
- the regression coefficient (r) should approach 0,
- the standard error of the estimate (SE) should approach 0,
- the $F/F_{0.05} \geq 4$,
- the total squared error (Cp) should be low, and,
- the Cp/P ratio ≤ 1.0.

3.3.2 Assumptions

A number of criteria must be met in order to make valid quantitative inferences using remote sensing data. The remote sensing study should conform to the following assumptions (Whitlock and Kuo, 1979):

1) The correct form of the equation has been chosen (radiance of each band is linear for concentration, for all channels involved).
2) The data are representitive of the whole range of environmental combinations in the remote sensing scene.
3) The observation of the dependent variable (surface truth concentration values) are uncorrelated and statistically independent.
4) All observation of the dependent variable have the same (but unknown) variance.
5) The distribution of uncontrolled error is normal.
6) All independent variables (radiance values) are known without error.

These criteria are met when:

1) Minimal time lapse between sensor overpass and surface sampling occurs.
2) The noise contributed by both instruments and the atmosphere is sufficiently low.
3) The number of surface truth data points should exceed the number of channels by a wide margin, for each classification.
4) Water depth greater than secchi depth (remote sensing penetration depth).
5) Constant vertical sediment concentration profile within the remote sensing penetration depth.

CHAPTER 4

METHODS

The methods described in this chapter are designed to evaluate the empirical relationships between multispectral image brightness and surface sampled SSCs. The simultaneous measurement of SSC and the remotely sensed apparent radiance spectrum was extremely important in order to reduce temporal variability.

4.1 Sensor System and Field Site Description

4.1.1 The Imaging System

The remote sensing system used in this study included both electro-optical imaging sensors and photographic systems. The multispectral sensor system was comprised of four video cameras with optical filters transmitting blue, green, red, and reflected infrared wavelengths, respectively (Figure 8). Additionally, two 35mm cameras were used with Ektachrome and infrared Aerochrome film

The video system (Roberts and Evans, 1986) consisted of one RCA Newvicon and three Sony Xc-37 CCD (charge-coupled device) low light television (LLTV) cameras. Figure 9 shows the spectral sensitivity curves for the detectors used in these video cameras. Matched variable focal length (12.5mm - 75mm) lenses were used on each camera. The Newvicon and two CCDs were outfitted with blue (415-485nm), green (515-585nm), and red (615-685nm) band-pass interference filters, respectively, and the third CCD was used with a glass near infrared sharp-cut filter (88A: 700-1100+nm). The spectral ranges of these filters are illustrated in Figure 1. Aquired imagery was recorded on four individual Sony 8mm metal video cassette recorders (VCRs). Proper exposures were set with the aid of a Hatachi V-099 waveform monitor. Imagery from each individual camera was viewed during data aquisition on a 4 inch Sony Trinitron monitor (system operator) and a 1.5 inch Akai V10U monitor (pilot) through a switching system.

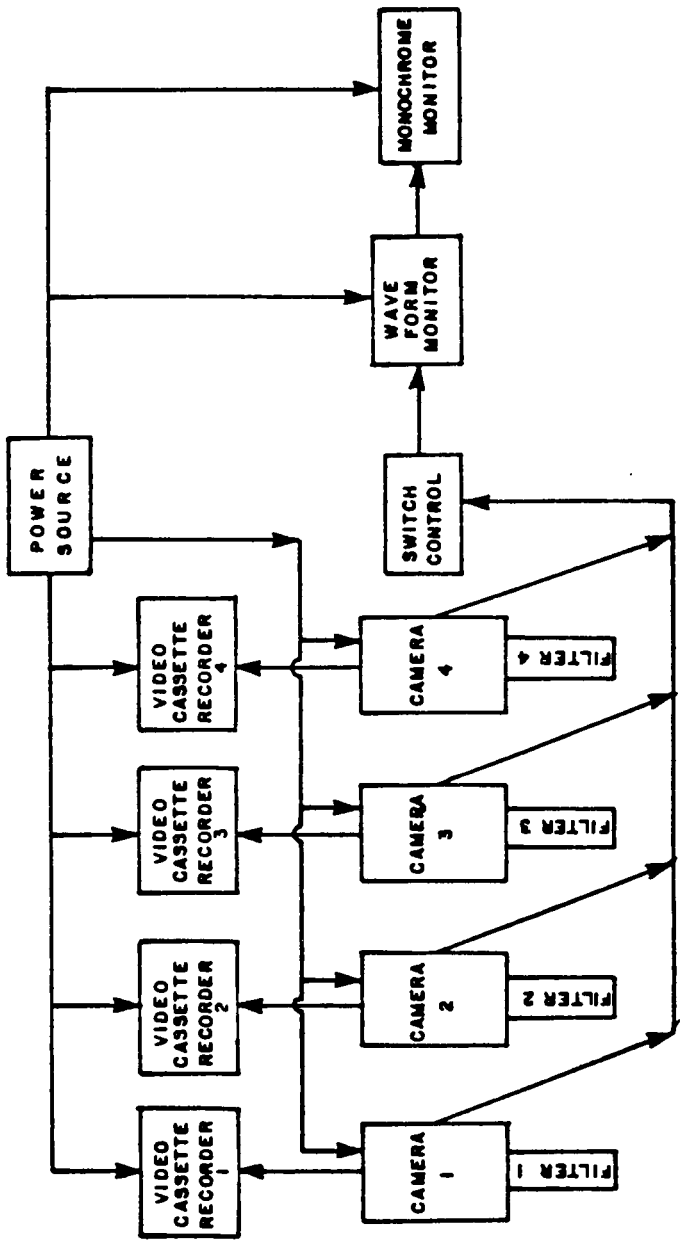

Figure 8: SCHEMATIC OF THE MULTISPECTRAL VIDEO SYSTEM (after Sherwood, 1987).

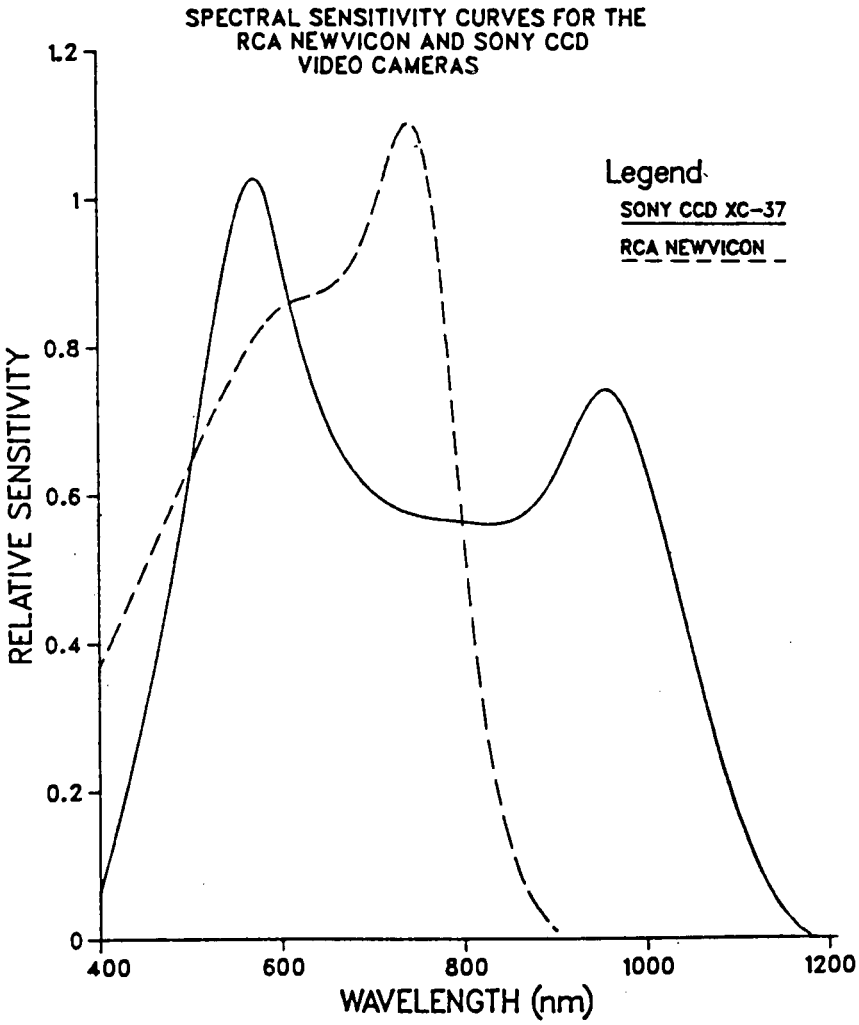

Figure 9: SPECTRAL SENSITIVITY CURVES FOR THE NEWVICON AND SONY CCD VIDEO CAMERAS.

Two 35mm reconniassance cameras were used to supplement the MSV imaging system. The Nikon F250s (with Nikkor 24mm *f*-2.8 lenses) were used with:

1) Kodak Infrared Aerochrome 2443 and a Wratten 22 filter for haze penetration and blue light removal; and
2) Kodak Ektachrome 5037 color film with a 85B filter for haze penetration and color balance.

Imagery from these cameras provided broad-band information covering the spectral gaps between the sensors of the MSV system, and allowed comparisons with the video imagery. The photographs were also useful to show visual contrasts simply, quickly, and inexpensively.

4.1.2 Field Site Characteristics

Throughout most of the year Fraser River discharge is relatively low and the small suspended sediment load is dominated by silt and clay-sized material. From midsummer through early spring SSC has been generally less than 50mg/l, and often less than 20mg/l during high tide (Milliman, 1980). Post-freshet flow in summer has relatively high discharge, but low SSC. During low tide in August 1975, Milliman (1980) measured SSC offshore in the Strait of Georgia. Values seldom exceeded 10mg/l, and decreased significantly with water depth greater than 10 meters.

Fraser River discharge often peaks in early May, depending on timing of warm weather. Milliman found that suspended material during LLT (Low-low tide) was primarily sand, while during LHT (Low-high tide) sand concentrations were less than 1 mg/l, with most of the suspended material being silt and clay. High turbulence during freshet creates high suspensions offshore, sometimes in excess of 400 mg/l of silt and clay (Milliman, 1980).

Saltwedge effects and density differences between fresh river water and salt water cause the river water (containing suspended sediment) to flow over the more dense sea water. The Fraser River water column is about 14 meters deep at the mouth of the main stem, and gradually thins to approximately one meter as it disperses across the

Strait of Georgia in a south-southwest direction towards the Gulf Islands and Strait of Juan de Fuca (Thomson, 1981). Little mixing occurs between the river and marine water, facilitating a sharp contact delineated by a 'foam line' between turbid river water and relatively clear marine water. Thomson also reported that the momentum of the river water flowing from the main stem caused it to initially be directed southwesterly. The runoff was then affected by winds and tidal currents that ebb to the southeast and flood to the northwest.

4.2 Field Sampling Project

4.2.1 Aerial Survey Project

In order to estimate SSC in the Fraser River plume in the Strait of Georgia, large scale (1:5000 - 1:25000) reconnaisance aerial photography and MSV imagery was acquired on August 8, 1986. Infrared and color photography was used for mapping and some spectral identification of surface and submerged vegetation, suspended sediment, bottom reflection and the land/water interface. The MSV cameras provided discrete spectral data for spectral identification of suspended sediment concentration in the Fraser River plume.

Imagery was collected on August 8 between 10:00 and 10:50 am (Daylight Time) on a moderately clear sunny day. Winds were 15 knots from the north, and the sea-state was moderately choppy with occasional whitecaps. A weak flood tide, approaching slack tide, was the predominite condition. Hence, the momentum of the runoff resulted in the sediment plume being driven southwesterly with the flood tide keeping it close to the west coast ($\simeq$ 8 km.).

The aircraft utilized was a Cessna 185-c (turbo, photo conversion) outfitted with two photo hatches covered with optical glass. The fore hatch was 18 inches in diameter and housed the two photographic and one Newvicon (video) cameras. The three CCD cameras were mounted over the aft hatch measuring 8 inches in diameter. All cameras were boresighted for nadir (i.e., vertical) viewing.

Correct camera exposures were determined over the highest sediment conditions (i.e., the brightest feature) in the Fraser River plume at 2000 feet. The exposure settings were not adjusted for the duration of the mission to allow direct comparisons to be made between altitudes. The lens aperture settings were determined using the waveform monitor for the video cameras. Exposures for the photographic cameras were determined with a light meter.

Three passes over the surface sampling transect were flown at increasing altitude to measure atmospheric effects on image data. Overflights were at 2000, 4000, and 8000 feet A.M.S.L. Time between first and last overflight was about an hour. Flight direction was west; each overflight began over land in the Tsawwassen jetty area and passed over the Westshore Terminals coal facility (see Figure 10). The spectral return from coal was used in some atmospheric correction procedures (see section 4.5.1). Time of each overpass was noted to correlate with the sediment samples.

4.2.2 Surface Truth

Collection of ground data is an important and integral component of any remote sensing process. Due to the dynamic nature of tidal marine environments, simultaneous water samples have to be collected concurrent with sensor overpass, and complex energy-water interactions must be taken into account to insure meaningful results. The results and conclusions can only be as good as the field data, and inadequacies in surface measurements will necessarily affect the results.

In many past remote sensing experiments, sensor overpass has not been synchronous with surface sampling due to logistical difficulties (Bowker *et al.*, 1975; Johnson, 1975, 1978; Miller *et al.*, 1977). However, these studies were conducted in somewhat calm waters (ie. lakes, bays, and low velocity rivers). In a dynamic environment such as the Fraser River coastal marine environment, it was crucial to synchronize surface sampling and sensor overflight.

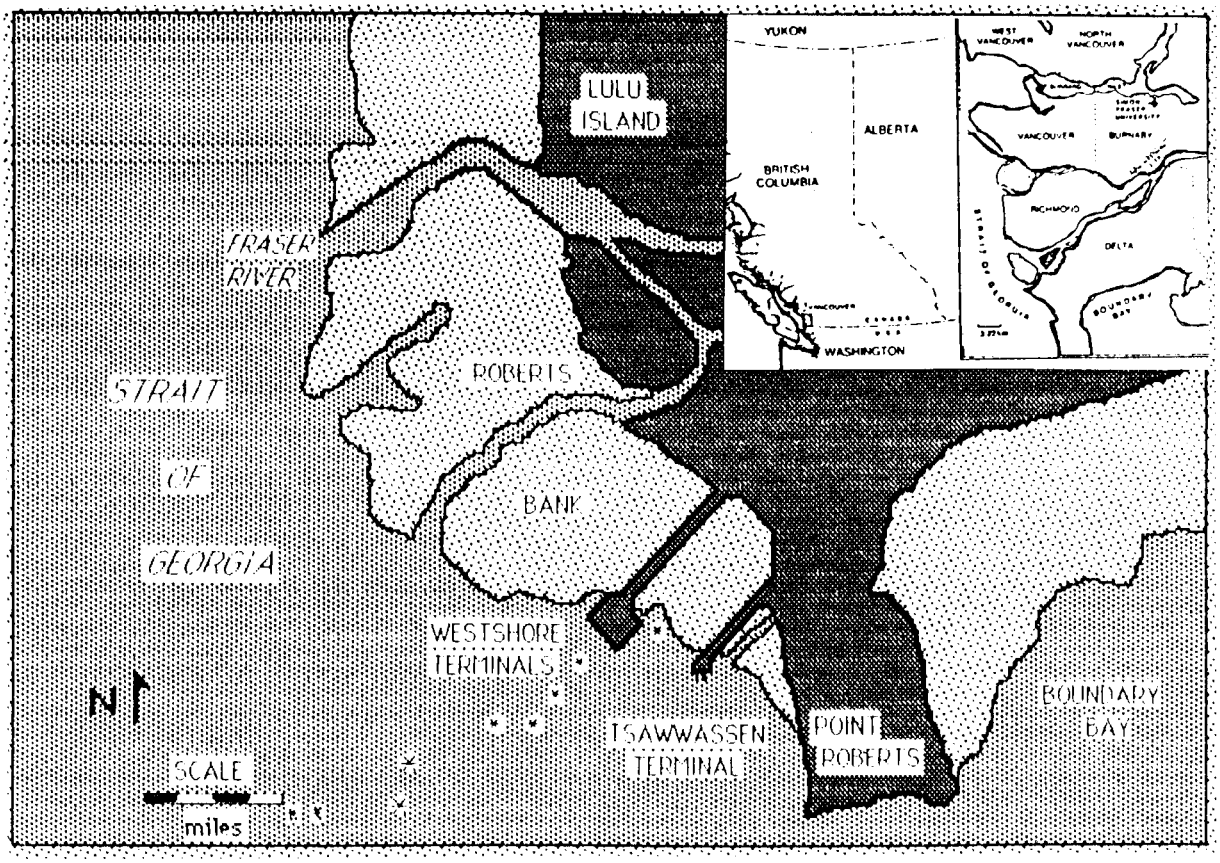

Figure 10: MAP OF THE FRASER RIVER DELTA, BRITISH COLUMBIA. SURFACE TRUTH SITES ALONG THE SAMPLING TRANSECT INTO THE STRAIT OF GEORGIA ARE INDICATED.

Knowledge of the maximum sensor penetration depth was required so that the water samples were not obtained below this zone. Secchi depth is a measure of turbidity; a (usually) white disk is lowered in the water until it is no longer visible, and is known as the 'extinction depth'. Turbidity is an optical property, and is affected by many types of particles suspended in water. Other constituents which are frequently measured are chlorophyll-*a*, which is related to amount of phytoplankton in water, and suspended sediment. Both of these are specific parameters that affect turbidity, but turbidity cannot be directly translated to SSC or chlorophyll-*a* concentration (Amos and Alföldi, 1979). Klemas *et al.* (1973) measured secchi disappearence depth with green and red disks and found that neither "color" exceeded the readings obtained with the white disk. Depending on the scattering and absorption characteristics of the suspended material, sensor penetration depth was on the order of 20% to 50% of secchi disk disapperance depth (Whitlock and Kuo, 1979).

4.2.3 Surface Sampling Transect

Suspended sediment samples were collected at selected sites arranged along a sampling transect in the Strait of Georgia. Six sampling sites were spaced between 500m and 1000m apart and represented variable suspended sediment conditions. A Canadian Coast Guard hovercraft and two small boats with outboard motors were used in surface sampling. The versitility of the hovercraft was instrumental in the formulation of the sampling procedure. Onboard navigation systems were used to set up a straight transect in open waters and provided communication links between aircraft and sampling crews. Additionally, boat crews were comforted by knowing their safety was assured, allowing them to concentrate on their sampling duties.

The sampling transect set-up involved anchoring targets[6] in five locations along a straight line. The transect began in shallow water adjacient to Westshore Terminals

---

6 The targets were 4x4 feet plywood painted flat white. A tire innertube was fixed to the underside to prevent submergence of the target. On each corner an inflated 55-gallon orange trash liner was tied, resulting in an overall target size of about 8x8 feet.

and extended west 240° (magnetic) into the Strait of Georgia until clear water was encountered — 8 km from Westshore Terminals (see Figure 10). The two small boats were launched from the Westshore Terminals boat launch and travelled to sample sites 1 and 2, where they remained for the duration of the sampling period. These crews collected samples every 5 minutes for 45 minutes beginning at 10:45 am, Daylight Time. The hovercraft travelled between the remaining four sample sites collecting suspended sediment samples. Sites 3, 4, and 5 were sampled twice; however, because the targets drifted south due to winds and tidal currents, these sample sites were not coincident with each other. No target was laid at the clear water site (site 6), and only one sample was obtained since SSC was assumed to be low and remain constant. Sediment concentrations ranged from 10.6 mg/l to 16.8 mg/l; the 'clear water' site had a concentration value of 2.1 mg/l.

4.2.4 Surface Sampling Procedure

The secchi disappearence depth was determined for each sampling position as an estimate of the remote sensing penetration depth. This also allowed the identification of areas influenced by bottom reflection when the white disk was visible on the seabed. Two sampling baskets containing three and four weighted sampling bottles, respectively, were lowered to a depth slightly less than secchi disappearence depth and raised at a constant rate to obtain 7 simultaneous integrated sediment samples. The time between submergence and emergence of the sampling baskets was about 12 seconds so that the sample bottles were not filled before reaching the surface insuring the preservation of the intergrated sample

The water samples were then transferred to 250 ml nalgene containers labled with the time, depth of sample, and sample site so that each container could be matched to a sample location on the airborne imagery. The sampling bottles were then washed with distilled water and redistributed into the sampling baskets in readiness for the next sample site. Samples were stored at cool temperatures and time between sample collection and analysis was less than four days.

Another surface sampling study was conducted on August 12, 1986, in order to investigate the temporal and spatial variability of SSC within the Fraser River sediment plume. Five suspended sediment samples were collected simultaneously at the same depth every 5 minutes for 45 minutes (8 groups) at two different locations. For both locations, variation between the 8 groups was not was not significantly different, nor was the variation of the entire sample significantly different when compared with each of the 8 groups. These results indicate that representitive samples may be obtained with short time lags (15 minutes) between surface observations and airborne collection of remote sensing data.

4.2.5 Laboratory Study

Since the sediment range encountered in the field study was relatively narrow (10.6 mg/l to 16.8 mg/l), the laboratory experiments were deemed necessary in order to futher test the analytical capibilities of both the MSV and photographic systems. Sediment concentrations ranged from 31.5 mg/l to 378 mg/l. Suspended sediment concentrations more than 250 mg/l are rarely found in nature (Pionke and Blanchard, 1975). Whitlock (1976) reported that the usual SSC range for estuaries and rivers was between 3 and 45 mg/l.

These experiments used natural sunlight for illumination in order to represent a more realistic spectral distribution of upwelling radiance from turbid water. It was hoped that these laboratory studies would provide insights on camera response to different light conditions and and broader ranges of SSC, and help to identify upper limits of camera sensitivity to high concentrations of sediment.

The first lab test was conducted on the mornings of Febuary 6-7, 1987, between 9:00 and 12:00 am, P.S.T. Both mornings were sunny with occasional clouds of different densities resulting in variable light intensities. The interiors of nine 45 gallon drums, with a diameter of 2 feet and a depth of 3 feet, were painted flat black to reduce reflection from the insides of the barrels influencing the spectral character of the

water/sediment mixture. The nine barrels were placed along a straight line on the shady side of a building (i.e., the light source was diffuse), and imaged from a nearly vertical position from the overhanging roof eight feet above the water surface. The drums were filled with unprocessed tap water and different amounts of sediment; one drum contained no sediment and was imaged before and after water was added, for control. The camera/filter configuration was identical to that used for the field experiment. Imagery was collected using the blue-sensitive Newvicon and three CCD cameras (green, red, and infrared), along with two 35mm photographic cameras with color (5037) and false-color infrared (2443) film. Since all the VCRs but one were required for another unrelated remote sensing study, imagery of the barrels was acquired using one camera at a time. The desired spectral image was acquired by selecting the appropriate camera through a switching system, and all imagery was recorded using the same VCR. Optimum exposure (1.0 volt) for each camera was set by first imaging the barrel with the highest SSC using the waveform monitor. After stirring and allowing the surface to stablize, imagery of each sediment condition, and clear water, was obtained using each video camera (i.e., blue, green, red, and infrared) and photographic camera (i.e., color and false color infrared). Secchi disappearence depth was noted and 7 intergrated suspended sediment samples were obtained using the same proceedure as in 4.2.4. After the first round of data collection, more sediment was added to all the drums except the control and the drum representing the highest sediment condition. Again, the mixtures were stirred and imaged and sampled, resulting in data for 22 sediment conditions.

Another laboratory experiment was conducted on March 21, 1987, to study the effects of direct sunlight on upwelling in turbid waters. The 45-gallon tanks were coated with aluminum foil for reflection to simulate side scattering of light (i.e., open ocean conditions), with matte black bottoms to minimize bottom reflection. Five tanks were placed on a concrete slab which had a slightly higher albedo than the highest sediment condition. Reflectance from the concrete would have scattered into the sensors' FOV, but the spectral distribution of this scattered light was assumed to be uniform

(and diffuse) for all bands since the concrete was white. Two additional tanks were filled with clear unprocessed tap water for control. The interior of one tank was flat black, while the other was coated with aluminum foil with a matte black bottom.

The camera, filtration, and imaging equipment was identical to the setup of the first laboratory experiment. Again, all the VCRs were not available so that imagery was acquired using the cameras in sequence. The exposures were set by first imaging the highest sediment condition, and not adjusted for the duration of the experiment. The sampling procedure was to stir three barrels to create a 'uniform' sediment concentration, then image them using a video camera sensitive to a particular wavelength. There was a short time-lag between stirring the barrels and imaging them, which undoubtedly caused some small amount of sediment to settle out of suspension. Then, the other two barrels were stirred and imaged in the same manner (plus the clear water control barrel) using the same camera. Imagery of the same barrel (i.e., the same sediment condition) was acquired in the same manner using a different camera until all four video and two photographic cameras had been used. Then the barrels were sampled to determine sediment concentration in the same fashion as described in the field test. After sampling, more sediment was added to some of the barrels, while water was added to others in order to dilute the existing sediment concentration. Thus, while the sun angle was increasing, SSC may have increased or decreased. This procedure was followed three times in total, resulting in 4-band multispectral video imagery, and color and infrared photographs of 15 sediment conditions. Total time from start to finish was about two hours, from 11:00 am to 1:15 pm.

Suspended sediment consisted of about 65% fine sand (≥63um), determined gravimetrically; approximately 33% silt, and about 2% clay (≤ 2um), determined on a Micrometrics sedigraph.

4.2.6 Film Densitometry

Ektachrome color 5037 and Infrared Aerochrome 2443 films were analyzed with an Eseco transmission densitometer with red, green, and blue filters (WRATTEN 92, 93, 94, respectively) that allowed measurement of film density for each of the three dye layers of the color and color infrared film. Film density was inversely related to scene reflectivity, where a high optical count on the densitometer corresponded to low reflectivity. The color film was sensitive to blue, green, and red wavelengths, while the color infrared was sensitive to green, red, and reflected infrared wavelengths. Optical density counts were taken using the 1 milimeter aperture. The 1mm aperture corresponded to a ground distance of 20 and 90 meters (diameter) for imagery collected at 2000 feet (601 meters) and 8,000 feet (2424 meters), respectively. Densitometric analysis of film used in the laboratory tests resulted in optical count values averaged for a 'ground area' of 9 centimeters on the water surface. Five densitometric readings were averaged for each sample point on all photographic images. The optical counts were then regressed with SSC and analyzed on the SFU mainframe computer.

4.3 Analysis of Video Imagery

The video remote sensing system used in this study was treated as a spectro-radiometer. This was done to avoid image registration difficulties, posed by both the sensor system and the lack of easily identifiable ground reference points over water. Additionally, camera and lens distortions were reduced, thus avoiding complex camera and radiometric calibration procedures. This approach also allowed complete control of radiance data manipulation, and avoided unknown (and perhaps unrepeatable) scaling and stretching procedures performed by the image processor after mathematical manipulation of image data. Spectral values at the image center (i.e., nadir values) were extracted using a VAX11-750 I^2S (Model 70/F4) image processing system and analyzed using the SFU mainframe computer.

Sample site locations were pin-pointed on the imagery by using Loran-C navigation (coordinates) information from both hovercraft and aircraft. The Coast Guard navigation system also provided digitized maps of sample site locations. After the video imagery in one band was scaled and sample sites located, the other multispectral images were selected by the VCR counter and a stop watch.

Video imagery lends itself to computer image processing due to its electronic format. The imagery was digitized in a straight-forward manner from video tape with good radiometric reproduction without the use of optical filters. The spectrally discrete video images were individually entered into the image processing system from a VCR. The VCR was interfaced with a time base corrector (TBC) which synchronized the scan rate of the digitizer and the output signal of the VCR. The waveform monitor was linked between the TBC and the video digitizer in order to accurately adjust the level of the video signals produced by the TBC. This insured that all the information on the video tape ($\leq$ 1 volt) was being 'captured' by the video digitizer without exceeding 1 volt, which would result in image saturation and loss of information. The different video image intensities, representd by .01-1 volt (100 divisions), were transformed into DNs between 0 and 255 by the digitizer. Imagery was visually inspected on a 19 inch RGB monitor during the process to permit proper image selection

The I^2S System 500 software BLOTCH function was used to select digitized video data from each band separately. These 'BLOTCHED' regions were analogous to the densitometric spot readings from the film. In order to overcome problems of detector noise, and noise in the image data due to sea-state or surface orientation, the data extracted from the video images for the regression analysis were not from a single pixel corresponding with the sample sites. Instead, areas (groups of pixels) incorporating multiple surface reflections were selected from the image nadir, with no attempt to impose a rigid shape or size. The number of pixels analyzed for the 'BLOTCHED' regions in each image was approximately 300 for the field study sites, and about 150 for the laboratory studies. The number of pixels, means, and standard deviations of

these selected regions were obtained with the HISTOGRAM function. While the analyzed regions of the multiple images making up the ground scene were not exactly coincident, they were from essentially the same area. Spatial and/or radiometric variability between images was 'smoothed over' by using the mean values for the areas analyzed.

4.3.1 Dark-Object Subtraction/Addition

Clear water has low reflectance and can be used as both a dark object for subtraction and a standard with which to compare turbid water bodies (Ahern *et al.*, 1977; Moore, 1978; Snydor, 1980). Subtraction of the minimum radiance of clear water from turbid water (in each band) results in the subtraction of approximately the atmospheric reflectance from the water surface and the volume reflectance of clear water. Thus, the resulting residual radiance is attributed only to suspended sediment concentration (Scarpace *et al.*, 1979; Scherz and Van Domelen, 1975; Sydor, 1980).

Such atmospheric corrections can significantly reduce the effects of atmospheric radiance components from the imagery, thereby increasing the image contrast for the scene and enhancing the sensitivity and accuracy of suspended sediment classification.

In an attempt to reduce atmospheric influences, the dark DNs from both coal and clear water were used to adjust image DNs in the field study. The DNs of coal from the video imagery were '0'; therefore, only the clear dark water values were used. These clear water DNs from both altitudes were subtracted from the sample site DNs obtained from the corresponding altitudes.

Since an increase in atmospheric scattering results in a *decrease* in film density (the photograph is lighter), the optical count density values of these dark objects were actually added to the image density values in order to increase the film density (and make the photograph darker). Thus, adding film density values was approximately analogous to subtracting reflectance values (see 4.3.1). However, neither dark object used with this technique improved the results. This prodedure was probably

inappropriate because it altered the spectral relationship between bands as well as between flight lines.

Clear water values from the black barrel and aluminum-coated barrel were used as dark objects to adjust the image DNs of the different sediment conditions in the laboratory study. Again, the video imagery was not sensitive to these dark values so that dark-object subtraction techniques could not be assessed. The dark DNs were added to the appropriate DNs of each light-sensitive layer of the color and infrared films, in the same manner as in the field study.

4.3.2 Regression Analysis

Linear and non-linear multiple regression empirically correlated the reflectance spectra (independent variable) from the sediment-laden water with the concentrations of suspended particles. Environmental and optical conditions (water and atmospheric conditions) were summarized in the regression coefficients. In order to help define a reliable relationship between SSC and reflectance, certain criteria and conditions were identified and measured. These included environmental, sampling, and statistical procedures:

1. Analysis of image data from water depths deeper than secchi disappearance depth. The flat-black bottom of the barrels in the laboratory study were not considered to be reflective, and these data were included in analyses.
2. A wide range of sediment conditions within the scene were measured in both the field survey and the laboratory experiment.
3. Time lags between image aquisition and surface sampling were small.
4. SSCs were determined from 7 integrated samples collected from the remote sensing penetration depth.
5. Only data subjected to consistent handling techniques were analyzed.
6. Only the central portion of the images were analyzed. Pixels from a representitive area in the image nadir were averaged to reduce system and environmental noise. These distributions were normal.

7. The field survey sample size was 14 when data from the two flight lines were combined. There were 13 sediment conditions analyzed from the laboratory experiment. While the number of observation were not large, they were more than three times the number of sensor channels, and probably constituted a representitive sample.

CHAPTER 5

RESULTS AND DISCUSSION

5.1 Introduction

The analytical capability of the airborne multispectral remote sensing system was evaluated in terms of sensitivity and precision. The analytical range of the reflectance-sediment relationship was subsequently examined in a laboratory experiment. The first step was to determine which bands responded best to various sediment concentrations then to evaluate the predictive capabilities of these bands using linear and log-linear multiple regression techniques.

With regards to the field study, imagery was analyzed from the 2000- and 4000-foot altitude flight lines, with the data collected at 8000 feet omitted. Imagery acquired at 8000 feet was not analyzed because about an hour had elapsed between sensor overflight and surface sample data collection. The optical density counts for each dye layer of the color and infrared films, representing film density, were ratioed one to another and regressed with SSC. The neutral density optical counts were not analyzed because they represented general irradiance (i.e., overall albedo), not radiance at discrete wavelengths. Consequently, neutral density values were correlated with each of the film's light-sensitive layers.

The data plotted in Figure 11 are the optical density counts from the different light-sensitive layers of the color and color reversal infrared film for the field study at 2000 feet. They illustrate the strong relationship between SSC and film density, showing that reflection increases with increasing SSC. Multiple and simple linear regression analyses were conducted in order to quantitatively evaluate this relationship. Reflectance in the different spectral bands (i.e., film layers) was used to predict SSC – the dependent variable.

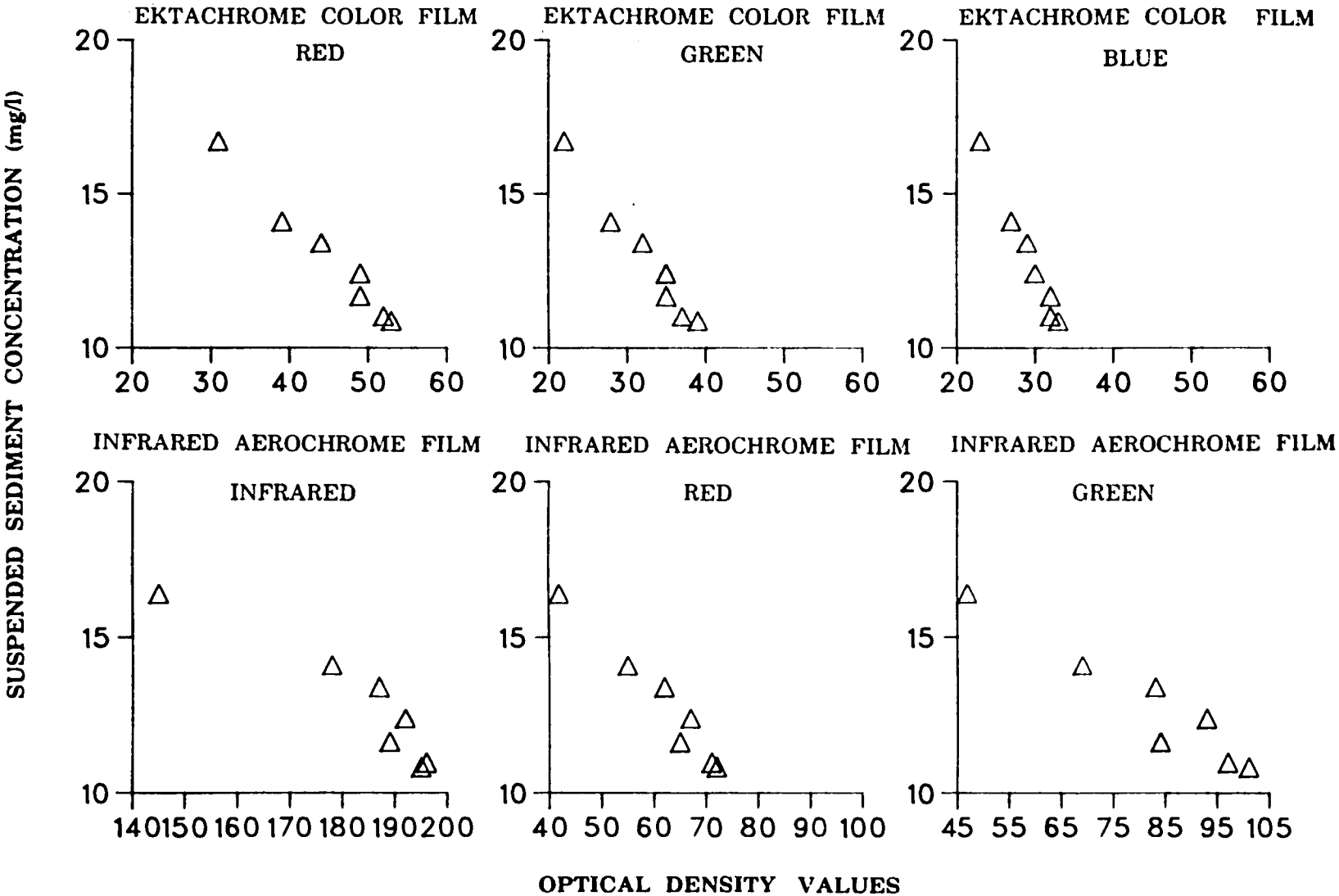

Figure 11: OPTICAL DENSITY VALUES FOR THE DIFFERENT LIGHT-SENSITIVE LAYERS OF COLOR AND INFRARED FILM TAKEN AT 2000 FEET, AS A FUNCTION OF SUSPENDED SEDIMENT CONCENTRATION

Only regression equations with coefficients of determination (r^2) greater than .70 were considered (Mace, 1983). Various statistical parameters were used to measure the precision of the regression solution, as described in the previous chapter. Briefly, the criteria used for selecting an appropriate regression equation were (Whitlock *et al.*, 1982):

1) Values for the regression coefficient (r) should approach 1,

2) the standard error should approach 0,

3) the $F/F_{0.05}$ ratio should be $\geq$ 4.0 for predictive utility,

4) the total squared error, Cp, should be low, together with,

5) a Cp/P ratio $\leq$ 1.0.

This information is tabulated for color and color infrared film in tables 3 and 4.

The tables show that several trends were evident. All of the film layers of both film types were good predictors of SSC for individual flight lines at both altitudes, with stronger results from the imagery collected at 2000 feet. Perhaps the most striking observation was that the best predictive equations for both the single flight lines and the two flight lines combined were essentially all single-term. Thus, simple regression solutions were adequate for the statistical prediction of SSC.

When data from both flight lines were combined, regression coefficients and number of variables meeting the various criteria generally decreased. However, all the values for the infrared film (see Table 4) remained high, indicating that it was relatively unaffected by atmospheric and sun angle differences between 2000 and 4000 feet. The principle reason for the reduced atmospheric effect on the infrared film was due to the filtration (Wratten 22) blocking wavelengths shorter than 560nm. Since the shorter wavelengths are scattered more than longer wavelengths, atmospheric scattering had a reduced effect on infrared film, and a stronger influence on the color film.

Table 3

Linear Regression Test Parameters Associated with the August 8, 1986 Aerial Survey; Ektachrome Color Film

	BAND	r	r^2	SE	F	$F/F_{0.05}$	RSS	Cp	Cp/P
A	R	.989	.979	.326	236.12	35.7	.53180	2.00	1.00
	G	.986	.973	.371	180.96	27.37	.68960	2.00	1.00
	B	.993	.986	.267	354.46	53.62	.35670	2.00	1.00
	R/B	.913	.833	.924	25.07	3.79	4.26500	1.99	1.00
	G/B	.919	.844	.892	27.17	4.11	4.46800	2.60	1.30
B	R	.893	.797	1.020	19.73	3.11	5.230	2.00	1.00
	G	.863	.745	1.143	14.62	2.21	6.53600	2.00	1.00
	B	.903	.815	.974	22.02	3.33	4.74500	2.00	1.00
	R/G	.924	.855	.863	29.41	4.45	3.72600	2.00	1.00
	R/B	.900	.811	.983	21.55	3.26	4.8300	1.99	1.00
C	R	.870	.760	1.009	38.33	9.00	12.2300	2.01	1.00
	G	.826	.680	1.166	25.71	6.03	16.3200	2.12	1.06
D	R	.921	.849	.804	67.44	10.2	7.7479	1.99	0.99
	G	.915	.837	.835	61.63	9.32	8.3598	1.99	1.00
E	R	.918	.843	.8181	64.65	15.18	8.0300	2.00	1.00
	G	.840	.705	1.122	28.73	6.74	15.1100	2.00	1.00
F'			No $r^2 \geq .700$						

A = 2000 feet A.M.S.L.
B = 4000 feet A.M.S.L.
C = 2000 and 4000 feet A.M.S.L., combined.
D = 2000 and 4000 feet A.M.S.L., combined, with Sun Angle Correction.
E = 2000 and 4000 feet A.M.S.L., combined, with Sun Angle Correction, and Clear Water Addition.
F' = 2000 and 4000 feet A.M.S.L., combined, with Sun Angle Correction, and Coal Addition
r = regression coefficient.
r^2 = coefficient of determination.
SE = standard error.
F = F-statistic.
$F/F_{0.05}$ = F-ratio, at the 95% confidence level.
RSS = sum of squares of residuals.
Cp = Total squared error
Cp/P = estimate of bias ($Cp/P \leq 1.0$ = negligible bias)

Table 4

Linear Regression Test Parameters Associated With The August 8, 1986 Aerial Survey; Infrared Aerochrome Film.

	BAND	r	r^2	SE	F	$F/F_{0.05}$	RSS	Cp	Cp/P
A	R+IR/G	.997	.995	.177	369.51	86.74	.12613	3.02	1.01
	R+G	.993	.985	.295	137.12	32.18	.33684	2.87	0.95
	IR	.934	.873	.771	34.42	5.21	2.9721	1.99	1.00
	R	.978	.957	.448	111.79	16.91	1.0031	1.99	1.00
	G	.957	.916	.624	55.08	8.33	1.9497	2.00	1.00
	IR/R	.977	.955	.455	107.94	16.3	1.9497	2.01	1.00
	IR/G	.95	.90	.673	46.71	7.07	2.2654	2.00	1.00
	R/G	.88	.787	.998	18.52	2.80	4.9803	2.00	1.00
B	IR	.90	.817	.924	22.45	3.39	4.2680	1.99	1.00
	R	.85	.72	1.136	13.16	1.99	6.4502	1.99	1.00
	G	.87	.757	1.066	15.62	2.36	5.6812	1.99	1.00
	IR/R	.847	.718	1.149	12.74	1.92	6.6033	2.00	1.00
	IR/G	.909	.827	.900	23.91	3.62	4.0521	2.00	1.00
	R/G	.933	.87	.779	33.62	5.08	3.0335	1.99	1.00
C	IR	.914	.836	.801	61.106	14.34	7.6918	1.98	0.99
	R	.898	.807	.868	50.24	11.79	9.0347	1.99	1.00
	G	.903	.816	.848	53.21	12.49	8.6234	1.99	1.00
	IR/R	.88	.77	.938	41.22	9.67	10.5650	2.00	1.00
	IR/G	.908	.824	.829	56.23	13.20	8.2413	1.99	1.00
	R/G	.88	.77	.932	41.94	9.8	10.425	1.99	1.00
D	IR	.914	.834	.803	60.59	14.22	7.7463	2.01	1.01
	G	.856	.733	1.021	32.94	7.73	12.513	2.00	1.00
E	IR	.880	.780	1.235	46.31	9.91	19.8240	1.99	0.99
	R	.936	.876	.926	92.34	19.77	11.1600	2.01	1.01
	G	.923	.850	1.017	74.50	12.44	13.4360	1.99	1.00
	IR/R	.835	.700	1.450	29.99	6.42	27.3450	2.00	1.00

A = 2000 feet A.M.S.L.
B = 4000 feet A.M.S.L.
C = 2000 and 4000 feet A.M.S.L., combined.
D = 2000 and 4000 feet A.M.S.L., combined, with Clear Water Addition
E = 2000 and 4000 feet A.M.S.L., combined, with Coal Addition
r = regression coefficient.
r^2 = coefficient of determination.
SE = standard error.
F = F-statistic.
$F/F_{0.05}$ = F-ratio, at the 95% confidence level.
RSS = sum of squares of residuals.
Cp = Total squared error
Cp/P = estimate of bias (Cp/P≤1.0=negligible bias)

The blue-sensitive layer for the color film had very high regression coefficients for individual flight lines (see Table 3), but when the data for the two altitudes were plotted together (Figure 12), the curves were separated due to the difference in atmospheric scattering and higher sun angle. The green- and red-sensitive layers were affected somewhat less by the atmosphere.

In order to compensate for increased sun angle, film density counts were multiplied by the cosine of the sun angle[7] (see Figure 12-D). Since the red-sensitive layer was theoretically affected least by additional atmospheric scattering, this procedure alone provided an adequate correction for the red band at these low altitudes. Sun angle correction also improved the response of the green- and blue-sensitive layers, but the curves remained separated due to residual effects from increased atmospheric scattering.

While the literature suggested that the relationship between SSC and spectral reflectance were nonlinear (e.g., see Munday and Alföldi, 1979), the narrow range of sediment values (10.6 mg/l - 16.8 mg/l) from the field observations resulted in a linear relationship. This did not hold true for the wider ranges of SSC values found in the laboratory experiments.

The four video bands analyzed were reflected infrared, red, green, and blue. The DNs were proportional to reflectance so that a large DN represents high reflectivity. Results of the regression analyses and the summary statistics are compiled in Table 5. From this table, linear relationships are evident between variable SSC and reflectance. The red, green, and blue image bands collected at 2000 feet met the criteria for SSC prediction. The response of the blue band was similar to color film in that it is highly sensitive to changing SSC at low altitudes. As expected, the r^2 for the blue imagery collected at 4000 feet fell below .70, probably due to the increased atmospheric scatter.

When data from both flight lines were combined to examine atmospheric effects between flight line altitudes, the red band proved to be the least affected by the change

---

7 The sun angle for the 2000-foot flight line was 42°, and the sun angle for the 4000-foot flight line was 45°.

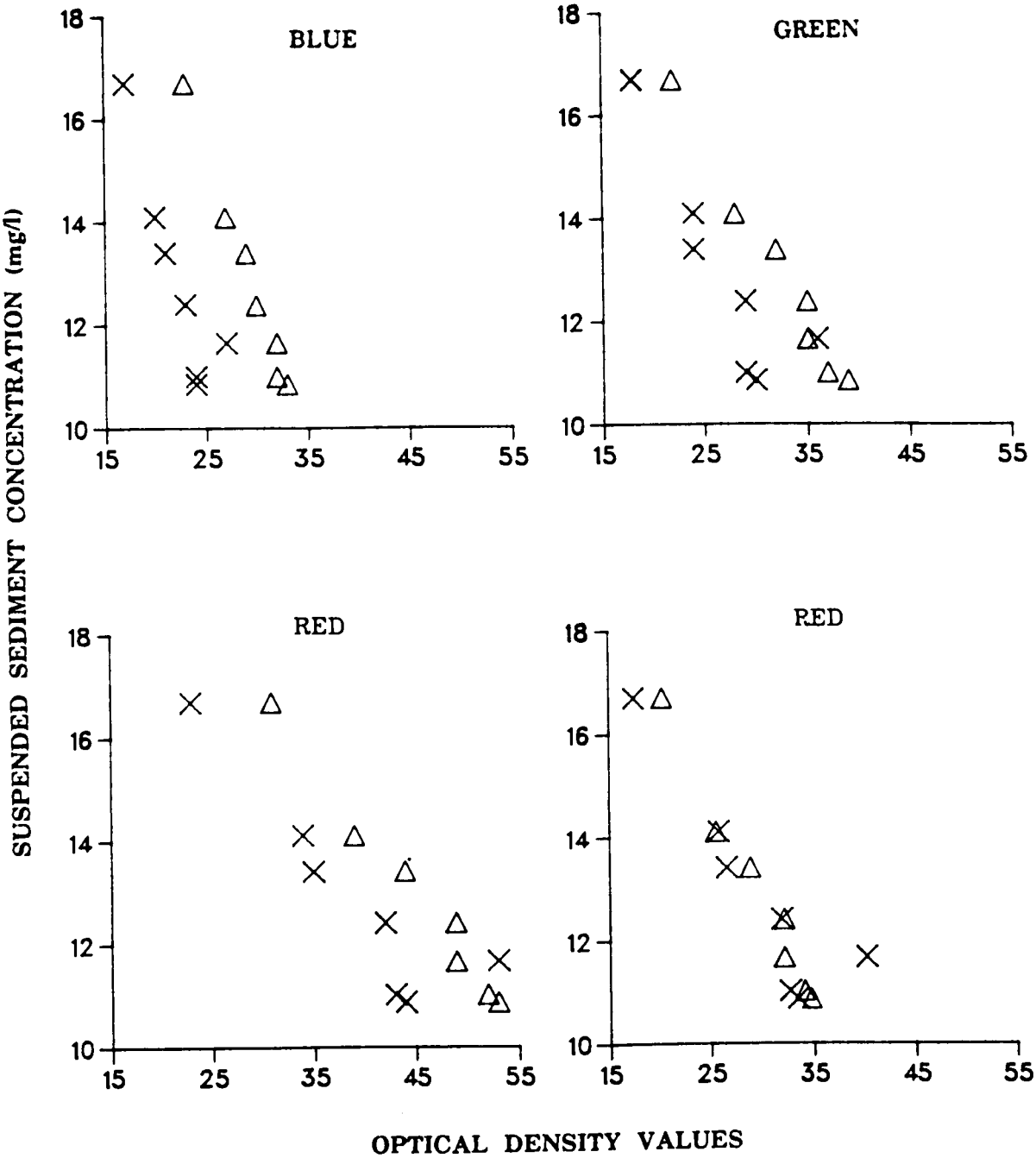

Figure 12: OPTICAL DENSITY VALUES FOR BLUE (A), GREEN (B), AND RED (C) SENSITIVE LAYERS OF EKTACHROME COLOR FILM TAKEN AT 2000 FEET (△) AND 4000 (×), AS A FUNCTION OF SEDIMENT CONCENTRATION. FIGURE "D" IS THE RED-SENSITIVE LAYER CORRECTED FOR SUN ANGLE DIFFERENCES BETWEEN THE ALTITUDES.

Table 5

Linear Regression Test Parameters Associated with the August 8, 1986 Aerial Survey; Multispectral Video Imagery

	BAND	r	r^2	SE	F	$F/F_{0.05}$	RSS	Cp	Cp/P
A	R	.835	.700	1.217	11.56	1.74	7.400	1.99	0.99
	G	.859	.739	1.131	14.15	2.14	6.400	1.99	1.00
	B	.930	.866	.809	32.4	4.90	3.270	1.99	1.00
B	R	.964	.929	.590	65.32	9.88	1.740	1.99	1.00
	G	.896	.800	.986	20.26	3.06	5.370	2.53	1.26
	R/B	.939	.880	.761	37.36	5.56	3.520	3.07	1.53
C	R	.888	.788	.929	44.77	10.51	10.360	2.00	1.00
D	R	.889	.791	.924	45.47	9.57	10.237	1.99	1.00
E	IR	.826	.680	1.140	25.7	5.4	16.270	2.51	1.25
	R	.811	.658	1.181	23.08	4.86	16.760	2.03	1.01
F'	R	.893	.797	0.911	47.04	9.90	9.960	2.00	1.00

A = 2000 feet A.M.S.L.
B = 4000 feet A.M.S.L.
C = 2000 and 4000 feet A.M.S.L., combined.
D = 2000 and 4000 feet A.M.S.L., combined, with Sun Angle Correction.
E = 2000 and 4000 feet A.M.S.L., combined, with Clear Water Subtraction
F' = 2000 and 4000 feet A.M.S.L., combined, with Sun Angle Correction, and Clear Water Subtraction
r = regression coefficient.
r^2 = coefficient of determination.
SE = standard error.
F = F-statistic.
$F/F_{0.05}$ = F-ratio, at the 95% confidence level.
RSS = sum of squares of residuals.
Cp = Total squared error
Cp/P = estimate of bias (Cp/P≤1.0=negligible bias)

in atmosphere, similar to the color film. The r^2 changed only slightly when the DNs were multiplied by the sine of the sun angle, increasing from .788 to .791. Slight exposure adjustments (see Appendix A) by the time-base-corrector saturated the pixels of the coal to black, so that only clear water values were used as dark object corrections for atmospheric interference. Clear water DNs were subtracted from the other sample site DNs in the appropriate images. Dark-object-subtraction (DOS), together with sun angle correction improved the results, increasing the r^2 from .788 to .797, with both the F-ratio and the Cp/P ratio values meeting the predetermined criteria. There was some indication that clear water DOS did compensate for some atmospheric effects. However, this technique cannot be fully evaluated because the time-base-corrector was thought to be automatically adjusting low image-DNs.

5.2 Laboratory Experiments

5.2.1 Experiment 1

The SSC range encountered in the field study was narrow. This obviously affects and limits the utility of the findings based on this narrow sediment range. Therefore, a need to examine the performance of the remote sensing system with higher concentration values and broader concentration ranges was evident. To satisfy this, a laboratory study was chosen over another field study in order to reduce expenses and logistical difficulties, while insuring a broad SSC range. A laboratory study also reduced or eliminated many environmental variables such as atmospheric absorption and scattering between the sensors and the desired targets, ie., variable SSC.

McCluney (1976) recommended the use of black, non-reflecting containers in laboratory experiments studying the spectral return from suspended sediment. This seems intuitively obvious since the color of the container will influence the total signal measured by the sensor. The first laboratory study utilized matte-black 45-gallon drums in which varying SSCs were measured and imaged.

Initial examination of the data uncovered some shortcomings of this method. The radiative transfer of light in both clear and sediment-laden water was seriously hampered by the dark interiors, the relatively small diameter of the barrels, and the diffuse light source. Subsequent observations noted better discrimination of SSCs in these black barrels in direct sunlight, but it was obvious that scattering was affected by the relatively low sun angle and dark interiors.

McCluney suggests that results from studies employing these methods are valid only if the vertical depth of light penetration was less than the diameter of the container. Therefore, SSC must be high enough such that the remote sensing penetration depth was only 2.5 feet. This required SSCs on the order of about 1000 mg/l - not very realistic concentration values for an applications-oriented remote sensing study.

Another problem encountered was that variable cloudiness resulted in variable skylight conditions that were extremely difficult to control for. These effects were acerbated by the dark background of the barrels. The net effect was that the sky, with haze and thin clouds, was prominantly mirrored on the water surface. This laboratory setup needed furthur study in order to assess its value in providing 'realistic' data. Data and experience obtained from this laboratory study were instrumental in formulating and implementing a second laboratory experiment.

5.2.2 Experiment 2

The laboratory setup for the second experiment was similar to the first experiment. The principal difference between the experiments was that the 45-gallon barrels were coated with aluminum foil to reflect sunlight in order to simulate the side scattering of light found in open water conditions, and also allowed deeper penetration of light in the barrels. Direct sunlight was used for illumination, and data was also collected from aluminum-coated and flat-black barrels containing clear water for control. The scattering of natural light in the sediment-laden water appeared much more realistic, and the results indicated that this method may represent a more realistic

model of the environment.

5.2.3 Photographic Imagery

The optical density numbers from both the aluminum-coated and matte-black control barrels containing clear water were added to the values obtained from the different sediment conditions. This was done to partially account for water surface reflections contributing to the total signal returned from the sediment laden water.

The resulting r^2 values and other statistics for the color film are presented in Table 6. The variable demonstrating the strongest relationship to sediment concentrations was the red:green ratio. In fact, it was the only significant variable in four cases, and had the highest r^2 value in the remaining two cases. Transforming SSC to logarithmic values resulted in higher r^2 values for the red:green ratio in all cases.

Thus, the ability of the color film to detect higher sediment concentrations decreased towards the upper boundary of the SSC range (see Figure 13).

The laboratory test took about 2 hours from start to finish. The increased sun angle had a small affect on the overall return from the sediment-laden water because the volume reflectance from these barrels was much larger than the surface reflection, in contrast to the first laboratory study. Dark-object addition did compensate for some surface reflections as shown by the improvement of the r^2 values of the non-linear red:green ratio. The r^2 of the uncorrected ratio, .702, was improved with dark-object-addition techniques using both the black barrel (.824), and the aluminum-coated barrel (.853).

The results from the linear and logarithmic multiple regression analyses using infrared film are compiled in Table 7. The infrared-sensitive layer provided the most meaningful results. The r^2 and F-ratio values for linear regressions were high, .920 and 12.4, respectively. This indicated that the infrared-sensitive layer was responsive to broad ranges of SSC. Dark-object addition techniques had little affect on the absolute

Table 6

Linear and Non-Linear Regression Test Parameters Associated with the Laboratory Experiment; Fujichrome Color Film

	BAND	r	r^2	SE	F	$F/F_{0.05}$	RSS	Cp	Cp/P
A	R/G	.838	.702	54.679	25.98	5.37	32727.8	1.95	0.97
B	R/G	.891	.793	0.155	42.32	8.74	.2650	2.03	1.01
	R/B	.856	.732	0.177	30.15	6.23	.3440	2.10	1.05
C	R/G	.898	.806	44.110	45.84	9.47	21377.7	1.98	0.99
D	R/G	.907	.824	0.189	80.16	16.56	.14109	2.05	1.02
E	R/G	.858	.737	51.42	30.826	6.369	29081.0	2.0	1.00
F'	R/G	.925	.853	.131	63.87	13.20	.18875	1.99	1.00
	R/B	.879	.773	.163	37.44	7.74	.29174	1.98	0.99

A = Raw Optical Density Numbers, untransformed.
B = Raw Optical Density Numbers, log10(SSC).
C = Black-Barrel Clear Water Addition, untransformed.
D = Black-Barrel Clear Water Addition, log10(SSC).
E = Aluminum-Coated Barrel Clear Water Addition, untransformed.
F' = Aluminum-Coated Barrel Clear Water Addition, log10(SSC).
r = regression coefficient.
r^2 = coefficient of determination.
SE = standard error.
F = F-statistic.
$F/F_{0.05}$ = F-ratio, at the 95% confidence level.
RSS = sum of squares of residuals.
Cp = Total squared error
Cp/P = estimate of bias ($Cp/P \leq 1.0$ = negligible bias)

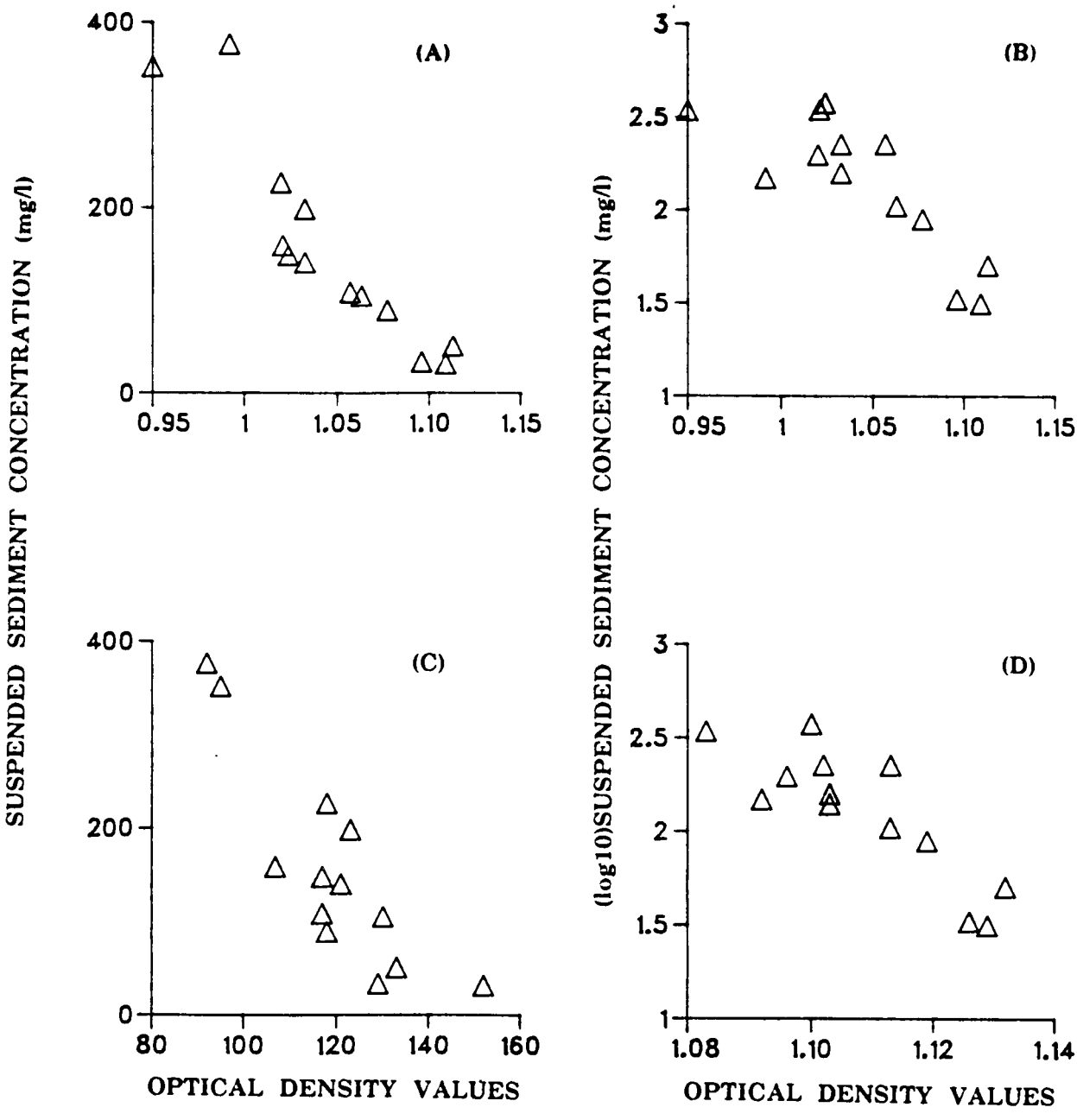

Figure 13: OPTICAL DENSITY VALUES FROM THE LABORATORY EXPERIMENT

A = Ratioed Red:Green optical density values for Fujichrome color film as a function of suspended sediment concentration.
B = Ratioed Red:Green optical density values for Fujichrome color film as a function of log10-sediment concentrations.
C = Infrared-sensitive layer of the infrared Aerochrome (2443) film.
D = Ratioed Red:Green optical density values after aluminum-barrel clear water addition (color film), as a function of log10 sediment concentration.

DNs. Logarithmically transforming SSC enhanced the ability of the red:green ratio to predict SSC, but the resulting red:green ratios were not as strong as those from the color film. The response from the red-sensitive layer was also improved by a logarithmic transformation, coupled with the black barrel addition.

5.2.4 Video Imagery

The DNs obtained from the video imagery of the laboratory experiment were treated in a similar manner as the film. No dark-object-subtraction (DOS) procedures were used because the dark values from both the black and aluminum coated control barrels of clear water were saturated to black (DN = 0) in the digitization process and provided no information. Linear and logrithmic multiple regressions were performed only on 'uncorrected' absolute and ratioed DNs. Additionally, the infrared imagery was seriously under-exposed and was consquently not used in the analyses.

The results of these regressions can be found in Table 8. The significant variables were the unratioed red and green bands. The r^2 of the green band was only slightly improved by logarithmic transformation, while the r^2 of the red band was improved from .720 to .790. The r^2 of the red and green bands was greater than .700, and the F-ratio was greater than 4.0, but the Cp/p ratio was greater than 1.0, indicating that the derived equations were biased. Inspection of the plots of residuals (see Figure 14) indicated that some of the errors were not random, but systematic. Therefore, the simple linear equation using the green reflectance appeared to be the best predictor of SSC.

The performance of the video system in the laboratory experiment was not as good as expected for a variety of reasons which are discussed below. The problems were not inherent to the video system *per se*, but resulted from equipment used inconjunction with the sensors and some aspects of the experimental design. The results do indicate, however, that video imagery can provide useful remote sensing data over broad SSC ranges.

Table 7

Linear and Non-Linear Regression Test Parameters Associated with the Laboratory Experiment; Infrared Aerochrome Film (2443)

	BAND	r	r^2	SE	F	$F/F_{0.05}$	RSS	Cp	Cp/P
A	IR	.920	.846	39.4	60.23	12.44	17076.0	2.00	1.00
B	R/G	.850	.727	.17854	29.3	6.05	35.063	1.99	1.00
C	IR	.920	.846	39.4	60.23	12.44	17076.0	2.00	1.00
D	R/G	.844	.713	.18312	27.31	5.6	.36887	2.00	1.00
E	IR	.920	.846	39.40	60.23	12.44	17076.0	2.00	1.00
F'	R	.844	.716	.18218	27.71	5.70	.36509	2.00	1.00
	R/G	.855	.732	.17704	29.98	6.20	.34479	2.00	1.00

A = Raw Optical Density Numbers, untransformed.
B = Raw Optical Density Numbers, log10(SSC).
C = Black-Barrel Clear Water Addition, untransformed.
D = Black-Barrel Clear Water Addition, log10(SSC).
E = Aluminum-Coated Barrel Clear Water Addition, untransformed.
F' = Aluminum-Coated Barrel Clear Water Addition, log10(SSC).
r = regression coefficient.
r^2 = coefficient of determination.
SE = standard error.
F = F-statistic.
$F/F_{0.05}$ = F-ratio, at the 95% confidence level.
RSS = sum of squares of residuals.
Cp = Total squared error
Cp/P = estimate of bias ($Cp/P \leq 1.0$ = negligible bias)

Table 8

Linear and Non-Linear Regression Test Parameters Associated with the Laboratory Experiment; Multispectral Video Imagery

	BAND	r	r^2	SE	F	$F/F_{0.05}$	RSS	Cp	Cp/P
A	G	.848	.720	53.027	28.32	4.28	30930.1	1.99	1.00
B	R	.889	.790	.156	41.47	6.27	.3142	2.90	1.45
	G	.869	.755	.169	33.97	5.14	.1.156	30.4	15.2

A = Raw Optical Density Numbers, untransformed.
B = Raw Optical Density Numbers, log10(SSC).
r = regression coefficient.
r^2 = coefficient of determination.
SE = standard error.
F = F-statistic.
$F/F_{0.05}$ = F-ratio, at the 95% confidence level.
RSS = sum of squares of residuals.
Cp = Total squared error
Cp/P = estimate of bias ($Cp/P \leq 1.0$ = negligible bias)

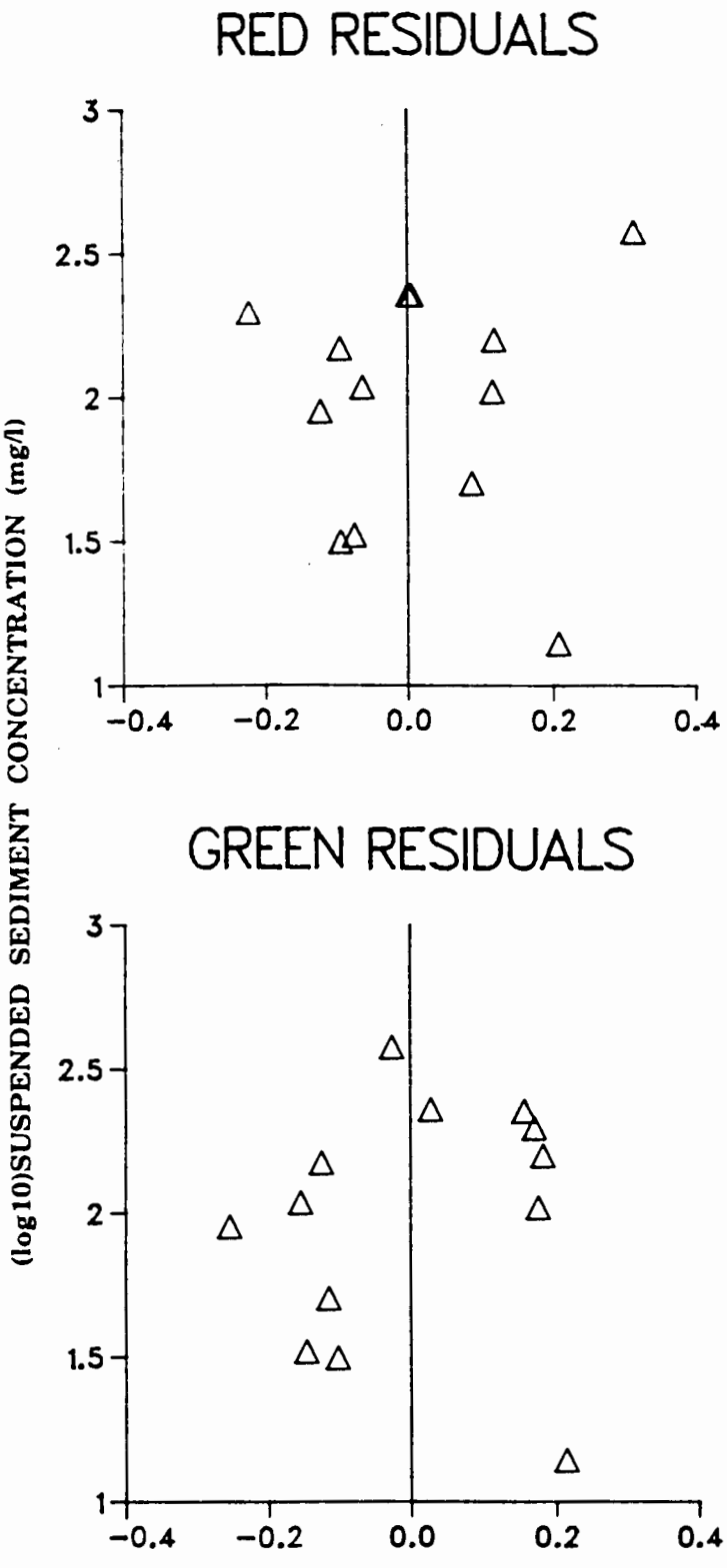

Figure 14: VIDEO RED AND GREEN BANDS: PLOTS OF RESIDUALS FROM THE REGRESSION ANALYSIS.

5.3 Results in Perspective

These results demonstrate that suspended sediment concentrations can be estimated using practical remote sensing systems. The results from the individual flight lines were very good, with r^2 values greater than .90 in many cases, together with high F-values and minimum biases. Combining data from both flight lines reduced the statistical strength of the derived regression equations to predict SSC due to increased noise.

The decision of which set of results were more useful would depend on the remote sensing objective. If the purpose of conducting a remote sensing survey was to collect data for a one-time, specific, non-temporal application, then there is value in calibrating image reflectance values from a single sensor overpass to the phenomena of interest. For example, if the objective of a study was to determine the total quantity of surficial SSC in the entire sediment plume during a certain stage of freshet discharge, image reflectance values would simply need to be calibrated with the corresponding surface truth concentration values. The relationship, under conditions particular to that overflight, could be modeled with, for example, a regression equation. The surficial sediment concentrations could then be quantified and mapped across the entire plume with a variety of computer plotting routines. The shortcomings of this procedure are that the accuracy would depend on the number and quality of surface truth measurements, and perhaps more importantly, the results would only apply to that specific data set. This method may be adequate for ongoing studies if ground truth data could be easily and inexpensively acquired and processed.

If the remote sensing objective was to monitor water quality for management purposes, minimize the dependency on ground truth data[8], or temporal parameters were of interest, then controlling and/or quantifying extraneous factors contributing to the recieved remote sensing signal would be important. These factors would be mainly meteorological, physical environmental, and sensor system noise.

---

8 Ground truth data aquisition is often expensive, time consuming, and difficult, or even dangerous, to obtain.

The objective of this study was not to determine the suspended sediment load in the Fraser River plume *per se*. Rather, the objective was to quantify suspended sediment using a particular remote sensing system, thereby testing its analytical ability. This was facilitated by employing certain methods to quantify SSC under a variety of conditions sufficient to realistically assess the techniques used to predict suspended sediment. A subsequent result is an evaluation of the sensor system employed. Therefore, data from the two flight lines were combined to test certain procedures (e.g., dark-object subtraction) under increased noise conditions to broaden the utility of these findings.

In agreement with studies previously reviewed, the relationship between SSC and reflectance can be used to predict suspended sediment concentrations in surface waters. However, the spectral bands most sensitive to SSC fluctuations were different in some cases. This may have been due to the composition of the suspended particles and physical factors affecting their suspension (coastal marine v.s. fresh water environments), in addition to the particular attributes of the sensor systems. Bartolucci (1977), Ritchie (1976), and Holyer (1978) all measured the spectral reflectance of sediment laden waters from just above the the water surface using spectro-radiometers. They all found that the channels most responsive to SSCs were in the near-infrared (700-800nm). Additionally, *in situ* measurements by Ritchie *et al.* (1974) and airborne data collected by Johnson (1975) showed strong relationships between SSC and reflectance at near-visible infrared wavelengths (700-800nm). In another airborne study, Poinke and Blanchard (1975) found that green wavelengths (530-580nm) were the most responsive to narrow sediment ranges, and orange (588-643nm) together with red (650-680nm) was the best combination to predict broad ranges of SSC (13-232 mg/l). Johnson and Bahn (1977) reported that their best results were obtained using both blue (440-490nm) and red (620-660nm) channels, but chlorophyll-*a* was also in suspension with the mineral particulates.

The best overall results from the field study were obtained with the red-sensitive layer of the color film, corrected for sun illumination angle. The r^2 value from data with both flight lines combined, was .849, the standard error was low, and the F and F-ratio values were high. Thus, the suggested equation format was:

$$SSC = J + K(Rad)$$

where:

1. SSC = suspended sediment concentration, mg/l,
2. J = 21.87
3. K = - 0.3247
4. Rad = optical density count of the red-sensitive layer of color film, multiplied by the cosine of the sun angle.

The usefulness of the red band was not restricted to the color film. The performance of the red band was consistently good at both altitudes for virtually all imagery. Using the color film, the most outstanding difference between results of the laboratory and field study was that the red absolute DNs were the best predictors in the field study, while the red:green ratio provided the best results in the laboratory study. Because the range in sediment concentration was narrow in the field test (10.6-16.8mg/l), the spectral shift of peak reflectivity from green to red wavelengths was not evident. Therefore, both bands experienced a similar increase in overall reflectance, and the relative behavior of the increased reflectance was similar. The range of sediment concentrations in the laboratory study was much wider (31-377 mg/l). As a result, the relative increase in reflectance as SSC increased was greater for the red-sensitive layer than for the green-sensitive layer. This difference in relative reflectance was enhanced by dividing the red band by the green band.

Another important finding of the laboratory study was that, for color film, nonlinear (logSSC) equations gave higher correlation coefficients than linear models, except for narrow ranges of SSC (i.e., the field study). Non-linear models were also

better with the infrared film, excluding the infrared-sensitive layer. The two similar light-sensitive layers of color and infrared film (i.e., green and red) behaved similarly under similar conditions. The response of the red:green ratio with both color and infrared photography confirmed the consistancy and usefulness of this ratio for predicting SSC.

The absolute DNs of the infrared-sensitive layer provided the best results when regressed with untransformed SSC. This indicated that infrared reflectance was sufficiently low over the entire range of SSC values so as not to increase at an exponential rate with increasing SSC. Therefore, infrared reflectance did not reach some asymptotic value at high SSCs, and has a broader analytical range than the other light-sensitive layers in the color and infrared film.

5.4 Data Correction Techniques

High altitude atmospheric effects must be reduced or negated to increase the usefulness and accuracy of remote imagery for predictive purposes. The lower the altitude of image aqusition, the less atmospheric alteration of the remotely sensed signal. However, this may be at the expense of synoptic coverage, because of the smaller area imaged. Other problems were compounded at low altitudes, such as video image blur and difficulty in averaging ocean wave-frequencies to compensate for variable sea-state.

The techniques examined in this study were dark-object-subtraction (or addition, for film) to compensate for additive atmospheric effects, band ratioing to compensate for multiplicative effects, and sun angle correction for differences in sun illumination. The main difference between this dark-object addition procedure with film and dark-object subtraction of reflectance data was that the relative spectral separation between bands was reduced for the addition procedure. If a large constant (a dark-object DN) was added to the DNs of each band, the relative difference between the bands would be reduced; whereas the relative difference would be increased (enhanced) if the resulting DNs became smaller. It is the relative differences between bands that are compared in

multispectral remote sensing, and as sediment conditions change, these relative differences between bands change. Because these relationships were degraded, this dark-object addition procedure was probably inappropriate. However, if film density values were converted to reflectance values, the subtraction of dark-object DNs should enhance image data affected by additive atmospheric scattering. This point was illustrated by the fact that dark-object addition techniques did not account for differences in altitude for the color film, while clear water subtraction, together with sun angle correction, slightly improved the video results. Sun angle correction was valuable for correcting the red-sensitive layer of the color film, suggesting that atmospheric interference was not as important as changes in sun elevation at these relatively low altitudes.

To compensate for water surface reflections in the laboratory experiment, the addition of the aluminum-coated barrel clear water values enhanced the results, using color film. The results from adding the aluminum-coated barrel clear-water values were better than for the addition of the black barrel clear-water values; both of which were an improvement on the the results from the uncorrected DNs. Therefore, there may be some utility for using dark-object-addition techniques when using color film and an 85B filter. However, these image values should be converted (inversely) so that a subtraction procedure could be used. Again, dark-object-addition had little effect on the results from the infrared film, even though the sun angle (i.e., atmospheric scattering) increased significantly. These results indicate that changes in sun angle and altitude have a reduced effect on infrared film used with a Wratten 22 filter. The small increase in sun angle and altitude differences had little affect on the infrared film, and no correction were necessary.

Physical environmental effects, such as sea state, were compensated for by simply analyzing an area on the image large enough to incorporate a representitive sample of wave frequencies. Thus, the multiple reflections of surface waves were averaged, and no one wave-surface orientation, and its resulting reflection characteristics, was dominant. The resulting average DN, corresponding to a particular sample site and sediment

condition, was considered to be representitive of that sediment condition. It was extremely important to select the same area on the multiple video images. This must occur so that essentially the same reflectance information was being compared, and differences between the bands were attributed to changes in the reflectance spectra, rather than non-related spatial differences.

Sensor system noise was minimized by insuring proper camera exposures, and by only analyzing image nadir values (i.e., the center of the image). Nadir values were affected the least by lens and camera distortions, resulting in relatively consistent exposure (spatially), thereby allowing relative comparisons to be made between images without incorporating vignetting effects in the analysis.

5.5 Realized and Potential Problems

5.5.1 The Field Experiment

The logistics of arranging personnel and equipment from government agencies and universities along a straight sediment sampling transect in adverse field conditions, extending from shallow water to 8 kilometers in the Strait of Georgia, concurrent with airborne sensor overflight proved to be difficult. Relatively short time lags between sediment sampling and sensor overflight resulted.

Strong winds and currents swept some of the 'anchored' sample-site location targets offline and out of sight. Sampling sites were located on the video imagery using the Loran-C navigation information from both aircraft and hovercraft, and smaller-scale aerial photography. Consistancy of surface sampling techniques between sea-sick sampling crews was assumed, as was the laboratory techniques employed to determine SSC.

5.5.2 The Laboratory Experiment

The main problem with the laboratory study involved the method of acquiring the video imagery. Because of equipment constraints, imagery of the different barrels was collected separately, rather than using all the cameras simultaneously. Therefore, the imagery was not 'multispectral' in the true sense of the word. Infrared, red, green, and blue imagery was collected of each barrel, but the surface orientations, and the resulting multiple reflections, were different for each image. In other words, surface reflection coefficients were different between images of a particular barrel. It would be difficult to circumvent this problem using the present MSV system. If the water surface in a barrel is thought of as a continuously moving plane in 3-dimensional space, it would be extremely difficult, or impossible, to register the same water surface orientations between different images, even if they were acquired simultaneously. Additionally, SSCs between the images of the same barrel may have been slightly different if the energy used to suspend the particles (in stirring) was slightly variable.

These problems were 'reflected' in the results of the laboratory study. The spectral shift of peak reflectivity between green and red wavelengths could not be detected because of the variablity introduced by the different multiple reflections between bands. The relatively small amount of bias indicated by the Cp/p statistic was probably due to some systematic errors associated with the same problems. However, despite these inadequacies, the results indicated that there is potential to achieve very good results with the MSV system for predicting SSC.

It is interesting to note that these problems were not realized with the film because all of the 'bands' were exposed simultaneously, and were, of course, 'registered' by design.

5.5.3 Video Imagery

Video cameras and other equipment are designed to provide optimum exposure over a wide range of light intensities. This is commonly facilitated through the use of automatic exposure controls which automatically adjust image brightness to an 'optimum' level. Because apparent feature reflectivity values are changed, these adjustments invalidate digital comparisons of these features between scenes.

One such exposure control function present in the video cameras is called 'automatic-gain-control' (AGC). The AGC was adjusted so that it was considered to be inoperative, but since it was not totally disabled until after the field study (and before the laboratory study), small exposure adjustments may have been made.

During the digitization process, there was some evidence that the time base corrector was making some exposure adjustments. In some scenes containing dark objects (e.g., the Westshore Terminals coal facility), the dark objects were saturated to 'black'. This may also have been a result of the black pedestal being set too high. Stated differently, dark DNs below a certain threshold value were assigned a DN of '0' (black). In either case, these factors essentially reduced the dynamic range of the video imagery, resulting in some loss of information. Proper adjustment or control of such factors would improve the performance of the video imagery for the spectral identification of features and phenomena.

5.5.4 Photographic Imagery

Portions of the study relied more heavily on photography because the results were better than for video imagery. Because the principle system of concern in the study was the video, some techniques of calibrating photographs were overlooked. These techniques included developing a grey-scale step-wedge with each photographic frame in order to measure density differences due to film development. Another technique is to calibrate density differences to a standard reflector within the scene, e.g., black shadows. Film developer and storage effects may have varied slightly between frames, and would

have been incorporated in the optical density counts. This unaccounted variability could influence the accuracy of the results. Other problems associated with multi-layered films included chemical development variabilities (e.g., 'cracked' emulsion), film storage effects, overlapping spectral sensitivity between layers, and dye absorption in areas other than those of its primary design. Many of these complications are less important with relative ratio comparisons between bands due to the compensating effects of ratioing procedures. Additionally, optical density values were obtained from the center of the individual photographic frames to reduce vignetting and other camera/lens distortions.

5.5.5 Measurement of Suspended Sediment Concentration

SSC is typically measured in terms of a weight of dry sediment per unit volume of water (mg/l). The reason for this type of measurement is simplicity and low cost. A problem exists with this convention of measurement. Volume reflectance is mainly a function of particle size, not their texture or color. Composition and size of particulates obviously affect the measurement of weight. Many clay-sized particles are required to produce the same weight as a few sand-sized particles; but an equal weight of clay- and sand-sized particles produce drastically different volume reflection spectra. Hence, mg/l is an measurement relative to a certain particle size or composition (density) and it may be inappropriate to compare such measurements between studies unless the comparisons were being made between the same sized particles. If discharge could be related to a certain particle size distributions, then remote sensing data of similar discharge rates could be compared.

CHAPTER 6

CONCLUSIONS

6.1 Towards an Universal Multispectral Model to Determine SSC

The ideal remote sensing scenario is that an algorithm could be developed which would allow the quantification of SSC without surface truth. Additionally, the algorithm would apply universally to various geographic regions under a variety of environmental conditions. The only way this could be accomplished is to model all variables which affect the spectral return from sediment-laden water. This would require knowledge of the conditions under which the different constituents are suspended due to the nature of suspended sediment measurements and their relationship with reflectance of electro-magnetic energy.

Several researchers have reported that particle size is the most important factor in relating SSC to reflectance, rather than color and texture of the particles (Bowker *et al.*, 1975; Whitlock, 1976; Holyer, 1978; Moore, 1978) Hence, there is some hope for developing an universal algorithm because the possible colors and textures of suspended sediment is infinite, whereas acccounting for different particle size may be a more manageable problem (Holyer 1978).

Developing such a model would still be a formidable task. Particle size would have to be corrrelated with time of year, discharge rates, and tidal conditions for a particular site, area, and region. If biological parameters are of interest, additional information would be needed, such as temperature, BOD, nutrients and time of day. Such a data base would take many years and require the efforts of many agencies and researchers. Therefore, the development of a universal algorithm is unlikely, and remote sensing of SSC would remain site-specific. If, however, the physical and environmental factors affecting the suspension of certain sediments can be adequately modeled so that a minimum of surface truth information was required, an "universal" model pertaining to a certain geographical region (e.g. the Fraser River delta) could be realized. Any

surface truth measurements would increase the accuracy of the classification, and these sample sites could be conveniently located to minimize time and cost.

The first step in the journey towards this "hybrid" classification of SSC would be to identify, quantify, and reduce the effects that distort and degrade classification accuracy with respect to the remote imagery. These effects are camera and lens distortions, system noise, atmospheric and sun angle differences, and sea state and surface reflection influences. The second step would be to quantify and correlate suspended partical size and other attributes to reflectance. Together, these 'steps' would provide a strong foundation on which to base an hybrid classification scheme to predict SSC.

6.2 Summary and Further Research

The aim of the research was to evaluate less costly methods of remote sensing data aquisition and analysis for monitoring water quality. The objective of the study was to develop a procedure to quantify variable suspended sediment concentrations using a combined multispectral video and small format photographic remote sensing system. It is concluded that the reflectance characteristics of sediment-laden water can be used to adequately predict SSC.

The following conclusions were reached:

1. A channel in the red portion of the spectrum can estimate narrow ranges of low SSCs (10 mg/l - 16.8 mg/l).
2. A ratio of the red and green channels can estimate broad ranges of variable SSCs (31 mg/l - 380 mg/l).
3. The relationship between suspended sediment concentration and radiance is non-linear, except for narrow ranges of SSC.
4. Correction for different sun angles can compensate for illumination differences in image data.

5. Averaged image nadir values are representitive of the reflectance spectra from different features/conditions in the ground scene. Thus, the sensors can be treated as a broad-band spectro-radiometer.

The fifth conclusion is valid only if the random variations affecting the reflectance characteristics of the sediment-laden water can be averaged. For example, variations in surface reflections can be averaged in an image of a large ground scene, whereas an image of only one surface reflection condition (e.g., the water surface in the barrels of the laboratory experiment) did not provide a representitive sample of surface reflection values.

Another important observation resulting from the research was that reflective containers used in the laboratory study appeared to be more representitive of natural water conditions than black containers. A probable explaination is that the black interior absorbed the incident light before representitive radiative transfer interactions of light in water could occur. Conversely, a reflective container re-directed incident light deeper into the container, simulating the side-scattering of light found in open waters.

Statistical and graphical analyses have shown that both narrow and wide ranges of SSC could be estimated with multispectral video and small format photographic imagery. The utility of the red portion of the spectrum was evident in both the laboratory and field studies, and provided the most consistant information over the broadest range of sediment and atmospheric conditions. The green band was also useful, especially for broad SSC ranges where its behavior could be compared with that of the red band by ratio techniques. A channel in the reflected infrared portion of the spectrum is necessary to extend the analytical range and insure that image saturation does not occur at high SSCs. In addition, the infrared band can be used to help delineate shallow water and/or the land-water interface because of absorption within the first few centimeters of the water. If a narrow range of sediment values are expected, and a low ($\simeq$ 2000 feet) altitude flight is planned, a band in the blue-green portion of the spectrum would be benificial for good discrimination of sediment concentrations. A

blue-green channel would also allow good water penetration in clear water for identification of underwater features. Thus, the rationale for a multispectral approach to water quality remote sensing has been reaffirmed by these results.

To fully test the performance of the MSV system, imagery of a broad range of sediment concentrations needs to be aquired at a few different altitudes. Fraser River discharge during freshet conditions could provide this wide range of SSCs. Aerial survey would allow the averaging of water surface wave-frequencies and a more thorough examination of atmospheric effects. It is suggested that imagery of a dark object be aquired at the same time to adequately test the value of dark-object subtraction techniques. A combination of dark-object-subtraction with ratio procedures may provide adequate atmospheric correction, for practical purposes. Additionally, all automatic exposure devices of all video imaging, viewing, and digitizing equipment *must* be disabled in order to make relative comparisons between bands and sediment conditions. Futhermore, all video digitizing equipment must be properly adjusted for imaging the features of interest to minimize the reduction of the dynamic range of the sensors and subsequent loss of information.

The remote sensing procedures described herein addressed principal problems in quantifying SSC, and identified methods contributing to a better classification of different suspended sediment concentrations. These techniques appeared fundamentally sound, and such analyses should conform to both statistical and physical criteria and conditions encountered, and not be applied to data in which limiting factors are not met or are unknown.

REFERENCES

Abidoun, A.A., 1976. Satellite Survey of Particulate Distribution Patterns in Lake Kainji. *Remote Sensing of Environment* 5: 109-123.

Ahern, F.J., D.J. Goodenough, S.C. Jain, and V.R. Rao, 1977. Use of Clear Lakes as Standard Reflectors for Atmospheric Measurements. *Proceedings, 11th Symposium on Remote Sensing of Environment*, vol. 1, pp. 731-755.

Alföldi, T.T. and J.C. Munday Jr. 1978. Water Quality Analysis by Digital Chromaticity Mapping of Landsat Data. *Canadian Journal of Remote Sensing* 4:108-126.

Amos, C.L. 1976. Suspended Sediment Analysis of Seawater Using Landsat Imagery, Minas Basin, Nova Scotia. *Geological Survey of Canada*. Paper 76-1C, pp. 55-60.

Amos, C.L. and T.T. Alföldi. 1979. The Determination of Suspended Sediment Concentration in a Microtidal System Using Landsat Data. *Journal of Sedimentry Petrology* 49:159-174

Amos, C. L. and B. J. Topliss. 1985. Discrimination of suspended particulate matter in the Bay of Fundy using the Nimbus 7 Coastal Zone Color Scanner. *Canadian Journal of Remote Sensing* 11: 85-92.

Aranuvachapun, S., and P.H. LeBlond, 1981. Turbidity of Coastal Water Determined from Landsat. *Remote Sensing of Environment* 84: 113-132.

Bartolucci L.A., F.R. Barret, and L.F. Silva, 1977. Field Measurements of the Spectral Response of Natural Waters. *Photogrammetric Engineering and Remote Sensing* 43(5): 595-598.

Bowker, D.E., W.G. Witte, F. Fleischer, T.A. Gosnik, W.G. Hanna, and J.C. Ludwick, 1975. An Investigation of the Waters in the Lower Chesapeake Bay Area. *Proceedings. 10th International Symposium on Remote Sensing of Environment*. Volume 1, pp. 411-420.

Blanchard, B., and R. Leamer, 1974. Spectral Reflectance of Water Containing Suspended Sediment. Remote Sensing and Water Resources *Remote Sensing and Water Resources Management*. American Water Resources Association, Proceedings No. 17.

Bukata R.P., J.E. Bruton, and J.H. Jerome, 1983. Use of Chromaticity in Remote Measurements of Water Quality. *Remote Sensing of Environment* 13: 161-177.

_____, and S.C. Jain, 1979. Determination of Inherent Optical Properties of Lake Ontario Coastal Waters. *Applied Optics* 18(23): 3926-3932.

_____, and H.H. Zwick, 1981a. Optical Water Quality Model of Lake Ontario 1: Determination of the Optical Cross Sections of Organic and Inorganic Particulates in Lake Ontario. *Applied Optics* 20(9): 1696-1703.

_____, 1981b. Optical Water Quality Model of Lake Ontario. 2: Determination of Chlorophyll-*a* and Suspended Mineral Concentrations of Natural Waters from Submersible and Low Altitude Optical Sensors. *Applied Optics* 20(9): 1704-1714.

Carpenter, D.J., 1981. Inland Water Quality Assessment from Landsat Data. Proceedings, *15th International Symposium on Remote Sensing of Environment*, vol. 1, pp. 483-489.

Carpenter D.J. and S.M. Carpenter. 1983. Modeling Inland Water Quality Using Landsat Data. *Remote Sensing of Environment* 13:345-352.

Clark, D.K., J.B. Zaitzeff, L.V. Stress, and W.S. Glidden, 1974. Computer Derived Coastal Water Classifications via Spectral Signatures. *Proceedings, 9th International Symposium on Remote Sensing of Environment*, vol. 2, pp. 1213-1239.

Clark, G. L. and H. R. James. 1939. Laboratory analysis of the selective absorption of light by sea water. *J. Optical Society of America* 29(2): 43-53.

Coker, A., A. Higier, and C. Godwin, 1973. Detection of Turbidity Dynamics in Tampa Bay, Florida, Using Multispectral Imagery from ERTS-1. *Remote Sensing and Water Resources Management*, American Water Resources Association, Proceedings No. 17.

Colwell, R. N. (Editor). 1983. Manual of Remote Sensing, v. 2, pp. 1371-1496.

Cox, C., and W. Munk, 1956. Slopes of the Sea Surface Deduced from Sun Glitter. *Bulletin of Scipps Institution of Oceanography of the University of California* 6(9): 401-488.

Cracknell, A.P., 1981. Optical Scanners and Remote Sensing of Estuarine and Coastal Water Quality. Matching Remote Sensing Technologies?? pp. 285-297.

Daniel, C., and F.S. Wood, 1971. Fitting Equations to Data. *Wiley Inter Science*, New York.

Dave, J.V., 1970. Intensity and Polarization of the Radiation Emerging from a Plane-Parallel Atmosphere Containing Mono-dispersed Aerosols. *Applied Optics* 9: 2673.

DiToro, D. M. 1976. Light propagation in turbid estuarine waters: theory and application to San Francisco Bay Estuary. Final Report to Dept. of Water Resources. State of California. Hydroscience. Westwood, New Jersey.

Di Toro, D.M., 1978. Optics of Turbid Estuarine Waters: Approximations and Applications. *Water Resources* 12: 1059-1068.

Draper, N., and H. Smith, 1966. Applied Regression Analysis. *John Wiley and Sons*, New York.

Duntley, S., 1963. Light in the Sea.*Journal of the Optical Society of America* 53(2): 214-233.

Egan, W.G. 1974. Boundaries of ERTS and Aircraft Data within which Useful Water Quality Information can be Obtained. *Proceedings, 9th Symposium on Remote Sensing of Environment*, vol. 2, pp. 1319-1331.

El-Ashry, M. and H. Wanless, 1967. Shoreline Features and their Changes. *Photogrammetric Engineering* 33(2): 184-189.

Estes, J.E., and J.L. Star, 1986. Support for Global Science: Remote Sensing's Challenge. *Geocarto International* 1: 3-14.

Geraci, A. L., R. N. Colwell and S. Khorram. 1981. Remote sensing of water quality for estuarine enviornments; Matching Remote Sensing Technologies and their Applications, Proceedings of the Ninth Annual Conference of the Remote Sensing Society, pp. 199-219.

Goldman, C. R., R. C. Richards, H. W. Paerl, R. C. Wrigley, V. R. Oberbeck and W. L. Quaide. 1974. Limnological Studies and Remote Sensing of the Upper Truckee River Sediment Plume in Lake Tahoe, California-Nevada. *Remote Sensing of the Environment* 3: 49-67.

Gordon, H.R., 1973a. Simple Calculation of the Diffuse Reflectance of the Ocean. *Applied Optics* 12: 2803.

Gordon, H. R. 1974. A simple calculation of the diffuse reflectance of the ocean. To be published in *Appl. Optics* 13.

Gordon, H. R. 1974. Mie-Theory Models of Light Scattering by Ocean Color Spectra. Ph. D. Thesis, Oregon State University, Corvallis, Oregon.

_____, and O.B. Brown, 1973b. Irradiance Reflectivity of a Flat Ocean as a Function of its Optical Properties. *Applied Optics* 12: 1549.

_____, and W. McCluney, 1975. Estimation of the Depth of Sunlight Penetration in the Sea for Remote Sensing. *Applied Optics* 14(2): 413-416.

Green, W.B., 1983. *Digital Image Processing: A Systems Approach.* Van Nostrad Reinhold Company Inc., Toronto.

Griggs, M. 1973. A Method to Measure the Atmospheric Aerosol Content Using ERTS-1 Data. Third ERTS Symposium, Statler Hilton Hotel, December 10-14. Washington, D. C.

Gupta, J.N., and A.H. Ghovanlou, 1978. Radiative Transfer in Turbid Water. *Proceedings, Society of Photo-Optical Instrumentation Engineers, Vol. 160, Ocean Optics* 5: 132-147.

Helgeson, G. A. 1970. Water depth and distance penetration. *Photogrammetric Engineering* 36: 164-172.

Højerslev, N., 1979. On the Origin of Yellow Substance in the Marine Environment. *Proceedings, Workshop EURASEP Ocean Color Scanner Experiments.* Joint Resource Centre, Ispra, Italy, pp. 13-28.

Holyer, R.J., 1978. Toward Universal Multispectral Suspended Sediment Algorithms. *Remote Sensing of Environment* 7: 323-338.

Horvath, R., J.G. Braithwaite, and F.C. Poloyn, 1970. Effects of Atmospheric Path on Airborne MUltispectral Sensors. *Remote Sensing of Environment* 1: 203-215

Hovis, W., and K. Leung, 1977. Remote Sensing of Ocean Color. *Optical Engineering* 16(2): 158-166.

Huang, K., and K. Lulla, 1986. Modelling of Water Quality Using Thematic Mapper Data: Case of Lake Michigan. *Geocarto International* 2: 3-16.

Hulbert, E., 1945. Optics of Distilled and Natural Water. *Journal of the Optical Society of America* 53(2): 214-233.

Johnson, R.W., 1975. Quantitative Suspended Sediment Mapping Using Aircraft Remotely Sensed Multispectral Data. *NASA Earth Resources Survey Symposium* vol. 1-C, pp. 2087-2098.

_____, and G.S. Bahn, 1977. Quantitative Analysis of Aircraft Multispectral-Scanner Data and Mapping of Water-Quality Parameters in the James River in Virginia. *Nasa Technical Paper* 1021, 31 pp.

Johnson, R.W., and R.C. Harris, 1980. Remote Sensing for Water Quality and Biological Measurements in Coastal Waters. *Photogrammetric Engineering and Remote Sensing* 46(1): 77-85.

Johnson, R.W., J. Munday Jr., V. Carter, A. Kemmerer, B. Kendall, R. Legeckis, F. Polcyn, J. Proni, and D. Walter, 1983. The Marine Environment. *Manual of Remote Sensing*, Second Edition, vol. 1, pp. 231-291. Sheridan Press, Virginia.

Jones, B. C. 1957. Photogrammetric surveys for national charts. *Photogrammetric Engineering* 23: 291-298.

Kalle, K., 1966. The Problem of the Gelbstoff in the Sea. *Oceanography and Marine Biology Annual Review* 4(91).

Khorram, S., 1979. Remote Sensing Analysis of Water Quality in the San Francisco Bay Delta. *Proceedings, 13th International Symposium on Remote Sensing of Environment*, vol. 3, pp. 1591-1598.

Khorram, S., and H.M. Cheshire, 1985. Remote Sensing of Water Quality in the Neuse River Estuary, North Carolina. *Photogrammetric Engineering and Remote Sensing* 51(3): 329-341.

Klemas, V., D. Bartlett, W. Philpot, R. Rogers, and L. Reed, 1974a. Studies with ERTS-1 and Skylab. *Remote Sensing of Environment* 3: 153-174.

_____, J. F. Borchardt and W. M. Treasure. 1973. Suspended Sediment Observations from ERTS-1. *Remote Sensing of the Environment* 2: pp. 205-221.

Klemas, V., M. Otley, M. Philpot, C. Wethe, R. Rogers, and N. Shah, 1974b. Correlation of Coastal Water Turbidity and Circulation with ERTS-1 and Skylab Imagery. *Proceedings, 9th International Symposium on Remote Sensing of Environment*, vol. 2, pp. 1289-1318.

_____, D. Bartlett, and R. Rogers, 1975. Coastal Zone Classification from Satellite Imagery. *Photogrammetric Engineering and Remote Sensing* 51(4): 499-514.

Klooster, S.A., and J.P. Scherz, 1973. Water Quality Determination by Photographic Analysis. *Institute for Environmental Studies, Remote Sensing Program*, Report No. 21, 14 pp.

Kritikos, H., L. Yorinks and H. Smith. 1974. Suspended Solids Analysis Using ERTS-A Data. *Remote Sensing of the Environment* 4: 69-78.

Lillisand, T. M., F. L. Scarpace and J. L. Clapp. 1975. Water quality in mixing zones. *Photgr. Eng. and Rem. Sens.* 41: 285.

Lillesand, T.M., and R.W. Kiefer. 1979. *Remote Sensing and Image Interpretation*, John Wiley & Sons, Inc., New York.

Lindell, L.T., 1981. Mapping of River Quality Using Landsat Imagery. *Proceedings, 15th International Symposium on Remote Sensing of Environment*, vol. 3, pp. 1375-1385.

Mace, D., 1983. Lake Michigan Water Quality Report. Illinois Environmental Protection Agency.

Maul, G. A. and H. R. Gordon. 1975. On the use of the earth resources technology satellite (Landsat-1) in optical oceanography. *Remote Sensing of the Environment 4: 95-128.*

McCauley, J., H. Yarger, G. James, L. Magnuson, and G. Marzolf, 1974. ERTS-1 Reservoir Monitoring Studies in Kansas. Remote Sensing and Water Resources Management, American Water Resources Association, Proceedings No. 17.

McCluney, W.R., 1974a. Ocean Color Spectrum Calculations. *Hydrology and Oceanography Branch*, Goddard Space Flight Center, Greenbelt, Maryland, 35 pp.

_____, 1974b. Estimation of Sunlight Penetration in the Sea for Remote Sensing. *Hydrology and Oceanography Branch*, Goddard Space Flight Center, Greenbelt, Maryland, 30 pp.

_____. 1976. Ocean color measured off the Oregon Coast: Characteristics Vectors. *Appl. Opt.* 15: 394.

Moore, G.K., 1978. Satellite Surveillance of Physical Water-Quality Characteristics. *Proceedings, 12th International Symposium on Remote Sensing of Environment.* vol. 1, pp.445-462.

Moore, J., 1947. The Determination of the Depths of Extinction Coefficients of Shallow Water By Air Photography Using Color Filters. *Royal Society Philosophical Transcripts* 240(816), London.

Morel, A., and L. Prieur, 1977. Analysis of Variations in Ocean Color. *Limnological Oceanography* 22: 709-722.

Morse, P.M. and H. Feshbach, 1953.*Methods of Theoretical Physics*. Part 1, Chapter 8. McGraw-Hill Book Co. Inc., New York.

Mueller, J. L. 1973. The Influence of phytoplankton on ocean color spectra. Ph. D. Thesis, Oregon State University.

Mueller, J.L., 1976. Ocean Color Spectra Measured off the Oregon Coast: Characterstic Vectors. *Applied Optics* 15(2): 394-402.

Munday, J.C. Jr., 1975. Lake Ontario Water Mass Delineation from ERTS-1. *Proceedings. 9th International Symposium on Remote Sensing of Environment*, vol. 2, pp. 1355-1365.

_____, and T.T. Alföldi, 1975. Chromaticity Changes from Isoluminous Techniques Used to Enhance Multispectral Remote Sensing Data. *Remote Sensing of Environment* 4: 221-236.

_____, 1979. Landsat Test of Diffuse Reflectance Models for Aquatic Suspended Solids Measurement. *Remote Sensing of Environment 8: 169-183.*

Munday, J.C. Jr.; T.T. Alföldi; C.L. Amos. 1979. Bay of Fundy Verification of a system for Multidate Landsat Measurement of Suspended Sediment. *Satellite Hydrology.* American Water Resources Association, Minneapolis, MN., pp. 622-640.

Munday, J.C. Jr., 1983. Chromaticity of Path Radiance and Atmospheric Correction of Landsat Data. *Remote Sensing of Environment* 9: 25-39.

Norwood, V., and J. Lansing, 1983. Electro-Optical Imagery Sensors. *Manual of Remote Sensing*, Second Edition, vol. 1, pp. 335-367, Sheridan Press, Virginia.

Pestrong, R. 1968. The evaluation of multispectral imagery for a tidal marsh environment; Office Naval Research Contract NONR-4430(00), Technical Report.

Piech, K.R., and J.E. Walker, 1971. Aerial Color Analyses of Water Quality. *Journal of the Surveying and Mapping Division, Proceedings, American Society of Civil Engineers*, pp. 185-197.

Pionke, H.B., and B.J. Blanchard, 1975. The Remote Sensing of Suspended Sediment Concentrations of Small Impoundments. *Water Air and Soil Pollution* 4: 19-32.

Plass, G.N. and G.W. Kattawar, 1969. Radiative Transfer in a Atmospheric-Ocean System. *Applied Optics* 8: 455.

Polcyn, F., and C. Wezernak, 1970. Pollution Surveillance and Data Acquisition Using Multispectral Remote Sensing. *Water Resources Bulletin. Journal of the American Water Resources Association* 6(6): 920-934.

Richardson, A.J., R.M. Menges, and P.R. Nixon, 1985. Distinguishing Weed from Crop Plants Using Video Remote Sensing. *Photogrammetric Engineering and Remote Sensing* 51: 1785-1790.

Ritchie, J.C., F.R. Schiebe, and J.R. McHenry, 1976. Remote Sensing of Suspended Sediments in Surface Waters. *Photogrammetric Engineering and Remote Sensing* 42: 1539-1545.

Sabins, F., 1978. *Remote Sensing: Principles and Interpretation.* W.H. Freeman and Company, San Francisco.

Salomonson, V., T. Jackson, J. Lucas, G. Moore, A. Rangog, T. Schmugge, and D. Scholz, 1983. Water Resources Assessment. *Manual of Remote Sensing*, Second Edition, vol. 2, pp. 1497-1570, Sheridan Press, Virginia.

Scarpace, F.L., K.W. Holmquist, and L.T. Fisher, 1979. Landsat Analysis of Lake Quality. *Photogrammetric Engineering and Remote Sensing* 45: 623-633.

Scherz, J. P., D. R. Graff and W. C. Boyle, 1969. Photographic characteristics of water pollution. *Photogrammetric Engineering* 35: 38-43.

Scherz, J.P. and J.F. Van Domelen, 1974. Lake Superior Water Quality Near Duluth from Analysis of Aerial Photos and ERTS Imagery. *Remote Sensing and Water Resources Management, American Water Resources Association, Proceedings* No. 17.

_____, 1975. Water Quality Indicators Obtainable from Aircraft and Landsat Images and their Use in Classifying Lakes. *Proceedings, 10th International Symposium on Remote Sensing of Environment*, vol. 1, pp. 447-460.

Schmer, F.A., M.J. Tipton, D.W. Ryland, J. Hayden, and G. Beaver, 1972. Investigation of Lake Water Quality in Eastern South Dakota with Remote Sensing Techniques. *Proceedings, 8th International Symposium on Remote Sensing of Environment*, vol. 1, pp. 553-557.

Slater, P., F. Doyle, N. Fritz, and R. Welch, 1983. Photographic Systems for Remote Sensing. *Manual of Remote Sensing*, Second Edition, vol. 1, pp. 231-291, Sheridan Press, Virginia.

Smith, R. C. and K. S. Baker. 1978. Optical classification of natural waters. *Linmol. Oceanogr.* 23: 260-267.

Specht, M. R., D. Needler and N. L. Fritz. 1973. New color film for water photography penetration. *Photogrammetric Engineering* 39: 359-369.

Strandberg, C.H., 19--. Water Quality Analysis. Photogrammetric Engineering --: 234-248.

Swain, P. H. and S. M. Davis. 1978. Remote Sensing: the Quantitative Approach. McGraw-Hill Inc., p. 252-259.

Sydor, M., 1980. Remote Sensing of Particulate Concentrations in Water. *Applied Optics* 19(16): 2794-2800.

Theurer, C. 1959. Color infrared experimental photography for coastal mapping. *Photogrammetric Engineering* 25: 565-569.

Thompson, R.E., 1981. Oceanography of the British Columbia Coast. *Canadian Journal of Fisheries and Aquatic Sciences* 56, Special Publications, 291 pp.

Turner, R.E., W.A. Malila, and R.F. Nalpeka, 1971. Importance of Atmospheric Scattering in Remote Sensing, or Everything You've Always Wanted to Know about Atmospheric Scattering but Were Afraid to Ask. *Proceedings, 7th International Symposium on Remote Sensing of Environment*, vol. 3, pp. 1651-1669.

Tyler, J.E., Smith, R.C., and W.H. Wilson Jr., 1972. Predicted Optical Properties for Clear Natural Water. *Journal of the Optical Society of America* 62(1): 83-91.

Verdin, J.P., 1985. Monitoring Water Quality Conditions in a Large Western Reservoir with Landsat Imagery. *Photogrammetric Engineering and Remote Sensing* 51(3): 343-353.

Villemonte, J., J. Hoopes, D. Wu, and T. Lillesand, 1974. Remote Sensing in the Mixing Zone. *Remote Sensing and Water Resources Management, American Water Resources Association, Proceedings* No. 17.

Viollier, N., and N. Baussart, 1979. Enhancement of Landsat Imagery for the Monitoring of Coastal Waters, Application to the Southern Part of the North Sea. *Proceedings, 13th International Symposium on Remote Sensing of Environment*, vol. 2, pp. 1093-1101.

Wald, L., and Monget, J.M., 1983. Reflectance Contrast Observed by Landsat between a Calm and a Rough Sea. *Photogrammetric Engineering and Remote Sensing* 49(2): 241-242.

Whitlock, C.H., 1976. An Estimate of the Influence of Sediment Concentration and Type on Remote Sensing Penetration Depth for Various Coastal Waters. *Nasa Technical Memorandum* X-73906, Langley Research Center, Hampton, Virginia, 16pp.

_____, 1977. Fundamental Analysis of the Linear Multiple Regression Technique for Quantification of Water Quality Parameters from Remote Sensing Data. *Thesis. NASA Technical Memorandum* X-74600.

_____, W.G. Witte, and J.W. Usry, 1978. Penetration Depth at Green Wavelengths in Turbid Waters. *Photogrammetric Engineering and Remote Sensing* 44(11): 1405-1410.

_____, and C.Y. Kuo, 1979. A Regression Technique for Evaluation and Quantification for Water Quality Parameters from Remote Sensing Data. *Proceedings, 13th International Symposium on Remote Sensing of Environment*, vol. 3, pp. 1351-1365.

_____, and S.R. LeCroy, 1982. Criteria for the Use of Regression Analysis for Remote Sensing of Sediment and Pollutants. *Remote Sensing of Environment* 12: 151-168.

Williams, J. 1970. Optical Properties of the Sea. U. S. Naval Inst. Ser. Oceanogr., Annapolis, Maryland. 123 pp.

Williansmon, A. N. and W. E. Grabau. 1973. Sediment Concentration Mapping in Tidal Estuaries. Third Earth Resources Technology Satellite-I Symposium, Washington, D.C. December 10-14.

Williman, J.D., 1980. Sedimentation in the Fraser River and its Estuary, Southwestern British Columbia. *Estuarine and Coastal Marine Science* 10(6): 609-634.

Witzig, A.S., and C.A. Whitehurst, 1981. Literature Review of the Current Use and Technology of MSS Digital Data for Lake Trophic Classification. *Proceedings of the 1981 Fall Meeting of the American Society of Photogrammetry*, pp. 1-20.

Yarger, H. L., J. R. McCauley, G. E. James and L. M. Magnuson. 1973. Quantitative Water Quality with ERTS-1. Proceedings of the Third Earth Resource Tehnology Satellite-1 Symposium, Volume II, pp. 1637-1651.

APPENDIX A

Characteristics of Video Sensors

The purpose of the following description of video hardware and basic characteristics of video signals is to familiarize the reader with some of the terms and concepts which have bearing on theoretical design and practical problems encountered during the course of the study.

The Newvicon video camera is a black and white (b&w) single tube camera. The camera lens forms an image on the faceplate of a magnetic deflection tube, which is then electronically scanned to generate a video signal. The Sony Xc-37 video cameras are solid state detectors which consist of an array of photo detectors and read-out electronics etched onto a single (b&w) silicon chip. The density of the detector array for these sensors is 384 X 491 horizontal/vertical detectors.

The video image is made up of 'scan lines' in which the voltage level of the video signal is varied in proportion to image brightness. Thus, variable scene brightness is translated into a corresponding voltage level at each array detector in the video frame (CCD). The VCR recieves the electronic image signals from the detectors of the camera and records this information on a video tape. The VCR only records 240 lines of the possible 400 lines of information obtained by the camera. The VCR represents the 'weakest' link in the system in regards to resolution, and determines the baseline for the spatial resolution of MSV imagery.

The video cameras are designed to provide good imagery over broad illumination ranges utilizing exposure adjustment devices such as auto-iris and automatic-gain-control (AGC). With automatic exposure controls, the camera will adjust image scene brightness values to optimize exposure between dark and light fields within the ground scene.

These exposure controls are constantly making adjustments since the bright and dark objects within every new ground scene can be different. Because apparent feature reflectivity values change with exposure, these adjustments invalidate digital comparisons of these features between scenes. The AGC was disabled in all cameras, requiring that correct camera exposures be set manually with the aid of a waveform minitor. When optimum exposure is achieved, video output of scene brightness values range from 0 to 1 volt, with 100 divisions between these two values. This is referred to as the dynamic range of the sensor. If exposure is set too high, bright ground values produce a video signal greater than 1 volt; values greater than 1 volt are saturated and appear white, resulting in loss of information. Therefore, correct camera exposure is determined by setting the brightest object to be imaged to the maximum video output, insuring that all other scene brightness values are less than 1 volt.

Sources of System Noise

A perfect camera system will respond to light within a particular intensity range by producing digital intensity values that are linearly related to the light intensity of the ground scene (Green, 1983). Many remote sensing systems do not faithfully represent scene reflectivity due to noise introduced by the imaging system. Two major causes of radiometric distortions in imagery (Green, 1983) are:

1) the digital intensity values are not linearly related to the light intensities producing them; and,
2) the lack of spatial uniformity in the system's response to light levels; different regions within the camera's FOV respond differently to the same light intensity (e.g., vignetting and tube distortions). These distortions affect both photographic and electro-optical imagery. Each type of distortion for both systems will be briefly discussed in turn.

Nonlinear Camera Response to Light Intensities

The response of film to different light intensities is illustrated by the film's 'characteristic curve'. *"The characteristic curve of processed film is a plot of optical densities against the logarithm of the corresponding exposures, where exposure is the product of irradiance and the time during which the irradiance is incident on the emulsion surface"*, (Slater, 1983). A typical characteristic curve is shown in figure 15. The four important regions are: base-plus-fog, toe of the curve, straight line portion, and the shoulder of the curve. The base-plus-fog portion represents the baseline density of the film below which no information is available. The toe of the curve is the region where exposure is just above the threshold of the base-plus-fog. The slope of the straight line portion of the curve indicates the contrast level of the film, with a steep slope indicating high contrast for limited exposure ranges. Increased granularity and reduced resolution result for exposures on the shoulder of the curve. Processing conditions and other physical factors which influence the chemical response of film determine the shape and position of the curve. The characteristic curve will vary between rolls of film and between frames within the roll of film due to chemical changes in the developer. Therefore, absolute comparisons of film density are necessarily suspect, even with careful calibration (Egan, 1974).

The nonlinear response of the MSV system to varying light intensities is caused by noise within the system, and is primarily electronic in nature. System noise is any interference which degrades the radiometric clarity of an image, and is usually expressed as the ratio of the signal to the combined noise (S/N). The efficiency of a sensor system is simply the ratio of emitted electrons to incident photons, and will vary nonlinearly through a wide range of light intensities. These electronic aberations result from changing light intensities over a scene, solid

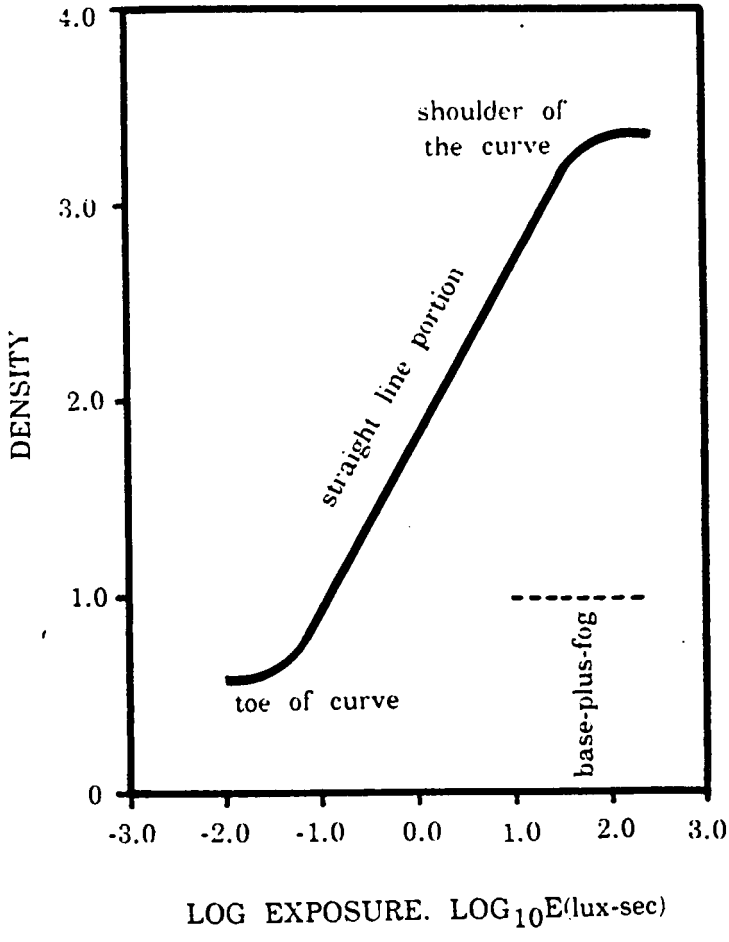

Figure 15: IDEALIZED CHARACTERISTIC CURVE FOR BLACK AND WHITE FILM, (after Slater *et al.*, 1983).

state circutry, dark current and thermal conductance, and the sensitivity of the individual detectors and/or scanning devices. Additional factors contributing to overall noise are the changes in pressure (aircraft altitude), aircraft electronic interferences, cabin temperature, and electronic interference from the photographic intervolometer. Nonlinear response characteristics of both photographic and MSV systems are influenced and acerbated by vignetting.

Shading Distortions

The remote sensing systems utilized in this study produce imagery through camera optics. Therefore, the imagery produced by the four video and two photographic cameras are all influenced by lens/filter absorption and refraction, resulting in uneven distribution of brightness in the focal plane and affecting the spatial and spectral sensitivity of the recording medium (film or magnetic tape).

Inherent in the imaging process of a lens is a $\cos^3$ dependence of incident light angle of incoming light (Egan, 1974). This $\cos^3$ dependence is quite pronounced and produces a vignetting of the image. Vignetting is a decline of light intensity away from the center of a lens, and is aperture dependent; smaller *f*-stops result in less vignetting. Camera lens transmission, and the resulting vignetting, differ between lenses (even 'identical' lenses) due to lens geometry. This fall-off in light intensity is not necessarily uniform, and depends on the geometry and the angle of collimated light striking the lens. Because different wavelengths of light refract differently, focal plane adjustments were made on each video camera to compensate for the different refractive index of the various bands. The blue camera required the smallest adjustment while the infrared camera required the largest adjustment.

Discrete bandwidths were determined by interference filters placed in front of each lens. Interference filters work on the principle of reflecting unwanted

radiation and transmitting the desired wavelength interval. These filters exhibit different bandpass characteristics for different angles if incidence. If the angle of incidence (for collimated light) is increased, the peak wavelength is shifted to shorter wavelengths (Oriel Corporation, 1983). The bandpass shift is not considered to be significant in this study as long as the channels do not overlap; however the additional refraction of light affects vignetting.

One more important source of shading distortions was the magnetic deflection tube in the Newvicon camera. Spatially variable response characteristics are caused by the geometry of the tube, with radiometric distortions extreme near the edges (Roberts and Evans, 1986).

All these nonlinear and shading distortions affecting an image can be significantly reduced with correct camera exposures, resulting in a more accurate representation of scene reflectivity. However, radiometric measurement uncertainty of less than 10% is extremely hard to achieve in remote sensing due to both sensor and environmental factors (Norwood and Lansing, 1983). Noise from this MSV system was estimated to be at least 10% of the recieved signal.

APPENDIX B

Laboatory Analysis

A filtration method was used for determination of total sediment concentration. The filtration method has several advantages over the Pyrex dish in the evaporating method (Environment Canada Sediment Laboratory New Westminster; and Geological Survey of Canada Sediment Laboratory, Patricia Bay, B. C.). Laboratory equipment necessary for filtering sediment are:

1. Millipore filtration funnel.
2. Filter manifold system with vacuum pump.
3. Dessicators.
4. Analytical balance.
5. Drying ovens.
6. 57 mm aluminum weighing dishes.
7. Millipore filters (pore size = .45 μm).
8. Graduated cylinders, flasks.

Filtration Method Laboratory Analysis

1. Number the sample bottles and corresponding 57 mm aluminum weighing dish.
2. Place the 4 um millipore filter in the weighting dish.
3. Place weighting dishes in oven at 105 C for 1 hour.
4. Transfer dishes into dessicators to cool to room temperature (1 hour).
5. Record the weight of the filters.
6. Record the gross weight of the sample bottle + the sample.
7. Record the volume of the sample (mL).
8. Place the filter in the millipore funnel and apply vacuum pressure of 100 to 300 mm Hg.
9. Wash filtrate through the milipore funnel, taking care to wash the graduated

cylinder, sample bottle and the funnel with distilled water to obtain all residue.

10. Let sample bottles air dry for several hours.

11. Place the filter + the residue in appropriate weighing dish.

12. Place weighing dishes in ovens to dry at 105 C for 3 hours.

13. Transfer dishes to dessicators to cool to room temperature (1.5 hours).

14. Record the weight of the filter + residue (grams).

15. Record the weight of the dry sample bottles.

16. Calculate the resultant total concentration as:

$$TC = (W_s * A * B) / W_{sm}$$

where:

TC = total concentration in mg/L

W_s = net weight of sediment in g. (#14 - #5).

A = 1000 mL per L.

B = 1000 mg per g.

W_{sm} = net weight of water-sediment mixture expressed in mL.

APPENDIX C

TABLES OF DATA

The following tables contain data from both the field survey and the laboratory experiment. These tables contain the absolute and ratio optical density values as well as the SSC values (mg/l).

Table 9

Absolute and Ratio Optical Density Numbers Associated With The August 8, 1986 Aerial Survey (2000 feet); Ektachrome Color Film

SITE	NEUTRAL	RED	GREEN	BLUE	N/R	N/G	N/B	R/G	R/B	G/B	SSC
Site1	24	31	22	23	.774194	1.090909	1.043478	1.409091	1.347826	.956522	16.7
Site2	30	39	28	27	.769231	1.071429	1.111111	1.392857	1.444444	1.03703	14.1
Site3	34	44	32	29	.772727	1.0625	1.172414	1.375	1.517241	1.103448	13.4
Site4	38	49	35	30	.77551	1.085714	1.266667	1.4	1.633333	1.166667	12.4
Site5	41	53	39	33	.773585	1.051282	1.242424	1.358974	1.60606	1.18181	10.86
Site6	40	52	37	32	.769231	1.081081	1.25	1.405405	1.625	1.15625	11.01
Site7	38	49	35	32	.77551	1.085714	1.1875	1.4	1.53125	1.09375	11.66
Clear Water	76	96	73	50	.791667	1.041096	1.52	1.315068	1.92	1.46	2.0
Coal	69	76	69	50	.907895	1	1.38	1.101449	1.52	1.38	

Table 10

Absolute and Ratio Optical Density Numbers Associated With The August 8, 1986 Aerial Survey (4000 feet); Ektachrome Color Film

SITE	NEUTRAL	RED	GREEN	BLUE	N/R	N/G	N/B	R/G	R/B	GB	SSC
SITE1	19	23	18	17	.826087	1.055556	1.117647	1.277778	1.352941	1.05882	16.7
SITE2	26	34	24	20	.764706	1.083333	1.3	1.416667	1.7	1.2	14.1
SITE3	26	35	24	21	.742857	1.083333	1.238095	1.458333	1.666667	1.14285	13.4
SITE4	32	42	29	23	.761905	1.103448	1.391304	1.448276	1.826087	1.26087	12.4
SITE5	33	44	30	24	.75	1.1	1.375	1.466667	1.833333	1.25	10.86
SITE6	32	43	29	24	.744186	1.103448	1.333333	1.482759	1.79166	1.20833	11.01
SITE7	38	53	36	27	.716981	1.055556	1.407407	1.472222	1.96296	1.33333	11.66
CLEAR WATER	60	79	57	34	.759494	1.052632	1.764706	1.385965	2.323529	1.676471	2.0
COAL	45	56	44	28	.803571	1.022727	1.607143	1.272727	2	1.571429	

Table 11

Absolute and Ratio Optical Density Numbers Associated with the August 8, 1986 Aerial Survey (2000 feet); Infrared Color Film

SITE	NEUTRAL	RED	GREEN	BLUE	N/R	N/G	N/B	R/G	R/B	G/B	SSC
SITE1	56	145	42	47	.386207	1.33333	1.191489	3.452381	3.085106	.893617	16.4
SITE2	70	178	55	69	.393258	1.27272	1.014493	3.236364	2.57971	.797101	14.1
SITE3	78	187	62	83	.417112	1.25806	.939759	3.016129	2.253012	.746988	13.4
SITE4	83	192	67	93	.432292	1.23880	.892473	2.865672	2.064516	.72043	12.4
SITE5	87	195	72	101	.446154	1.20833	.861386	2.70833	1.930693	.712871	10.86
SITE6	87	196	71	97	.443878	1.22535	.896907	2.760563	2.020619	.731959	11.01
SITE7	81	189	65	84	.428571	1.24615	.964286	2.907692	2.25	.77381	11.66
CLEAR WATER	149	220	137	204	.677273	1.087591	.730392	1.605839	1.078431	.671569	2.0
COAL	122	192	109	205	.635417	1.119266	.595122		1.761468	.936585	.531707

Table 12

Absolute and Ratio Optical Density Numbers Associated with the August 8, 1986 Aerial Survey (4000 feet); Ektachrome Color Film

SITE	NEUTRAL	RED	GREEN	BLUE	N/R	N/G	N/B	R/G	R/B	G/B	SSC
SITE1	51	139	38	42	.366906	1.342105	1.214286	3.657895	3.309524	.904	16.8
SITE2	70	181	54	66	.38674	1.296296	1.060606	3.351852	2.742424	.818182	14.1
SITE3	71	182	56	68	.39011	1.267857	1.044118	3.25	2.676471	.823529	13.4
SITE4	80	190	65	87	.421053	1.230769	.91954	2.923077	2.183908	.747126	12.4
SITE5	79	191	64	84	.413613	1.234375	.940476	2.984375	2.27381	.761905	10.86
SITE6	83	196	67	88	.423469	1.238806	.943182	2.925373	2.227273	.761364	11.01
SITE7	97	206	82	109	.470874	1.182927	.889908	2.512195	1.889908	.752294	11.66
CLEAR WATER	139	216	126	192	.643519	1.103175	.723958	1.714286	1.125	.65625	2.0
COAL	99	177	85	143	.559322	1.164706	.692308	2.082353	1.237762	.594406	

Table 13

Absolute and Ratio Density Numbers Associated with the August 8, 1986 Aerial Survey (2000 feet); Multispectral Video Imagery

SITE	NEUTRAL	RED	GREEN	BLUE	N/R	N/G	N/B	R/G	R/B	G/B	SSC
Site1	39.867	39	31.25	62.036	1.022231	1.275744	.642643	1.248	.628667	.50374	16.4
Site2	30.5	33.359	31.71	56.71	.914296	.961842	.537824	1.052003	.588238	.559161	14.1
Site3	35.25	37.82	29.7	55.39	.932047	1.186869	.636396	1.273401	.682795	.536198	13.4
Site4	28.8	27	25.75	40.47	1.066667	1.118447	.711638	1.048544	.667161	.636274	12.4
Site5	23.15	25.4	24.65	38.09	.911417	.939148	.607771	1.030426	.666842	.647151	10.6
Site6	25.59	26.61	25.33	32.62	.961669	1.010265	.784488	1.050533	.815757	.776517	11.01
Site7	20.52	20.67	22.99	38.21	.992743	.892562	.537032	.899087	.540958	.601675	11.66

Table 14

Absolute and Ratio Optical Density Numbers Associated with the August 8, 1986 Aerial Survey (4000 feet); Multispectral Video Imagery

SITE	NEUTRAL	RED	GREEN	BLUE	N/R	N/G	N/B	R/G	R/B	G/B	SSC
Site1	43.39	43.44	44.96	52.76	.998849	.96508	.822403	.966192	.823351	.852161	16.4
Site2	29.72	30.97	33.255	45.39	.959638	.8937	.65477	.931289	.682309	.73265	14.1
Site3	34.3	31.25	34.1	53.88	1.0976	1.00586	.6366	.91642	.57999	.63288	13.4
Site4	16.21	22.48	25.49	37.15	.721085	.635936	.436339	.881914	.605114	.686137	12.4
Site5	25.15	17.67	27.58	42.81	1.423316	.911893	.58748	.640682	.412754	.644242	10.6
Site6	30.04	20.12	22.99	46.39	1.493042	1.306655	.647553	.875163	.433714	.495581	11.01
Site7	30.58	26.57	31.39	44.24	1.150922	.974196	.69123	.846448	.600588	.709539	11.66

Table 15

Absolute and Ratio Optical Density Numbers Associated with the Laboratory Experiment; Fujichrome Color Film

NEUTRAL	RED	GREEN	BLUE	N/R	N/G	N/B	R/G	R/B	G/B	SSC
119.4	132.4	120.8	177.6	.901813	.988411	.672297	1.096026	.745495	.68018	33.2
116.4	127.1	118	175.857	.915814	.986441	.661901	1.077119	.722746	.671	89.3
135	151.2	136.4	184.4	.892857	.989736	.732104	1.108504	.819957	.739696	31.46
122.66	137.3	123.33	179	.893372	.994567	.685251	1.113273	.767039	.688994	50.6
103.43	111.7	105.7	163.7	.925962	.978524	.631827	1.056764	.682346	.645693	108.5
108.8	115.3	111.66	168.5	.943625	.974387	.645697	1.032599	.684273	.662671	140.1
118	128	120.4	173.2	.921875	.980066	.681293	1.063123	.73903	.69515	104.8
91	96.8	94.8	149.4	.940083	.959916	.609103	1.021097	.647925	.634538	158.8
83.2	83.4	87.8	138.4	.997602	.947608	.601156	.949886	.602601	.634393	228.1
104.6	110.2	107.6	167	.949183	.972119	.626347	1.024164	.65988	.644311	148.1
116.4	122.4	120	177.2	.95098	.97	.656885	1.02	.690745	.677201	226.7
112.4	119.4	115.6	171	.941374	.972318	.65731	1.032872	.698246	.676023	197.8
95	98.25	99	154.5	.966921	.959596	.614887	.992424	.635922	.640777	376.6

Table 16

Absolute and Ratio Optical Density Numbers Associated With The Laboratory Experiment; Infrared Color Film

NEUTRAL	RED	GREEN	BLUE	N/R	N/G	N/B	R/G	R/B	G/B	SSC
129	222	112	216	.581081	1.151786	.597222	1.982143	1.027778	.518519	33.2
118	221	100	205	.533937	1.18	.57561	2.21	1.078049	.487805	89.3
152	228	139	236	.666667	1.093525	.644068	1.640288	.966102	.588983	31.46
133	224	116	220	.59375	1.146552	.604545	1.931034	1.018182	.527273	50.6
117	217	99	207	.539171	1.181818	.565217	2.191919	1.048309	.478261	108.5
121	218	104	213	.555046	1.163462	.568075	2.096154	1.023474	.488263	140.1
130	223	113	219	.58296	1.150442	.593607	1.973451	1.018265	.515982	104.8
107	217	88	192	.493088	1.215909	.557292	2.465909	1.130208	.458333	158.8
95	211	75	173	.450237	1.266667	.549133	2.813333	1.219653	.433526	228.1
117	217	99	206	.539171	1.181818	.567961	2.191919	1.053398	.480583	148.1
118	216	100	210	.546296	1.18	.561905	2.16	1.028571	.47619	226.7
123	215	106	212	.572093	1.160377	.580189	2.028302	1.014151	.5	197.8
92	186	74	172	.494624	1.243243	.534884	2.513514	1.081395	.430233	376.6

Table 17

Absolute and Ratio Optical Density Numbers Associated with the Laboratory Experiment; Multispectral Video Imagery

RED	GREEN	BLUE	R/G	R/B	G/B	SSC
19.71	43.28	16.94	.455407	1.163518	2.5549	33.2
51.25	72.84	31.19	.703597	1.643155	2.335364	89.3
19.44	39.52	18.66	.491903	1.041801	2.117899	31.46
32.68	51.57	18.16	.633702	1.799559	2.839758	50.6
69.94	79.72	29.20	.877321	2.395205	2.730137	228.1
51.79	62.57	24.70	.827713	2.096761	2.533198	158.8
40.05	53.03	26.26	.755233	1.525133	2.019421	104.86
42.39	57.79	14.34	.733518	2.956067	4.029986	140.1
52.87	72.05	25.59	.733796	2.066041	2.815553	108.5
63.67	94.67	56.26	.672547	1.13171	1.682723	376.6
80.69	68.50	31.93	1.177956	2.527091	2.145318	197.8
69.52	72.55	46.93	.958236	1.481355	1.545919	226.7
63.87	77.82	45.83	.82074	1.393629	1.698014	148.1